UNIVERSITÀ DEGLI STUDI DELLA CALABRIA

Facoltà di Scienze Matematiche, Fisiche e Naturali
Dottorato di Ricerca in Fisica

XX Ciclo

Settore Scientifico-Disciplinare: FIS/03

TESI di DOTTORATO

A dynamical model for wave-particle interaction in collisionless plasmas

Rossana De Marco

Supervisore:
Prof. Vincenzo Carbone

Coordinatore:
Prof. Giovanni Falcone

2004-2007

Contents

Introduction

The theoretical discovery of wave damping without energy dissipation by collisions [1] is perhaps the most astounding result of plasma physics research. That is a real effect has been demonstrated in the laboratory. Although a simple physical explanation for this damping can be given, it is a triumph of applied mathematics that this unexpected effect was first discovered purely mathematically in the course of a careful analysis of a dispersion relation.

Landau damping results from resonant energy exchange between waves and plasma particles and it is a characteristic of collisionless plasmas, but it may also have applications in other fields. For instance, in the kinetic treatment of galaxy formation, stars can be considered as particles of a plasma interacting via gravitational rather than electromagnetic forces. Instabilities of the gas of stars can cause spiral arms to form, but this process is limited by Landau damping.

The absence of collisions is one of the main characteristics of space plasmas, but a great part of laboratory plasmas can be treated as collisionless. So wave-particle interaction, of which Landau damping is the most typical manifestation, is ubiquitous in plasma physics. One of its features is that it exhibits a locality in the velocity space: since all charged particles do not interact in the same manner with the self-consistent fields, a fluid description would fail to describe it and a kinetic description is required. The usual description of wave-particle interaction involves the Vlasov-Poisson system of equations for the electron distribution function and the perturbed field. Landau's theory is rigorous for waves of infinitesimal amplitude. For a finite-amplitude wave, particles which are near resonance, i.e. particles with velocity $v \approx v_{ph}$, with v_{ph} the wave phase velocity, will be trapped by the wave potential. Indeed, if the kinetic energy of a resonant particle is less than the potential barrier, the particle is trapped and experiences reflections at turning points (where the kinetic energy has the same value of the potential), exchanging energy with the wave. Particle bounce motion significantly limits the validity of linear Landau damping, that is equivalent to an integration in unperturbed orbits. The so-called nonlinear Landau damping problem is, in

general, not analytically tractable, as it requires explicit expressions for all particle trajectories as a function of initial position and time. Such trajectories cannot be explicitly calculated for a potential of arbitrary shape. In some cases, an approximate analytic expression for the wave profile shape is supposed and may be assumed to persist, while the wave amplitude varies. According to the first nonlinear analysis, done by O'Neil [23], the damping can be dramatically altered. The nonlinear energy exchanges between a wave and the resonant particles, trapped in its potential well, drive the wave amplitude through a sequence of oscillations, whose magnitude decreases as the particles become more and more phase mixed and unable to exchange energy with the electric field in any coherent manner. Thus, in the time-asymptotic limit the wave amplitude should reach a final nonzero constant value.

In recent years massive computer simulations have been accomplished, especially after the paper by Isichenko [24], in which the long-time evolution of generic initial perturbations in a Vlasov plasma is reconsidered, and an algebraic asymptotic damping is predicted, in spite of the non-linear interaction effects. These conclusions are based on the idea that the motion of the resonant particles is not simply oscillatory, but there is a significant number of them that escape from the potential troughs. In this way the energy balance between wave and particles is not kept. Isichenko's algebraic decay is presented as an exact asymptotic result, valid for a general initial perturbation. This conjecture has been first questioned by Lancellotti and Dorning [25], and it is not confirmed by numerical simulations. When starting with a sufficiently large initial wave amplitude, these show that in the final asymptotic state the wave energy displays an oscillatory behaviour and wave damping is stopped [28, 42]. As shown by Valentini *et al.* [31], the particles that get untrapped from the potential well, do not have a purely ballistic motion, since they can be retrapped later. The presence of a chaotic zone in proximity of the resonance zone in phase space, and the presence of particles that are always trapped could explain the observed oscillations.

Landau damping has been studied so far by using the kinetic plasma theory and only recently [33] it has been realized that the framework of dynamical systems can be useful to describe nonlinear features of the phenomenon.

In this thesis we study a dynamical model, in the form of a modified Fermi model [39], in order to investigate the wave-particle interaction. Our aim is to verify the phenomenology observed in numerical simulations, and in particular, we attempt to look into the behaviour in the long-time limit, where simulations cannot be conclusive. A simple model can also be useful to understand the underlying dynamics of the phenomenon, that cannot be easily inferred from the not intuitive analytical and numerical calculations.

The model describes the wave-particle interaction as the net result of a large number of collisions between an ensemble of particles of unitary mass moving between two infinitely massive walls with variable length. This varies following the collision dynamics of classical Newtonian physics. Using Monte Carlo simulations, it is possible to recover the phenomenology of Landau damping, with a special regard to the collective behaviour of particles. Landau damping appear as a threshold phenomenon: for initial amplitudes above a certain threshold determined from the initial conditions, after an initial decreasing, wave oscillates around a constant value. The period of this oscillations is bound to the initial amplitude as stated by O'Neil [23]. This is only a transitory phenomenon stemming from the dynamical approach towards equilibrium in the wave-particle conservative system. The equilibrium is reached via a phase mixing in phase space, where regions characterized by different density become more and more mixed, till the state of maximum entropy is reached. Correlations are created between trajectories in phase space. These facets cannot be investigated with the classic kinetic approach, since the latter, neglecting collisions between particles, cannot account for an entropy increase or the appearance of correlations. Moreover it cannot describe the phase mixing phenomenon, since it misses a characteristic distance that could be considered as a limiting distance, below which structures in phase space are no longer resolved.

In the first chapter of this thesis, the theoretical aspects of wave-particle interaction are outlined, and the numerical simulations of the last years are briefly discussed. In the second chapter, a general overview of dynamical systems, with a special regard to the *Fermi billiard* is proposed. In the third chapter the modified Fermi model is introduced, along with its principal results. In the fourth chapter we will see some statistical facts that can be derived from the model. Finally, in the fifth chapter, a comparison with the more rigorous (but even more expensive!) PIC code is presented.

The main result of our work is the analysis of how the system reaches the equilibrium state.

Chapter 1

Landau Damping

1.1 Introduction

In 1946 Lev Davidovich Landau published a landmark paper on the oscillations of plasma [1]. What Landau found was an impressive result, that there would be exponential decay of the coherent oscillations. This "Landau damping" was surprising since Landau's calculation was done in the collisionless limit where there is no explicit damping term in the equation. In fact, due to the subtleties inherent in the equations of motion, earlier treatments of the problem [2] had entirely missed this effect.

Initially, after Landau published his paper, it was not generally recognized that this kind of phenomenon could be observed in real system since Landau's analysis relied on rather restrictive assumptions. It was not until 1960's, after Landau damping had been put on a firm mathematical footing (Van Kampen [3] showed that the solution of the initial value problem can be represented as a superposition of a continuous set of singular eigenfunctions), and it had been observed experimentally [4], that the reality of the phenomenon was accepted.

Despite the mathematical and experimental confirmations, there has been some confusion over the physics behind Landau damping. This confusion is not helped by the complexity of the standard mathematical treatment. One minor problem in discussing Landau damping is that it manifests itself in different systems in different ways.

In plasma physics, that is the argument in which we are concerned, Landau damping causes the decay of coherent oscillations. But the importance of Landau's result lies beyond the domain of plasma physics and has been applied to different fields, as high energy particle beams [5], superfluids [6], and quarks [7]. Landau damping has even appeared in biological systems

[8] where it is involved in the question of the synchronization of oscillators. Such biological systems include flashing of fireflies [9], and the periodic firing of the pacemaker cells that control the beating of the heart [10]. Within a system of biological oscillators, Landau damping can be used to explain why there exists a threshold below which the feedback fails to synchronize any oscillators and why, below the synchronization threshold (at least within the framework of one particular mathematical model) the coherent signal can decay exponentially in time. The presence of Landau damping is due to the fact that the necessary conditions for the damping itself are easily satisfied: essentially, any system that can be modeled as a large collection of oscillators with feedback is a candidate for displaying Landau damping.

1.2 Landau damping in plasmas

The collisionless damping of high frequency vibrations of electronic plasmas was predicted by Landau [1] for Langmuir oscillations [11]. Since then, its presence has been identified in essentially all other modes of collective oscillations in plasma. Various modifications and refinements associated with non-Maxwellian particle distributions, background plasma non-uniformities, magnetic fields, multiple plasma species, nonlinear effects, and so on, have been made. Landau damping is a concept permeating the whole fabric of modern plasma physics. During the first 10–15 years after Landau's discovery, his paper was cited and used in only a few publications because of the absence of research programs in hot collisionless plasmas. Among these early publications was the paper by Bohm and Gross [12] where the electron distribution function was represented as a superposition of monochromatic beamlets, and that by Bernstein, Greene and Kruskal [13] who constructed exact nonlinear solutions (so-called BGK modes) in which Landau damping is absent. Generally, in the early years, a lot of attention was paid to interpretation of the singularities that appear in some versions of the theory, in particular, in the analysis of perturbations of the distribution function by a monochromatic wave. In fact, these "singularities" are, to a great extent, fictitious, not stemming from the physics of the initial-value problem but rather appearing in specific types of its mathematical description (see e.g. [14]). A nice intuitive interpretation of Landau damping and its nonlinear limits was presented by Dawson in 1961 [15]. First dedicated experiments were carried out by Malmberg and Wharton [4], which clearly demonstrated the reality of Landau damping. An explosion of interest occurred in the late 1950's early 1960's, when large-scale fusion research began in several countries and it was realized that Landau damping may strongly affect the phenomenon

of anomalous plasma losses from fusion devices. Nowadays Landau damping is almost ubiquitous in plasma physics: it is implied in supplementary heating of magnetically confined plasma in fusion devices [16], in the formation of high-energy tails of particle distribution functions, in fast relaxation of charged particle beams. It is also important in laser–plasma interactions [17], in particle acceleration by means of plasma accelerators [18], for the heating of coronal gas [19] and for that of interstellar medium [20].

1.2.1 Linear Landau damping

Let's now recall briefly the problem treated in the original paper by Landau, namely the initial value problem for a localized Langmuir perturbation. Consider the general Vlasov equation:

$$\frac{\partial f}{\partial t} + \mathbf{v}\frac{\partial f}{\partial \mathbf{r}} - \frac{e\mathbf{E}}{m}\frac{\partial f}{\partial \mathbf{v}} = 0 \tag{1.1}$$

where, $f(\mathbf{x}, \mathbf{v}, t)$ is the particle distribution function which gives the density of particles inside the element of volume $d\mathbf{x}d\mathbf{v}$ around the coordinates $(\mathbf{x}, \mathbf{v})$ of phase space, m and e mass and charge of electron, and $\mathbf{E}$ is the self-consistent electric field. Let us assume now that the electron plasma is initially stirred in a volume with a characteristic size L. If the frequency of vibrations is high enough, the collisions of electrons with ions and with each other are unessential. The distribution function of ions can be considered as invariable, whereas that of electron is assumed to be composed of a equilibrium distribution function $f_0(v)$, plus a small perturbation $f_1(\mathbf{r}, \mathbf{v}, t)$, introduced at $t = 0$, i.e.:

$$f(\mathbf{r}, \mathbf{v}, t = 0) = f_0(v) + f_1(\mathbf{r}, \mathbf{v}, t = 0) \tag{1.2}$$

By linearizing Vlasov equation, one finds:

$$\frac{\partial f_1}{\partial t} + v\frac{\partial f_1}{\partial x} - \frac{eE}{m}\frac{\partial f_0}{\partial v} = 0 \tag{1.3}$$

where, from linearized Poisson's equation,

$$\frac{\partial E}{\partial x} = n_0 - 4\pi e \int f dv \tag{1.4}$$

(n_0 is the density of the neutralizing positive background). For an initial value problem, the equations are simplified by taking their Fourier transforms with respect to spatial variables and their Laplace transforms in time. This reduces the differential equations to algebraic equations that can be solved for the desired transform variable. The problem is then inverting the Fourier and Laplace transforms.

Consider the case of long-wavelength electron plasma oscillations with $k^2\lambda_D^2 \ll 1$, where $\omega_{pe}\lambda_D = v_{th}^2$, λ_D is the Debye length, v_{th} is the thermal velocity and $\omega_{pe} = (4\pi n_0 e^2/m_e)^{1/2}$ is the plasma frequency. In this conditions, by solving Eqs. (1.3) and (1.4), one get the well known classic result of Landau for $t \to \infty$:

$$E(x,t) = E_0 \exp(\gamma_L t) \exp[i(kx - \omega_r t)] \tag{1.5}$$

where:

$$\omega_r^2 = \omega_{pe}^2(1 + 3k^2\lambda_D^2 + \cdots) \tag{1.6}$$

$$\gamma_L = \frac{\pi}{2}\frac{\omega_{pe}^3}{k^2}\left(\frac{df_0}{dv}\right)_{v=\omega/k}. \tag{1.7}$$

It is easy to see that the damping rate critically depends on the electron distribution function in vicinity of $v = (\omega/k) \equiv v_\phi$, the so called resonant region. In particular, for a Maxwellian equilibrium distribution function (centered at $v = 0$):

$$f_0(v) = n_0\left(\frac{m_e}{2\pi k_B T}\right)^{1/2} \exp\left(-\frac{m_e v^2}{2k_B T}\right)$$

one gets for γ_L the expression:

$$\gamma_L = -\left(\frac{\pi}{8}\right)^{1/2} \frac{\omega_{pe}}{(k\lambda_D)^3} \exp\left[-\frac{1}{2(k\lambda_D)^2} - \frac{3}{2}\right]. \tag{1.8}$$

Since the derivative of the distribution function in $v = v_\phi$ is negative the wave is damped in time. If $f_0(v)$ is increasing in the resonant region the wave amplitude will grow exponentially, on the basis of this linear theory.

In Appendix A is presented a nice derivation of Landau damping, in which the mathematical rigor has been sacrificed in order to convey an intuitive picture of the phenomenon.

1.2.2 Changes in the distribution function

Once that the evolution of the perturbed electric field is known, it is easy to follow the time behaviour of the electron distribution function f_1. In fact, by using Eq. (1.3) and Eq. (1.4) it is possible to show (see e.g. Ref. [21]) that for the Fourier transform of f_1 one gets:

$$f_k(t) = \bar{f}_b(t) \exp(-ik \cdot vt) + \sum_{\omega_k} \bar{f}_k \exp(-i\omega_k t) \tag{1.9}$$

where $\bar{f}_b(t)$ and $\bar{f}_k$ are some amplitudes. The terms in summation give the reaction of the particles to the waves. This damps in time as $E_1(t)$ does. The additional term $\bar{f}_b(t) \exp(-ik \cdot vt)$ is called *ballistic term* or *free-streaming*. This appears because a particle, perturbed at $t = 0$, brings memory of this perturbation. This memory is cancelled only by collisions, that are not included in Vlasov equation. Thus a fluctuation in the point (**x,r**,t) arises for two reasons: the first one is the wave, that propagates in space and time and reaches the point (**x,r**) at time t; the second one is due to the particles that arrive in (**x,r**) at time t, bringing with them memory of the initial perturbation. The ballistic term does not decrease with time (k and v are both real) but become highly oscillating in velocity space, and it does not give any contribution to the electric field because in the Poisson's equation, since $t \to \infty$ the integral becomes zero for the fast oscillations of the integrand. It has been shown [22] that the distribution function, properly mediated in time, forms a plateau asymptotically in time, in the region corresponding to the resonant trapped electrons.

1.2.3 The "surfer's picture"

To see what is responsible for Landau damping, we notice that the damping rate in Eq. (1.7) arises from the particles with velocity $v \approx v_\phi$. Consequently, the effect is connected with those particles in the distribution that have a velocity nearly equal to the phase velocity, the resonant particles. These

particles travel along with the wave, so they are able to exchange energy with the wave effectively. The easiest way to understand this exchange of energy is to picture a surfer trying to catch an ocean wave. If the surfboard is not moving, it merely bobs up and down as the wave goes by and does not gain any energy on the average. Similarly, a boat propelled much faster than the wave cannot exchange much energy with the wave. However, if the surfboard has almost the same velocity as the wave, it can be caught and pushed along by the wave. This is, after all, the main purpose of the exercise. In that case, the surfboard gains energy, therefore the wave must lose energy and is damped. On the other hand, if the surfboard should be moving slightly faster than the wave, it would push on the wave as it moves uphill; then the wave could gain energy. In a plasma, there are electrons both faster and slower than the wave. A Maxwellian distribution, however, has more slow electrons than faster ones (Fig. 1.1). Consequently, there are more particles taking energy from the wave than the vice versa, and the wave is damped. As particles with $v \approx v_\phi$ are trapped in the potential well, $f(v)$ is flattened near the phase velocity. This distortion is $f_1(v)$. Obviously, if

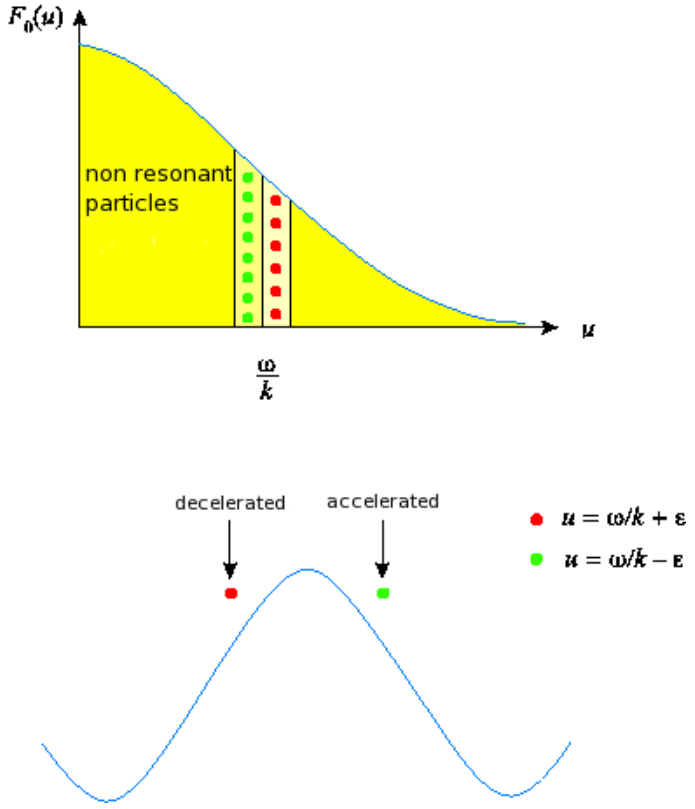

Figure 1.1: Representation of the resonant particles.

$f_0(v)$ contained more fast particles than slow particles, a wave can be excited. Waves with v_ϕ in the region of positive slope will be unstable, gaining energy at the expense of the particles. This is just a finite–temperature analogy of the two–stream instability.

1.3 Nonlinear theory: introduction

We have seen that little electrostatic perturbations in a uniform Maxwellian plasma are damped exponentially even in absence of dissipative terms in the equations. In this linear theory, the electric field is assumed to be a little perturbation in an equilibrium field-free situation. Landau's treatment is rigorous, but strictly linear, meaning that it is valid for infinitesimal initial perturbation. Indeed, the linearization holds true until the condition:

$$\frac{\partial f_1}{\partial v} \ll \frac{\partial f_0}{\partial v} \tag{1.10}$$

is verified, since the term $\partial f_1/\partial v$ is neglected in Vlasov equation. The effect that makes the linear treatment no longer applicable is the *trapping* of electrons in the potential well of the wave. As simple explanation of this point, consider the simple case in which the electric field $E(x,t)$ has the form of a purely sinusoidal travelling wave of infinite spatial extent:

$$E(x,t) = E_0 \sin(kx - \omega t) \tag{1.11}$$

where, without loss of generality, $E_0 > 0$ and $k > 0$. For the moment we ignore considerations on the self-consistency of $E(x,t)$ and assume $E_0 =$ const. In a frame of reference moving with the wave phase velocity the field is:

$$E(x,t) = E_0 \sin(kx) \equiv E(x). \tag{1.12}$$

The equation of motion for an electron moving in the electric field is:

$$m\ddot{x} = -eE(x) = e\frac{d\phi(x)}{dx} \tag{1.13}$$

where $\phi(x) = (E_0/k)\cos(kx)$ is the electrostatic potential in the wave frame. The total energy of the electron is then:

$$\frac{1}{2}m\dot{x}^2 - e\phi(x) = W. \tag{1.14}$$

Clearly, each electron with energy $W < -e\phi(x)$ is trapped and oscillates back and forth in the potential well (Fig. 1.2). This trapping imposes severe limitations to validity of linear Landau damping, that is equivalent to an integration in unperturbed orbits, namely $x(t) = x(0) + v(0)t$. For strongly trapped electrons, those with energy near the bottom of the well, we have:

$$m\ddot{x} = -eE_0kx = -m\omega^2 x \tag{1.15}$$

from which we see that the electron oscillates with a period:

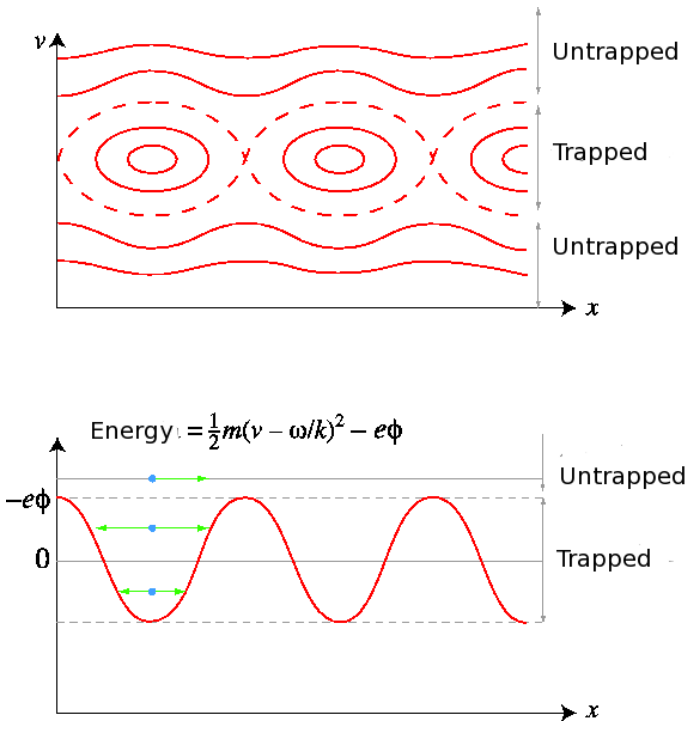

Figure 1.2: Representation of trapping of particles in a wave, with trajectories in the phase space (x, v) (top) and corresponding energy diagram (bottom).

$$\tau_{tr} \approx \omega_{tr}^{-1} = \sqrt{\frac{m}{eE_0 k}} \tag{1.16}$$

while for electrons at the top of the trough the oscillation period becomes infinite. These nonlinear orbits are then associated with the fact that the wave is not vanishing, so they are not included in the linear theory, whereas an electron with $W > eE_0/k$ is not trapped in the trough, it accelerates and decelerates as it passes over the potential, but the direction of its motion is not reversed from the initial sense. This simple harmonic motion in the potential well is a major perturbation of the particle orbit, and any linear calculation that depends on the distribution of these trapped particles cannot be valid on time scale $t > \tau_{tr}$. Landau damping depends on the distribution function of particles that move at nearly the speed of wave. Since these resonant particles are the first to be trapped Landau damping holds only if:

$$\tau_L \ll \tau_{tr} \tag{1.17}$$

where $\tau_L = \gamma_L^{-1}$, is the typical time in which linear effects take place and γ_L is given by Eq. (1.8). In other words the linear treatment is a good approximation only if the amplitude of the electric field is such that the wave damps before that electrons have time to perform oscillations in the potential well of the wave.

1.4 Nonlinear treatment of Vlasov equation

As a further demonstration of the fact that the time scale in Eq. (1.16) marks the end of validity of linear theory in the case of a single wave, let's study the linearized solution of the Vlasov equation for the electron distribution function $f(x, v, t) = f_0(v) + f_1(x, v, t)$ in an electric field given by Eq. (1.11) while for the initial condition on f_1 we consider $f_1(x, v, 0) = f_1(v, 0)\cos(kx)$. This form of f_1 is consistent, for small amplitudes, with the functional shape assumed for the electric field. The linearized Vlasov equation then is:

$$\left(\frac{\partial}{\partial t} + v\frac{\partial}{\partial x}\right) f_1 = \frac{e}{m} E_0 \sin(kx - \omega t)\frac{\partial f_0}{\partial v}. \tag{1.18}$$

The solution for the above equations may be found, integrating along the particle trajectories (method of characteristics), in absence of perturbed field. The quantity in the left hand side of Eq. (1.18) represents the temporal derivative of f_1, evaluated along an unperturbed trajectory in the field-free equilibrium:

$$\left(\frac{\partial}{\partial t} + v\frac{\partial}{\partial x}\right) f_1 = \frac{d}{d\tau} f_1. \tag{1.19}$$

Eq. (1.18) can be written as:

$$\frac{d}{d\tau} f_1[x_0(\tau), v_0(\tau), \tau] = \frac{e}{m} E_0[x_0(\tau), \tau] \left[\frac{\partial}{\partial v} f_0(v)\right]_{v=v_0(\tau)} \tag{1.20}$$

where x_0 and v_0 are the particle orbits in absence of electric field:

$$\frac{d}{d\tau} x_0(\tau) = v_0(\tau) \tag{1.21}$$

$$\frac{d}{d\tau} v_0(\tau) = 0 \tag{1.22}$$

and $x_0(\tau = t) = x, v_0(\tau = t) = v$. Integrating in time Eq. (1.20) and Eq. (1.21) we get:

$$\begin{aligned} f_1(x, v, t) = f_1[x_0(\tau = 0), v_0(\tau = 0), \tau = 0] + \\ \frac{e}{m} \int_0^t E_0(x_0(\tau), \tau) \cdot \left[\frac{\partial}{\partial v} f_0(v)\right]_{v=v_0(\tau)} d\tau \end{aligned} \tag{1.23}$$

and:

$$\int_\tau^t \frac{d}{d\tau} x_0(\tau) d\tau = \int_\tau^t v_0(\tau) d\tau \tag{1.24}$$

from which:

$$x_0(t) - x_0(\tau) = (t - \tau) v_0 = (t - \tau) v. \tag{1.25}$$

Since $v_0 = \text{const} \equiv v$ we have:

$$x_0(\tau) = x + v(\tau - t). \tag{1.26}$$

By substituting the above expression in Eq. (1.23) we get:

$$f_1(x, v, t) = f_1(x - vt, v, 0) + \frac{e}{m}\frac{\partial f_0(v)}{\partial v}\int_0^t E_0[x + v(\tau - t), \tau]d\tau. \tag{1.27}$$

If we put in this equation the expression of the electric field and that of the distribution function we have:

$$\begin{aligned} f_1(x, v, t) = f_1(v, 0)\cos[k(x - vt)] \\ + \frac{e}{m}\frac{\partial f_0(v)}{\partial v}E_0\int_0^t \sin[k(x + v(\tau - t)) - \omega t]d\tau. \end{aligned} \tag{1.28}$$

By solving the integral we obtain:

$$\begin{aligned} f_1(x, v, t) = f_1(v, 0)\cos(kx - kvt) \\ + \frac{e}{m}E_0\frac{\partial f(v)}{\partial v}\left[\frac{\cos(kx - \omega t) - \cos(kx - kvt)}{\omega - kv}\right]. \end{aligned} \tag{1.29}$$

Clearly, the resonant condition $v \approx v_\phi = \omega/k$ gives rise to a singularity in the second term of the right-side of the above equation. By taking the Taylor expansion of the numerator around v_ϕ , we get:

$$\begin{aligned} \cos(kx - \omega t) - \cos(kx - kvt) \approx \left(v - \frac{\omega}{k}\right)kt\sin(kx - \omega t) \\ + \frac{1}{2}\left(v - \frac{\omega}{k}\right)^2 k^2t^2\cos(kx - \omega t) + \cdots \end{aligned}$$

Using the last equation in Eq. (1.29) the following expression for the perturbation f_1 is finally found:

$$
\begin{aligned}
f_1(x,v,t) = f_1(v,0)\cos(kx-kvt) \\
+ \frac{e}{m}E_0\frac{\partial f_0(v)}{\partial v} \\
\times \left[t\cdot\sin(kx-\omega t) + \frac{t^2}{2}(\omega-kv)\cos(kx-kvt)\right].
\end{aligned}
\tag{1.30}
$$

Taking the velocity derivative of this equation and retaining only the dominant contribution for large t, we find:

$$
\left[\frac{\partial}{\partial v}f_1(x,v,t)\right]_{v=\omega/k} \approx -\frac{\partial f_0(v)}{\partial v}\left(\frac{eE_0k}{m}\right)\frac{t^2}{2}\cos(kx-\omega t). \tag{1.31}
$$

It is clear from this expression that the condition for the validity of the linear approximation ($|\partial f_1/\partial v| \ll |\partial f_0/\partial v|$) breaks down for

$$
t \approx \sqrt{\frac{m}{ekE_0}} \equiv \tau_{tr}. \tag{1.32}
$$

The diverging term in Eq. (1.31) is associated to the fact that unperturbed orbits, represented by the term $x - vt$ in Eq. (1.30), no longer describes the real dynamics of the resonant electrons for $t > \tau_{tr}$, at least for the case of a single wave.

1.5 O'Neil nonlinear theory

In 1965 T. O'Neil [23] took in consideration the dynamics of trapped particles to get a deeper insight into the nonlinear features of the wave-particle interaction. In his theory the amplitude of electric field is kept constant during the calculation, so it is possible to solve the exact Vlasov equation in the resonant region. Then the changes in amplitudes are obtained as a consequence of conservation of energy. In this way O'Neil extended to the nonlinear case the method used by Dawson [15], who derived the linear damping coefficient by equating the rate of increase of kinetic energy of particles to the rate of decrease of wave energy.

For a system with a spatial periodicity $2\pi/k$ the conservation of energy is expressed as:

$$\frac{d}{dt}\left[\int_{-\pi/k}^{\pi/k}\frac{E^2(x,t)}{8\pi}dx+\int_{-\pi/k}^{\pi/k}dx\int_{-\infty}^{\infty}\frac{mv^2}{2}f(x,v,t)dv\right]=0. \tag{1.33}$$

This is an exact consequence of non-linear Vlasov equation for generic $E(x,t)$ and $f(x,v,t)$. In the case of a monochromatic wave of the type $E(x,t)=E(t)\sin(kx)$, Eq. (1.33) can be written as:

$$\frac{d}{dt}\int_{-\pi/k}^{\pi/k}\frac{E^2(t)}{8\pi}sin^2(kx)dx=-\int_{-\pi/k}^{\pi/k}dx\int_{-\infty}^{\infty}\frac{m}{2}\left(v+\frac{\omega}{k}\right)^2\frac{\partial f}{\partial t}dv \tag{1.34}$$

where the variables are expressed in the wave frame of reference. The last relation can be written as:

$$\frac{d\mathcal{E}(t)}{dt}=-\int_{-\infty}^{\infty}\frac{m}{2}\left(v+\frac{\omega}{k}\right)^2\frac{\partial}{\partial t}<f(v,t)>dv \tag{1.35}$$

where $<f(v,t)>$ is the spatially averaged distribution function:

$$<f(v,t)>=\frac{k}{2\pi}\int_{-\pi/k}^{\pi/k}f(x,v,t)dx \tag{1.36}$$

and $\mathcal{E}(t)$ is the spatially averaged energy density of the electric field:

$$\mathcal{E}(t)=\frac{E^2(t)}{16\pi}. \tag{1.37}$$

To evaluate the term $\partial f/\partial t$, O'Neil found the exact nonlinear solution of Vlasov equation by noting that:

$$\frac{\partial f}{\partial t}+v\frac{\partial f}{\partial x}-\frac{e}{m}E_0\sin(kx)\frac{\partial f}{\partial v}=0 \tag{1.38}$$

just expresses incompressible flow in phase space. In the wave frame the solution can be written as:

$$f(x,v,t) = f[x_0(x,v,t), v_0(x,v,t), 0] \tag{1.39}$$

where $f(x_0, v_0, 0)$ is the initial distribution and (x_0, v_0) are the initial conditions. The evolution of this point is governed by equation:

$$m\ddot{x} = -eE\sin(kx). \tag{1.40}$$

This equation is exactly solvable in terms of elliptic functions. The final result (see Ref. [23] for details) is that the electric field energy density $\mathcal{E}$ is described by the equation:

$$\frac{d\mathcal{E}(t)}{dt} = 2\gamma(t)\mathcal{E}(t) \quad \Rightarrow \quad \mathcal{E}(t) = \mathcal{E}(0)\exp\left[2\int_0^t \gamma(t)dt\right]. \tag{1.41}$$

The expression for the parameter γ is:

$$\gamma(t) = \gamma_L \sum_{n=0}^{\infty} \frac{64}{\pi} \int_0^1 dy \left\{ \frac{2n\pi^2 \sin(\pi n t/yF\tau_{tr})}{y^5 F^2 (1+q^{2n})(1+q^{-2n})} + \frac{(2n+1)\pi^2 y \sin[(2n+1)\pi t/2F\tau_{tr}]}{F^2(1+q^{2n+1})(1+q^{-2n-1})} \right\} \tag{1.42}$$

where F is the elliptic integral of the first kind:

$$F(\beta, z) = \int_0^\beta \frac{dz'}{(1-\beta^2\sin^2 z)^{1/2}} \tag{1.43}$$

and

$$q = \exp(\pi F'/F), \qquad F = F(\alpha, \pi/2), \quad F' = F[(1-\alpha^2)^{1/2}, \pi/2]. \tag{1.44}$$

It is possible to show that the contribution of free-streaming electrons to $\gamma(t)$ is contained in the first term in curly brackets of Eq. (1.42), whereas the second term is associated to trapped particles. For $t \ll \tau_{tr}$ the term with $n = 1$ for free electron dominates and Eq. (1.42) reduces to $\gamma \approx \gamma_L$. For $t \gg \tau_{tr}$, $\gamma(t) \approx 0$, since the integrals over the sine and cosine terms phase mix to zero. Moreover it can be shown that:

$$\int_0^\infty \gamma(t)dt \approx O(\gamma_L \tau_{tr}). \tag{1.45}$$

Since $\mathcal{E}(t) = \mathcal{E}(0)\exp[2\int_0^t \gamma(t)dt]$, it follows that the relative loss of energy is of order of τ_{tr}/τ_L.

In conclusion, according to O'Neil theory, for the case $\gamma_L < 0$, the electric field damps exponentially as depicted in linear theory for $t < \tau_{tr}$. When $t \simeq \tau_{tr}$, the nonlinear effects start playing an important role. As a consequence the electric field amplitude exhibits an oscillatory modulation with a period of order of τ_{tr}. For larger times, $\gamma(t) \to 0$, and the field tends to a constant value, which is $O(\tau_{tr}/\tau_L)$ lower than its initial value. The nonlinear energy exchange between wave and trapped particles supports the wave, preventing the damping (see Fig. 1.3). Obviously the same considerations can be made in the case $\gamma_L > 0$.

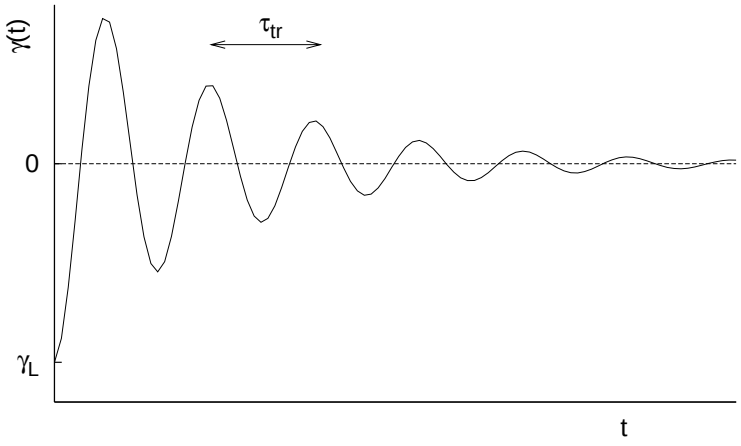

Figure 1.3: Qualitative time behaviour of damping rate $\gamma(t)$.

1.5.1 Physical interpretation

We make now some qualitative considerations about the results seen in the previous section. The physical interpretation may be given in terms of phase space picture.

Let's us first consider the linear theory of collisionless damping. Only those electrons whose velocities are such that $kvt \lesssim 1$ can give a significant contribution to the rate of change of kinetic energy; so, we may focus our attention to those electrons between two trajectories such as A and B in Fig. 1.4. Between these two trajectories, there is a net upward flow along direction 1 and a net downward flow along direction 2. For the case of damping, the initial distribution, plotted out of paper in Fig. 1.4, decreases as a function of velocity. This results in a net increase in the kinetic energy of the resonant electrons and a consequent damping of the wave.

On a nonlinear time scale, the trapped electrons make complete cycles with a period of order τ_{tr}. These electrons carry along the density from their original position and thus cause a cyclic variation in the density at any point. It is this variation in density that causes the oscillatory behaviour of the wave. The fact that $\gamma(t)$ phase mixes to zero as $t \to \infty$ is easily explained in term of ergodic theorem. Consider an initial distribution limited to the small patch of phase space represented by the shaded area in Fig. 1.5. The electrons with energy W have a shorter period than those with energy $W + \Delta W$. So, as

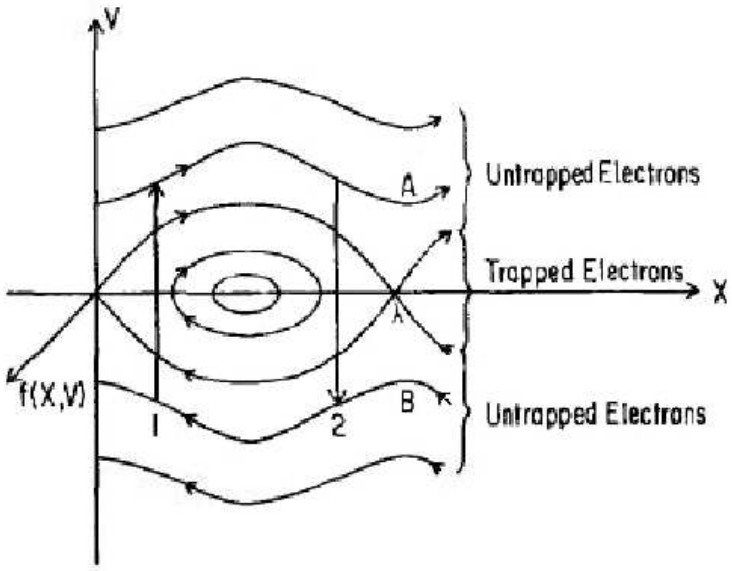

Figure 1.4: Particle orbits in phase space.

times goes by, the shaded area is stretched into a long spiral that fills the area between the two trajectories, W and $W + \Delta W$. Let $\tilde{f}$ be a coarse grain distribution obtained by averaging the actual distribution over the phase elements which are large enough to be traversed by many strands of the spiral. In Ref. [23] it is shown that the coarse grain distribution becomes constant along the trajectories, as $t \to \infty$ and the size of mesh used in the coarse grain distribution goes to zero. Since the coarse grain distribution becomes constant along any phase trajectory, it also becomes constant in time. As the size of the mesh decreases, the integral of any smooth function weighted by the distribution will depend only on the coarse grain distribution. Consequently, $\mathcal{E}$ becomes constant and $\gamma(t) \propto d\mathcal{E}/dt$ approaches zero as t/τ_{tr} approaches infinity.

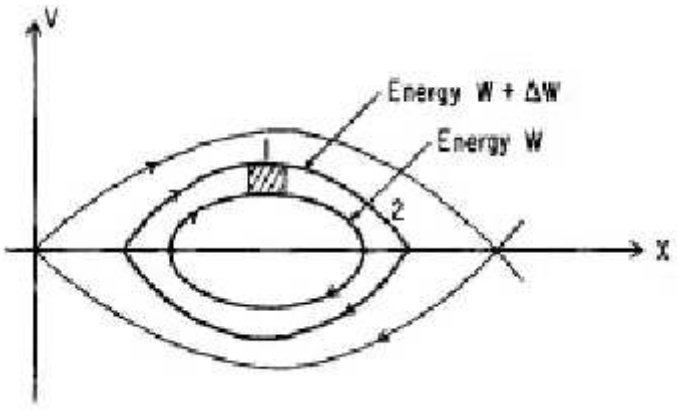

Figure 1.5: Schematic phase space representation

1.6 Numerical study of Landau damping

Today, after nearly 60 years after Landau's discover, the issue of collisionless damping is far from being solved. A satisfactory general quantitative analysis is still lacking, since O'Neil study deals only with a limiting case, namely that in which the trapping effect are so dominant that the amplitude of an isolated wave is approximately constant. At the opposite extreme, the standard linear theory is valid when strong initial Landau damping occurs before the nonlinear effects come into play.

In 1996, Isichenko [24] revisited analytically the nonlinear evolution of electrostatic perturbations. At variance with O'Neil result, he found that, even if nonlinear effects are present, the wave is finally completely damped,

but for long times the decay is algebraic rather than exponential. This conclusion is presented as an exact result, valid for a generic initial electric field, and hence not limited to infinitesimally small perturbations.

The underlying idea of Isichenko theory is that the motion of the resonant particles near the boundary of the resonant region is not simply oscillatory, but it is possible to have a certain number of detrapped particles which escape from the potential well and perform flights in the phase space, which are able, at least in principle, to dissipate the wave energy. Unfortunately, Isichenko made a little confusion in calculating the trajectories of the particles and the electric field, as pointed out from Lancellotti and Dorning [25]. In fact, crucial to Isichenko's analysis is his hypothesis that, as $E \to 0$, each single particle trajectory, which satisfies Newton's equation

$$\ddot{x} = E(x,t) \tag{1.46}$$

tends to a motion with constant velocity $x(a,b,t) = U(a,b)t$, where (a,b) is the initial phase-space point for the orbit and $U(a,b)$ is a constant velocity. But the damping rate resulting from Isichenko's analysis, namely, $E \sim t^{-1}$ as $t \to \infty$, does not justify this affirmation. Integrating Eq. (1.46) once gives the velocity:

$$v(a,b,t) = b + \int_0^\tau E(x(a,b,t),\tau)d\tau \tag{1.47}$$

which tends to a constant value $U(a,b)$ as $t \to \infty$ only if $E(x(a,b,t),t)$ is an *integrable* function of t. However, if $E \sim t^{-1}$ as $t \to \infty$, the function $E(x(a,b,t),t)$ is, in general, not integrable, so that $v(a,b,t)$ does not tend to a constant value, and the following analysis is inconsistent.

In 1998 an analytical study by the same authors [26] contributed to the discussion about the features of the asymptotic evolution of electrostatic perturbations. They focused the attention on the existence of a critical initial amplitude of the wave, below which a complete damping take place. The electric field $E(x,t)$ is represented as the sum of a transient and an asymptotical part $E(x,t) = T(x,t) + A(x,t)$. The Poisson's equation is split in the corresponding transient and asymptotical part. The theory of bifurcation is employed and the result is that, given a family of initial condition $f(x,v,t) = F(v) + h(x,v)$ (where F is the equilibrium solution and h the perturbation) a set of critical initial state exists, which mark the transition

between two different scenarios: the Landau scenario, in which the electric field is definitively damped to zero exponentially in time, as stated in Landau theory, and the O'Neil scenario, in which the electric field reaches an almost constant saturation value. A perturbation $h^0(x,v)$ is critical if $F(v)+h^0(x,v)$ gives rise to a solution in which $A=0$, but arbitrarily close to h^0 there exists another h for which the final result $A \neq 0$ (see Fig. 1.6 for a qualitative picture of this situation).

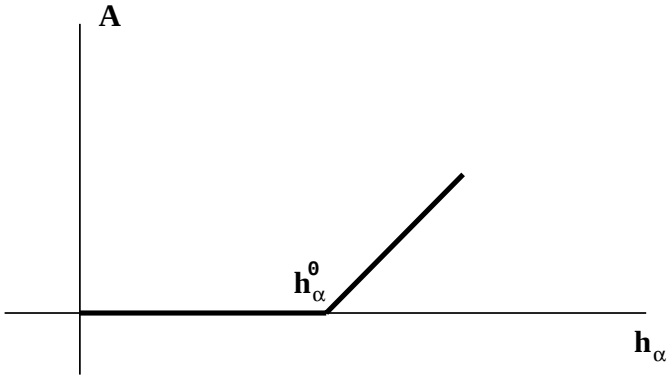

Figure 1.6: Schematic representation of a bifurcation [26]

Wave-particle interaction has been investigated in several kinetic simulations. Oscillations are excited by perturbing the equilibrium distribution function, then the 1D-1V Vlasov-Poisson system of equations, Eqs. (1.1) and (1.4), is integrated. This work is accomplished making use of the so called Vlasov codes, Eulerian codes which solve the Vlasov equation on a uniform mesh in phase space. Starting from the pioneering studies of Cheng *et al.* [27], and thanks to the impressive development of computer power of the last years, Vlasov codes are extensively used to perform high resolution simulations. The results obtained in this way are characterized by an oscillating behaviour of the wave amplitude around an approximately constant value.

Among others, we cite here the works by Manfredi [28] and Pegoraro *et al.* [29], in which the long-time evolution of nonlinear Landau damping is analysed by solving the Vlasov-Poisson system numerically. In the first paper the effects of changing the mesh size and the time steps of the simulations are discussed. Fig. 1.7 reports the evolution of the electric field for three different resolution in phase space [28]. In Ref. [29] the value of the parameter marking the transition between Landau's and O'Neil's regimes is determined and compared with analytical results. It is also shown the ions dynamics is found not to affect these behaviours significantly. Fig. 1.8 shows the spatial Fourier component of the electric field for large times and for a different

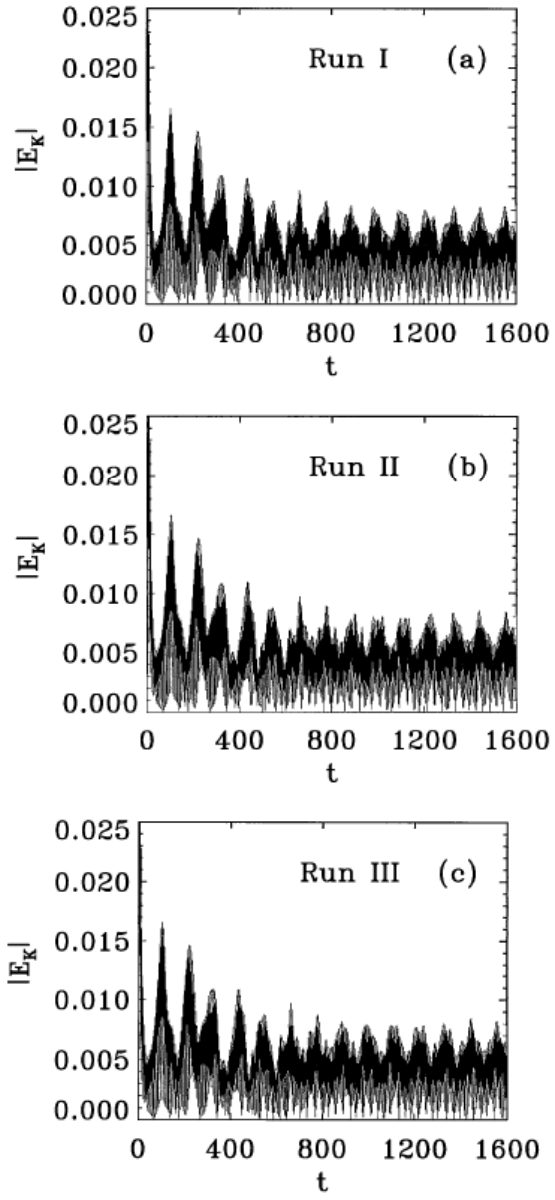

Figure 1.7: Evolution of the amplitude of the electric field. Spatial resolution increases from top to bottom [28].

values of the mesh size. In the figure only the nonlinear part of the evolution is plotted, namely after the damping has stopped.

Valentini *at al* [31] faced Landau damping problem from a different point of view: they studied the Lagrangian trajectories of resonant test-particles in a self-consistent way. Their analysis is based on the integration of the

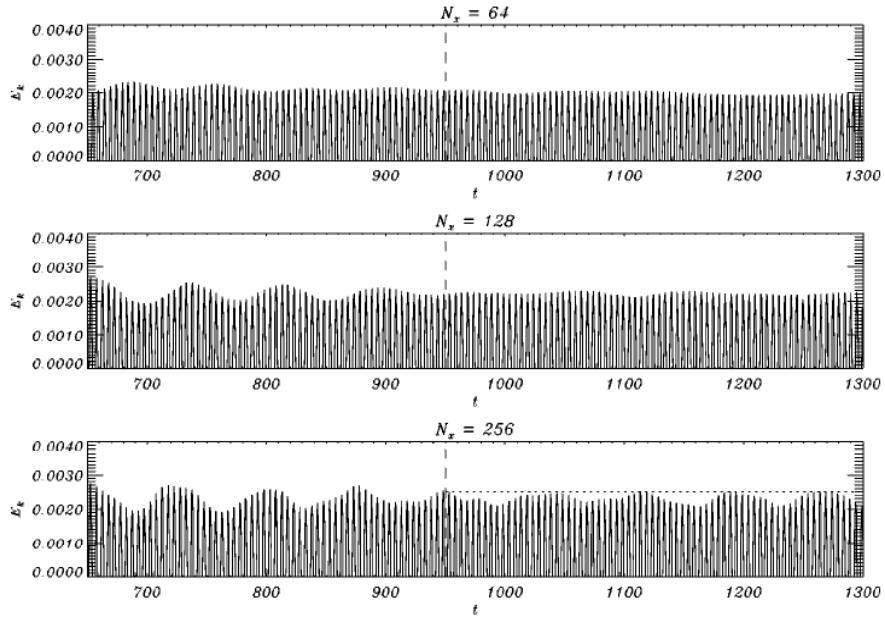

Figure 1.8: Spatial Fourier component of the electric field E_k versus t, for different resolution in the phase space. Resolution increases from top to bottom [29].

equation of motion $\dot{x} = v$ and $\dot{v} = -eE(x,t)/m$ in the phase space, where E is the self-consistent field, calculated by solving numerically the Vlasov-Poisson system. In this way, two kinds of motion have been observed. There are particles that are always trapped in the potential well of the field. They exhibits an oscillatory movement of the order of the wave length, and at every change in the velocity sign they interact with the wave (see top of Fig. 1.9).

The second type of trajectories are relative to particles that are initially trapped, but, as time goes on, they perform long flights in the phase space (a flight is defined as the portion of trajectory between two changes of sign of the velocity in the wave frame) before being retrapped (bottom of Fig. 1.9). The length of these flights is larger than 6-7 wavelengths. In phase space two regions are observed (see Fig. 1.10). One in which the behaviour of particles remain nonergodic and one in which the trajectories diffuse, displaying a chaotic behaviour. This result is affirmed also by the evaluation of Lyapunov exponents, which have a maximum in the zone of the separatrix.

A consequence of these facts is that the pure ballistic motion assumed for detrapped particles in Isichenko's view [24] is ruled out, since, in his investigation, the possibility of Lagrangian chaos and subsequent diffusion-induced retrapping is not considered. On the contrary, the set of self-consistent La-

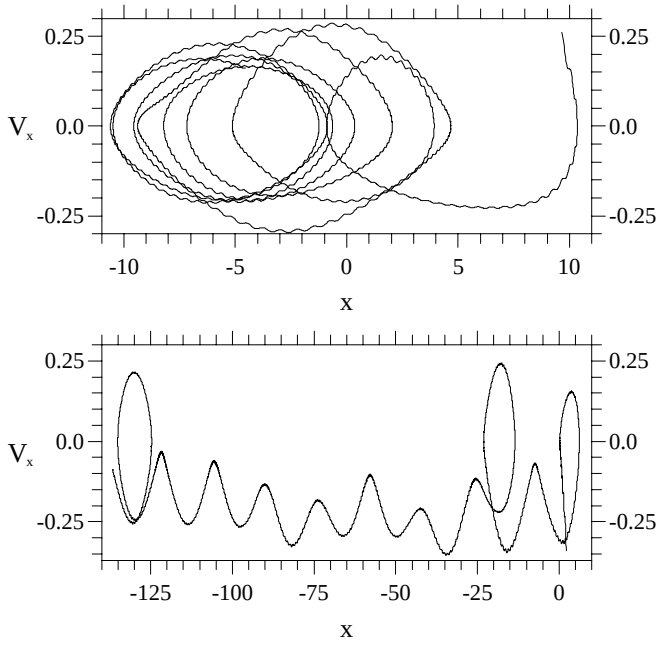

Figure 1.9: Trajectories in the wave reference frame of a trapped particle (top) and one at the edge of the resonant region (bottom) [31].

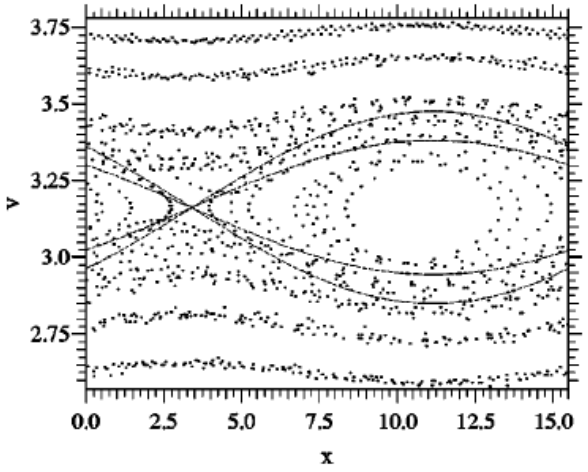

Figure 1.10: Poincaré section in phase space. The continuous line is the separatrix corresponding to the maximum and minimum values of the electric field envelope [31].

grangian equations which describes the motion of the particles is in general nonintegrable, and displays a chaotic behaviour in the region around the separatrix.

A different approach is the one by Firpo et al. [33]. In this work the attention is focused on the localization of chaos in phase space, and the framework of dynamical systems is used. The dynamics of N identical quasiresonant particles moving on the interval of length L with periodic boundary conditions, with unit mass and charge, and, respectively position x_r and momentum p_r, interacting with M waves with wave numbers $k_k = 2\pi j/L$, derives from the Hamiltonian:

$$H = \sum_{l=1}^{N} \frac{p_l^2}{2} + \sum_{j=1}^{M} \omega_{0j} I_j - N^{-1/2} \sum_{l=1}^{N} \sum_{j=1}^{M} \sqrt{2\eta I_j} \times \cos(k_j x_l - \theta_j)$$

where (I_j, θ_j) are the action-angles variables and the small parameter η denotes the ratio of the tail density over the bulk plasma density.
This system is studied in the reduced case in which two particles interact with only one wave. In this case the Hamiltonian in the reference frame of the wave can be written as:

$$H(p,q) = \frac{p_1^2}{2} + \frac{p_2^2}{2} - \sqrt{\eta}(\bar{P} - p_1 - p_2)^{1/2}(\cos q_1 + \cos q_2). \tag{1.48}$$

The wave-particle self-consistency manifests itself through a coupling potential whose strength depends, in a mean field way, on all particle velocities. The self-consistent interaction of two particles and one wave is the simplest non-integrable situation for the model. Nevertheless, by remembering that η is a small parameter, the system is close to integrability: $H_0(p_1, p_2) = p_1^2/2 + p_2^2/2$ is the energy of unperturbed state and the reduction to one-and-a-half degrees of freedom is used.

This study, as the previous one, shows that the regions of strongest chaos develop at the borders to the velocity domain swept by the wave resonance.

1.7 Laboratory experiments

As mentioned in section 1.2, for a lot of time people had doubts on the reality of Landau damping phenomenon. The experiment of Malmberg and Wharton brought clarity on the matter. A more recent experimental analysis is

the one by Danielson *et al.* [34], where waves are excited in a pure electron plasma column. Linear Landau damping and nonlinear wave-particle trapping oscillations are observed with standing plasma waves. For low wave amplitudes, the mode is seen to decay exponentially, (see Fig. 1.11), and the measured linear damping rate agrees quantitatively with linear Landau damping theory. In some case the wave is damped down to thermally excited levels. At larger amplitudes, as the exciting potential V_{exc} is increased, the overall mode decay rate is diminished and oscillations in the amplitude develop, with a frequency that increases as V_{exc} increases. Then a steady state is approached, as predicted by O'Neil.

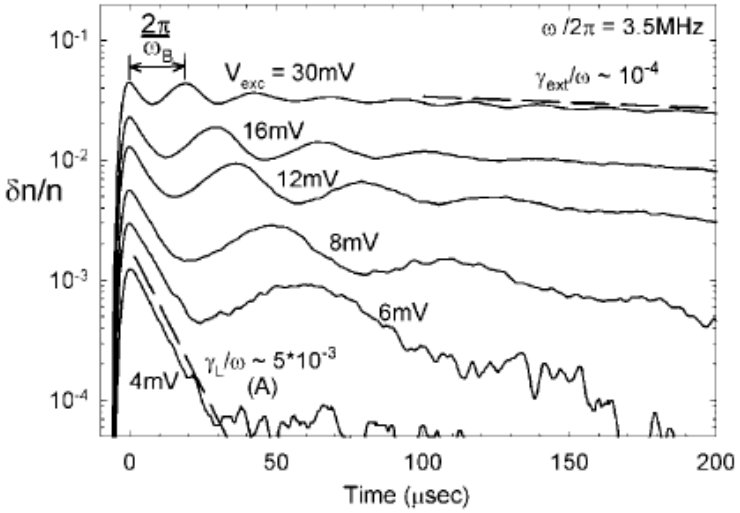

Figure 1.11: Detected amplitude versus time after ten cycle bursts for different exciting potentials V_{exc} [34].

Chapter 2

Dynamical systems

2.1 Introduction: dynamical systems

We have seen in the previous chapter how Landau damping had been investigated analytically in early times, and more recently by mean of kinetic simulations. In the last years the framework of dynamical systems has been successfully employed, especially for investigating chaos in the region where particles are resonant with the wave.

Dynamical systems became quite fashionable after the pioneering review of May [35], who demonstrated their usefulness in many applications. There are two main types of dynamical systems:

1. System of differential equations of the form:

$$\dot{\mathbf{x}} = \mathbf{f}(\mathbf{x},t) \tag{2.1}$$

   where $\mathbf{x} = (x_1, x_2, \ldots, x_N)$ is a N-dimensional vector, and the dot denotes derivative with respect to continuous time t.

2. Maps (or mapping) of the form:

$$\mathbf{x}_{n+1} = \mathbf{f}(\mathbf{x_n}) \tag{2.2}$$

   where $\mathbf{x}_n$ is a vector of N-dimensions $\mathbf{x}_n = (x_{n1}, x_{n2}, \ldots, x_{nN})$, and $\mathbf{f}$ is a set of N functions $(f_1, f_2, \ldots, f_N)$. Maps can be considered as describing the time evolution of a vector $\mathbf{x}$ at a discrete time $t = n$ (integer).

The similarity between maps and systems of differential equations allows the use of very simple maps to illustrate the properties of generic dynamical systems that are described by differential equations, since the calculation of maps is much simpler and faster than the solution of differential equations. For this reason maps have been used extensively in the last decades, especially in order to understand chaos.

The study of dynamical systems is by no means complete, nevertheless in the last 20 years the threads of chaos and nonlinear dynamics have spread across many scientific disciplines.

Dynamical systems display some features which differentiate them and according to which they are studied. The usual classification includes integrable systems, ergodic systems, mixing systems, Kolmogorov and Anosov systems.

There's a certain number of dynamical systems that are rather popular and are widely investigated. As a example we mention the Lorentz system, the logistic map, the double pendulum, the tent map, the Henon and baker's maps.

In this context we will not go into more depth in the study of dynamical systems in general, but rather we will focus our attention on some systems that are particularly interesting for our purposes.

2.2 The standard map

We consider now the situation of a charged particle moving in an electrostatic field due to collective oscillations of a plasma, as the Langmuir oscillations of Landau damping. We will show that this situation is fit to be representable with a map.

Let's assume an electrostatic wave field given by $\mathbf{E}(x,t) = E_x(x,t)\mathbf{x}_0$, with:

$$E_x(x,t) = \sum_{\kappa,\omega} E_{k,\omega} \exp(i\kappa x - i\omega t). \tag{2.3}$$

In the special case where there is only one wavenumber, $\kappa = \pm k_0$, the frequencies ω form a discrete set $\omega = 2\pi n/T$ (where T is the fundamental period and $n = \ldots, -2, -1, 0, 1, 2, \ldots$), and the amplitudes $E_{\kappa,\omega}$ are real and independent of ω and κ, $E_{\kappa,\omega} = E_0/2$, the above expression for E_x reduces to:

$$\begin{aligned} E_x(x,t) &= E_0 \cos(k_0 x) \sum_n \exp(2\pi i n t/T) \\ &= E_0 \cos(k_0 x) \sum_m \delta(t - mT) \end{aligned} \tag{2.4}$$

where $\delta(\ldots)$ denotes the Dirac function. With this expression for the electric field the Hamiltonian of the system composed by wave plus particle is:

$$H(x,p,t) = \frac{p^2}{2m} - \frac{eE_0}{k_0} \sin(k_0 x) \sum_m \delta(t - mT) \tag{2.5}$$

(e is the elementary charge). The times mT indicate the instant in which the particle "collides" with the wave. If we take $m = 1$, $k_0 x = \theta$ and $eE_0/k_0 = K$, the resulting equations of motion are:

$$\frac{dp}{dt} = K \cos\theta \sum_m \delta(t - mT) \tag{2.6}$$

$$\frac{d\theta}{dt} = \frac{p}{m} \tag{2.7}$$

From Eq. (2.6) we see that p_θ is constant between the kicks but changes discontinuously at each kick. In order to obtain the equations of motion in form of a map of the type in Eq. (2.1), let's call p_n and θ_n the values of p_θ and θ at times $t = n\tau + 0^+$, where 0^+ denotes a positive infinitesimal. By integrating Eq. (2.6) through the δ function from $t = n\tau$ to $t = (n+1)\tau$, we get:

$$p_{n+1} - p_n = K \cos(\theta_{n+1}) \tag{2.8}$$

and from Eq. (2.7):

$$\theta_{n+1} - \theta_n = p_n \tau / m \tag{2.9}$$

Without loss of generality we can take $\tau/m = 1$, to obtain the map:

$$p_{n+1} = p_n + K\cos(\theta_{n+1}) \tag{2.10}$$
$$\theta_{n+1} = \theta_n + p_n \tag{2.11}$$

in which we considered $\tau = 1$. This kind of map is known in literature as the standard (or Chirikov-Taylor) map [36]. It is an area-preserving chaotic map from a square with side 2π into itself. Its name is due to the fact that it has become widely used. In the general case, this map describes the motion of the simple mechanical system called the kicked rotor. This is formed by a bar of moment of inertia I and length l, which is fastened at one end to a frictionless pivot. The other end is subjected to a periodic force of impulsive strength K/l applied at times $t = 0, \tau, 2\tau, \ldots$. There is no gravity. Using canonically conjugate variables p_θ (the angular momentum) and θ (the angular position of the rotor), we have the Hamiltonian for this system:

$$H(\theta, p_\theta, t) = \frac{p_\theta^2}{2I} + K\cos\theta \sum_n \delta(t - n\tau). \tag{2.12}$$

With the method described above, and after some simplification, we recover the equation of the map.

Let's now briefly examine the behaviour of the particle by studying the map. By picking a set of initial condition for (θ_0, p_0) one can draw the *orbit* in the phase space, the path followed by the system as it evolves with time. Setting the potential strength to zero, $K = 0$, the standard map becomes:

$$\theta_{n+1} = (\theta_n + p_n) \mod 2\pi \tag{2.13}$$
$$p_{n+1} = p_n \mod 2\pi \tag{2.14}$$

In this case trajectories are just the lines of constant p (Fig. 2.1). This is true whatever the initial condition. We are reproducing now the case of the free particle. On each line the orbit is given by $\theta_n = (\theta_0 + np)$ modulo 2π and if $p_0/2\pi$ is an irrational number, a single orbit densely fills the line $p = p_0$. If $p_0/2\pi$ is a rational number, then orbits on the line return to themselves after a finite number of iterates. Increasing K slightly from zero (these cases

are represented from Fig. 2.2 to Fig. 2.4) introduces small perturbation to the orbit, the velocity of the particle is no more constant since now there is an electric field. In this case, particles differentiate according to the initial condition. If this is on an invariant torus the trajectory traces out the closed curve corresponding to the torus, i.e. the particle is trapped. If the initial condition yields a chaotic orbit, then it will wander throughout an area densely filling that area.

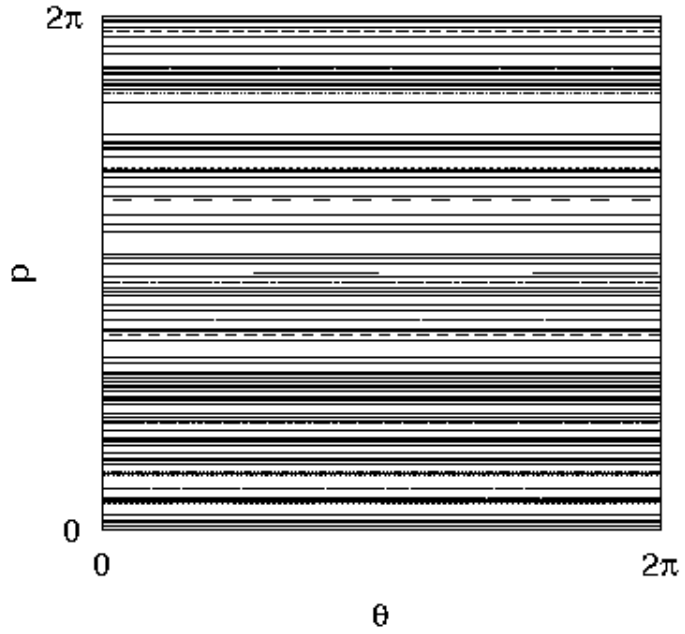

Figure 2.1: Plots of (θ, p) modulo 2π for the map in Eq. (2.11) for $K = 0$.

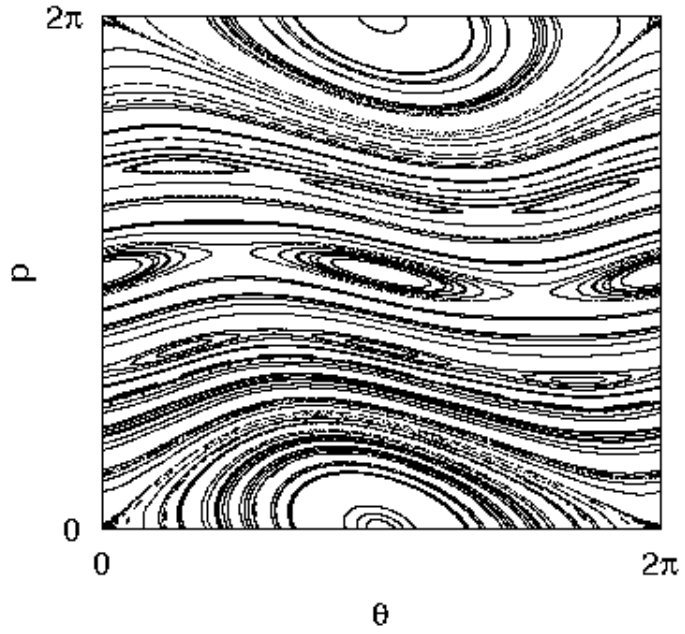

Figure 2.2: Plots of (θ, p) modulo 2π for the map in Eq. (2.11) for $K = 0.5$.

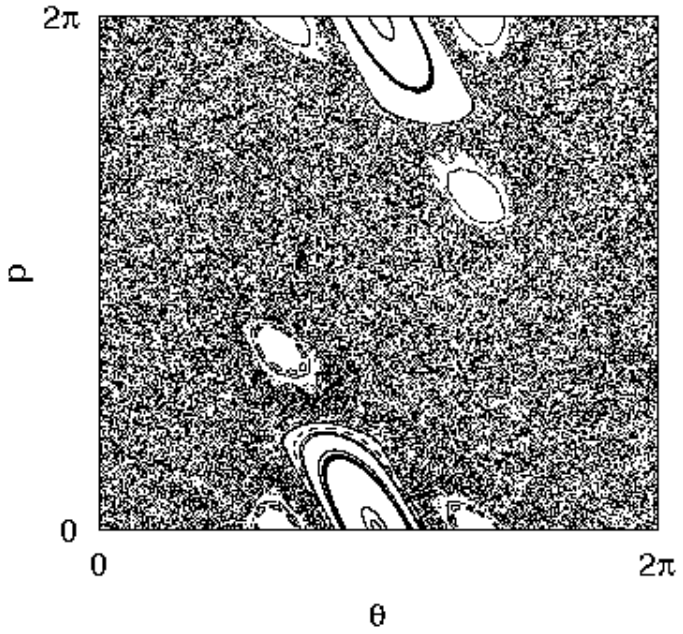

Figure 2.3: Plots of (θ, p) modulo 2π for the map in Eq. (2.11) for $K = 2.5$.

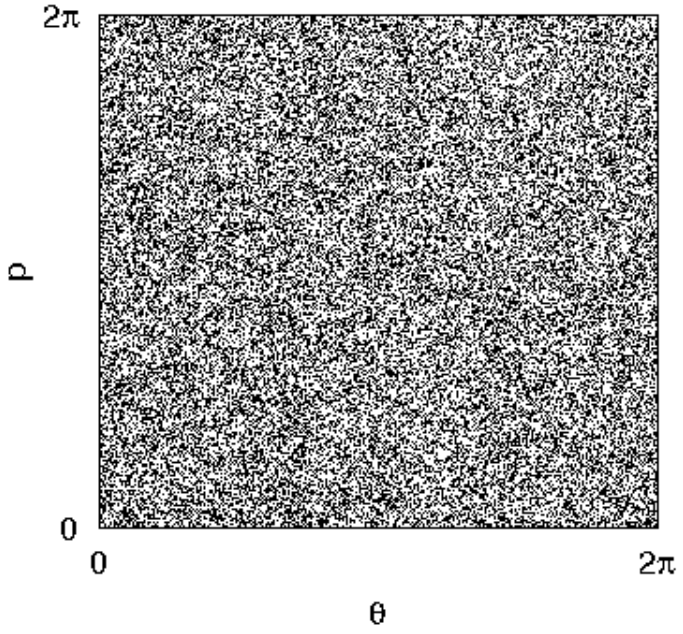

Figure 2.4: Plots of (θ, p) modulo 2π for the map in Eq. (2.11) for $K = 8$.

2.3 The Fermi accelerator model

Another model that deals with the acceleration of particles is the Fermi accelerator model. It belongs to a particular type of dynamical system called *billiards*. They appear as natural models in many problems of optics, acoustics and classical mechanics. Billiards are Hamiltonian models that make use of perfectly elastic collisions of an object with either boundary walls or with other objects. If the confining region is rectangular or circular, then it turns out that all the orbits are periodic or quasi-periodic. However, if the boundary is shaped like a stadium (Fig. 2.5), with straight side walls and semi-circular ends, or if a round obstacle is placed inside a rectangular boundary (Sinai billiard, Fig. 2.6), then the motion can be chaotic, at least for some trajectories.

In 1949 Fermi [37] proposed an acceleration mechanism of cosmic ray particles interacting with a time dependent magnetic fields. It was designed to answer to the fundamental question if a particle, in a classical system that gives/takes energy to it, can have unlimited gain of energy. Since its first appearance, different versions of the problem (simplifications, gravity, external fields, dissipation, quantum and relativistic effects) have been the subjects of extensive theoretical and experimental studies, as they are simple to conceive but hard to understand in that their behaviour is quite complex (see e.g. Ref. [38] and references therein). One of these versions is the well known Fermi-Ulam model (FUM) [39]. The FUM consists of a particle confined between two rigid walls, one of them is fixed and the other is moving periodically in time (a representation of this situation is given in Fig. 2.7). The particle collides elastically with the walls and moves freely between impacts.

To be definite consider a particle of mass m and two parallel walls, one of them is fixed at the origin ($X = 0$) and the other is moving periodically in time. The position of oscillating wall is given by

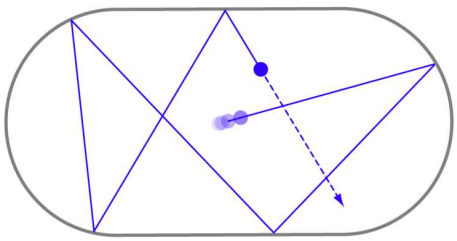

Figure 2.5: The Bunimovich stadium: it was designed to show that the orbits beyond the focusing point of a concave region exhibit exponential divergence.

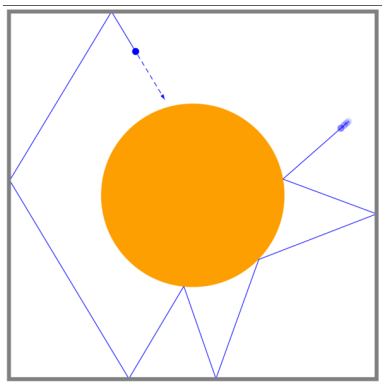

Figure 2.6: The Sinai billiard: its result is that a gas of two hard balls is strongly ergodic.

$$X_W(t') = X_0 + \epsilon' \cos(\omega t' + \phi_0) \tag{2.15}$$

where X_0 is the equilibrium position, ϵ' is the amplitude of oscillation, t' is the time, ω is a frequency and ϕ_0 is the initial phase.

We now construct the map. Consider the situation just after a collision with the moving wall. In order to define the instant of the next collision with this wall, it is useful to distinguish between two different cases:

1. The particle undergoes a collision with the fixed wall before hitting the oscillating wall again.

2. The particle has successive impacts with the moving wall.

In the first case, the particle leaves the moving wall at time $t_0 = 0$ from

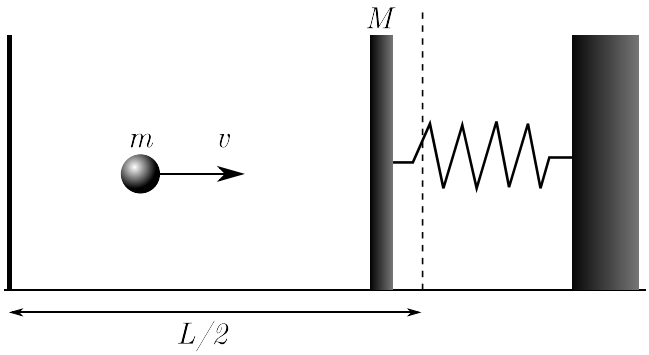

Figure 2.7: Cartoon of the Fermi-Ulam model.

the point $x(0) = x_W(0) = 1 + \epsilon\cos\phi_0$ with velocity $\mathbf{v}_0 = -v_0\mathbf{i}$ (we have chosen v_0 to be positive in the direction of the inner normal of the oscillating wall). It hits the fixed wall, rebounds with velocity $\mathbf{v}_b = v_0\mathbf{i}$ and then hits again the oscillating wall at time t_1 given (implicitly) by:

$$v_0 t_1 - (1 + \epsilon\cos\phi_0) = 1 + \epsilon\cos(t_1 + \phi_0). \tag{2.16}$$

The velocity $\mathbf{v}_1 = -v_1\mathbf{i}$ of the particle after the new impact with the oscillating wall can be easily found, performing the calculations in a referential frame in which the wall is instantaneously at rest. In this frame the velocity of the particle just before the collision is $\mathbf{v}'_b = \mathbf{v}_b - \mathbf{v}_W(t_1)$, where $\mathbf{v}_W = -\epsilon\sin(t_1 + \phi_0)\mathbf{i}$ is the moving wall velocity. After the collision we have that $\mathbf{v}'_a = -\mathbf{v}'_b$. Since $\mathbf{v}_a = -\mathbf{v}'_b + \mathbf{v}_W(t_1)$ we obtain that $\mathbf{v}_1 = 2v_W(t_1) - \mathbf{v}_b = -[2\epsilon\sin(t_1 + \phi_0) + v_0]\mathbf{i}$. In the second case, the time t_1 for the second collision with the oscillating wall is determined by:

$$1 + \epsilon\cos\phi_0 - v_0 t_1 = 1 + \epsilon\cos(t_1 + \phi_0) \tag{2.17}$$

and the velocity after the impact is given by $\mathbf{v}_1 = 2\mathbf{v}_W(t_1) + v_0\mathbf{i}$. Note that Eqs. (2.16) and (2.17) can have more than one solution and that t_1 is given by the smallest positive solution. The map that describes the system can be written as

$$v_{n+1} = \pm v_n + 2\epsilon\sin\phi_{n+1} \tag{2.18}$$

$$\phi_{n+1} = \phi_n + t_{n+1} \mod 2\pi \tag{2.19}$$

where $\Delta t_{n+1} = t_{n+1} - t_n$ is given by the smallest positive solution of

$$v_n\Delta t_{n+1} - (1 + \epsilon\cos\phi_n) = \pm(1 + \epsilon\cos(\Delta t_{n+1} + \phi_n)). \tag{2.20}$$

The plus sign in equations above corresponds to case 1 and the minus sign to case 2. Note that Eq. (2.20) should be solved numerically.

A standard simplification widely used in literature is the Simplified Fermi Ulam model [40] (SFUM), in which the oscillating wall keeps a fixed position $x_W = 1$ but, when the particle suffers a collision with it, the particles exchanges momentum and energy as if the wall were moving. This simplification carries the huge advantage of speeding up numerical time-consuming simulations. The map for the simplified model can be written as:

$$v_{n+1} = |v_n - 2\epsilon \sin(\phi_{n+1})| \tag{2.21}$$
$$\phi_{n+1} = \phi_n + 2/v_n \mod 2\pi \tag{2.22}$$

The modulus in the equation of the velocity was introduced artificially in order to prevent the particle leaving the region between the walls.

Maps of the kind described so far may outline, to some extent, the movement of a particle in a field. Anyway, even though collisions with the wave are present, with the term $\delta(t - mT)$ in Eq. (2.5) for the standard map and the collision with the wall in the Fermi model, and the particle changes its velocity as stated by the equations of motions, there is no feedback on the wave itself: the forcing term is always the same. Moreover the maps are written for a single particle at a time. For these reasons these maps may only represent a starting point for a more complex model, that takes into account the behaviour of the particles as well as the evolution of the wave.

The map we are going to introduce and study in the continuation of this work has been formulated on the basis of the simplified Fermi model described above.

2.4 The Simplified Fermi Ulam model: a first generalization

A first generalization of the SFUM can be made by thinking walls with length that changes in time with a given law. So let's consider the following situation, illustrated in Fig. 2.8. The billiard is composed by two vertical rigid walls set at a certain distance L, fixed once and for all. In a Cartesian frame of reference, without loss of generality, walls are placed at $x = -1$ and $x = 1$, so that $L = 2$. They have infinite mass. The walls length $A(t)$ changes in time. To be definite, with reference to the picture in Fig. 2.8, points A and B are fixed, but point C and D change their position according to the law:

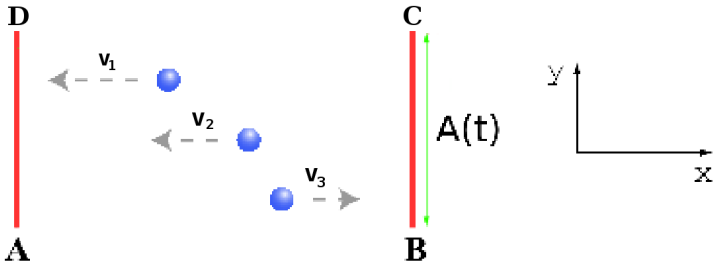

Figure 2.8: Cartoon of the billiard used for the map.

$$A(t) = A_0|\cos(\omega t)|. \tag{2.23}$$

A particle moves between the walls and suffers elastic collisions with them. The particle is identified by its random initial position x_0 and by a constant velocity u, which may only change sign. We assume that the y coordinate is equal to the square velocity:

$$y = u^2. \tag{2.24}$$

The velocity u of the particle, the amplitude A_0, and the frequency ω are assigned quantities. When a particle arrives to a barrier, since the altitude of the upper end of the wall changes in time, the particle can undergo to two different situations:

- $y_n > A_0|\cos(\omega t_n)|$;
- $y_n \leq A_0|\cos(\omega t_n)|$;

where with t_n we indicate the time t at which the n-th collision happens. In the first case the particle overtakes the barrier and, if we consider the system as made by periodic boxes, it enters, with velocity unchanged, the next box. In the second case the particle simply reflects back.

We want to check the frequency of collisions of the particle with walls with the variation of u and ω. Obviously we expect to find a correlation between the altitude of the particle and the possibility of escape from the trap. The upper part of Fig. 2.9 reports the sign of the velocity as a function of the number of iterations for a particle with speed $u = 0.94$ ($y = 0.88$), and for four different value of the frequency ω. If we call $\Omega = 2\pi u/L$ the period of oscillation of a particle in the trap, we see that the dynamics is

different according to the ratio $r = \omega/\Omega$. If $r \ll 1$ or $r \gg 1$, intermittency can be noted: the particle switches between two states characterized by long flights with the same sign of the speed, interrupted by brief intervals of fast inversions. In the case $r \approx 1$ particle and walls are in a kind of resonance, and the particle gets to the barrier when this has more or less always the same altitude. In Fig. 2.9 on the bottom, the particle has velocity $u = 0.6$ ($y = 0.36$) and the situation is very different. Since this particle lies lower then the previous one, the probability to get trapped is greater. This is shown in the frequent inversion in the sign of the velocity. No more long flights are observed and also the frequency of oscillation of the walls makes no important differences.

Differently, we can choose the frequency of oscillation ω as fixed and perform the test with particles with different velocities. In this case we have the situation sketched on Fig. 2.10. As we can see from the figure, as velocity increases, the flights of the particle become longer.

2.5 Conclusions

This model describes in a very simplistic way, the interaction between a particle and a wave which oscillates with frequency ω, the process being schematized as a sequence of collisions. We have seen that the behaviour of the particle is not trivial. It can perform more or less long flights, during which the velocity does not change sign. The spatial extent of these flights varies according to the ratio between the bounce frequency Ω and the oscillation frequency ω. In the situation in which these two frequencies are comparable, a little perturbation could induce a chaotic behaviour of the particle. These considerations could be very interesting from the point of view of the theory of dynamical systems. However they go beyond the scope of the present work.

In the next chapter we will deal with the discussion of the selfconsistent model.

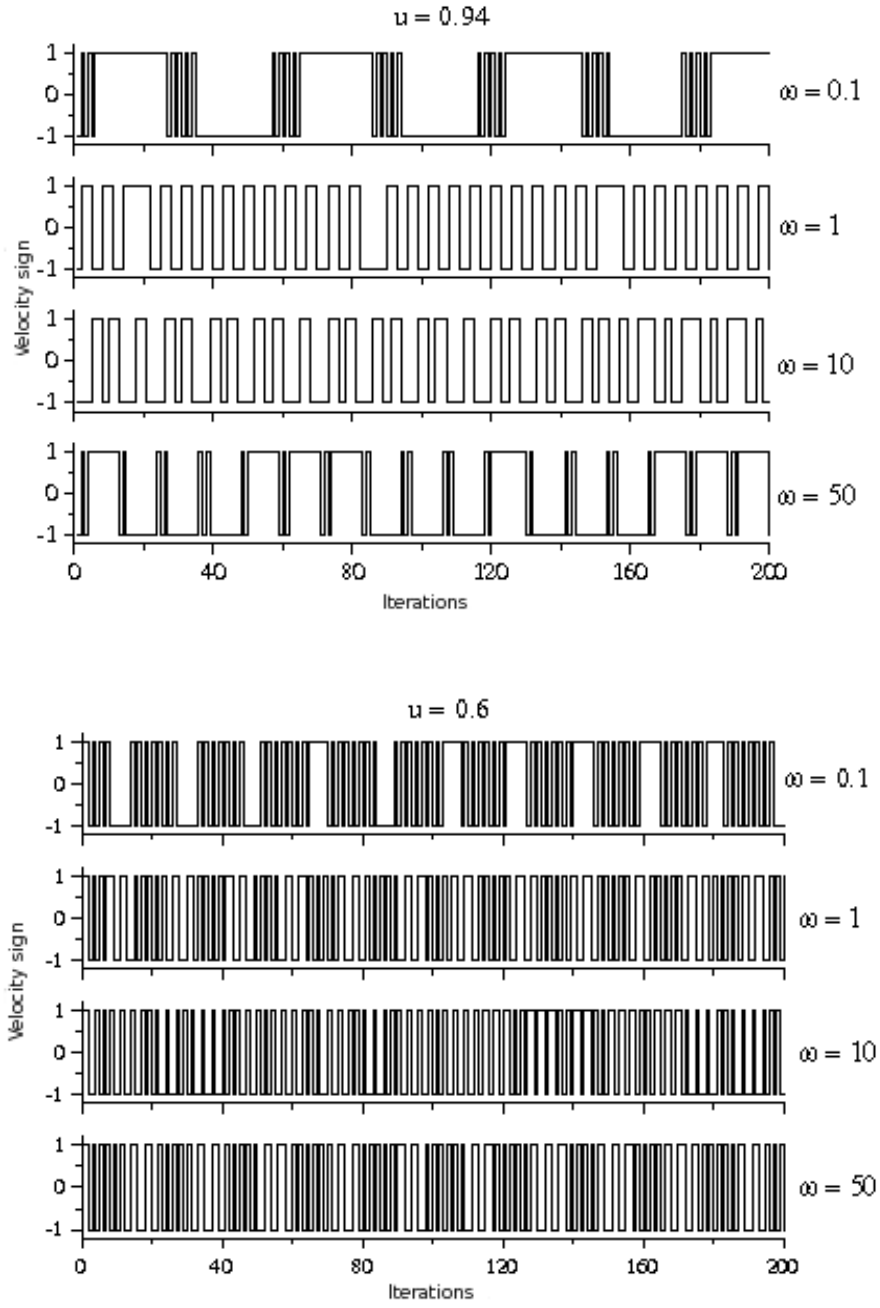

Figure 2.9: Changes in the velocity sign for two particles with velocity $u = 0.94$ (top) and $u = 0.6$ (bottom) and different pulsations indicated in figure.

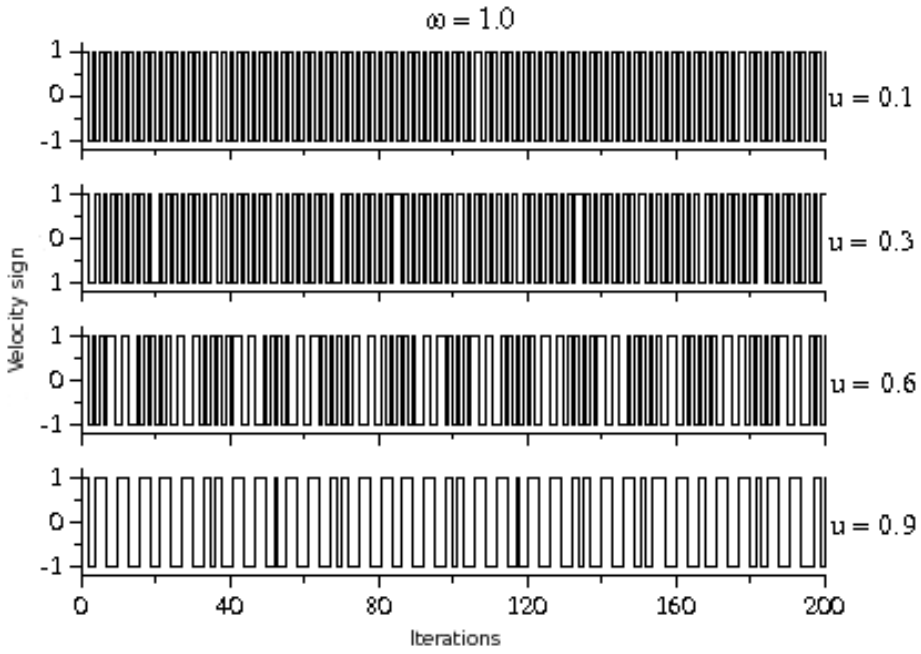

Figure 2.10: Changes in the velocity sign for four different particles trapped in a time dependent square potential well. Particle velocities are reported on figure.

Chapter 3

The modified Fermi model

3.1 Introduction

In the previous chapter we briefly discussed a modification of the Simplified Fermi Ulam model, in the sense that the length of the walls were considered as oscillating with a frequency that can be chosen equal to, for example, that resulting from analytical or numerical calculations. However, such a model, still doesn't present any feedback on the wave. Moreover it considers only a single particle. In order to depict the time evolution of the wave as well as collective phenomena involving all the particles we introduce a further generalization of the SFUM. As the latter is a system composed by only one particle, our *modified Fermi model* [41] regards many particles and considers changes in the term representing the potential. The model schematizes the basic mechanism of Landau damping, that is, the exchange of energy between wave and particles, by mean of a system in which a certain number of test-particles, with a defined kinetic energy, moves between two walls, whose length is proportional to the amplitude of the wave. The exchange of energy between particles and walls will modify the length of the walls themselves. Following this dynamics we are able to recover all the phenomenology of Landau damping.

3.2 The poor man's Landau damping model

The billiard that we are going to study is still that shown in Fig. 2.8. As the one described in sec. 2.4, it is composed by two vertical, rigid, infinitely heavy walls, placed at $x = \pm 1$ so that the distance between them is $L = 2$. The length of the walls $A(t)$, i.e. the length of the segment AD and BC in the picture, represents the amplitude of the wave (we will refer to it as

the "amplitude" in the following). At variance with the model previously described, it does not vary with a predefined law, but rather it can change according to the dynamical state of the particle that, from time to time, hits the wall. At every instant of time we identify the energy of the wave E_W as proportional to the squared amplitudes of the barriers:

$$E_W(t) = [A(t)]^2. \tag{3.1}$$

Between the walls N particles are placed. These particles move back and forth in the x-direction. Each particle is identified by an initial position $x_j(0)$ in the range $[-1 : 1]$ and a velocity v_j $(j = 1, 2, \ldots, N)$. The whole system travels horizontally with constant speed v_p with respect to an inertial frame of reference, so that the quantities v_j are to be referred to the frame of reference of the barriers. We can identify the quantity v_p as the wave phase velocity. As before, we assume that the position y_j is given by the squared velocity, $y_j = v_j^2$. In the frame of reference of the barriers, each elastic collision of a particle with a wall will reverse the direction of motion of the particle, so we have:

$$v_a = -v_b \tag{3.2}$$

(v_b and v_a are the speeds before and after the collision). In the reference frame at rest, where the system has velocity v_p we have:

$$v_{bR} = v_b + v_p \tag{3.3}$$
$$v_{aR} = v_a + v_p \tag{3.4}$$

where the he subscript R indicates the quantities measured in the rest frame. By substituting Eq. (3.2) in Eq. (3.4) we have:

$$v_{aR} = -v_b + v_p. \tag{3.5}$$

We define the amount of energy gained or lost by the particle in collision as:

$$\Delta E = v_{aR}^2 - v_{bR}^2 = (-v_b + v_p)^2 - (v_b + v_p)^2 = -4v_b v_p. \tag{3.6}$$

For the conservation of energy, ΔE is assigned (with opposite sign) to the energy, and thus to the amplitude, of the barriers. However, since our aim is to simulate the interaction of a gas of particles with a wave, the quantity ΔE has to be referred to all particles. In other words, we require that the energy exchanged by a single particle in collision is proportional to $1/N$, so that the energy exchanged by a single particle is:

$$\Delta E = \frac{4vv_p}{N} \tag{3.7}$$

and the amplitude, at the time t' after a collision is

$$A(t') = [E(t) + \sigma(t)|\Delta E|]^{1/2} \tag{3.8}$$

where $\sigma(t) = vv_p/|vv_p|$ and t is a time before the collision. According to the phenomenology of Landau damping, the increase or decrease of the amplitude at a given time, depends on the relative sign $\sigma(t)$ between v and v_p. Particles with velocity lower than v_p ($v_j < 0$ in the frame of the barriers) cause a decreasing of the amplitude of the barriers (ΔE is negative), and this is equivalent, in our rough approximation of Landau damping, to taking energy from the wave. On the contrary, particles with velocity greater than v_p ($v_j > 0$) raise the barriers, thus giving energy to the wave.

3.3 Map and numerical algorithm

We derive now the dynamical map that describes the system.

The velocities v_j ($j = 1, 2, \ldots, N$) of the particles are constant in modulus, consequently the positions $x_j(t)$ are easy to calculate:

$$x_j(t) = x_j(t_0) + v_j(t - t_0) \tag{3.9}$$

where t_0 is the initial time. It is possible to write a recurrence relation with

non constant time steps, identified by the index n. For each particle we consider the time interval $\Delta t_j^{(n)}$ it requires to reach the wall towards which it is directed, at the step n. We select the minimum of this intervals, say that of the k-th particle. This means that after a time $\Delta t_k^{(n)} = \min_j\{\Delta t_j^{(n)}\}$ the k-th particle will reach the barrier (formally identified by the sign $\sigma_k^{(n)}$ of the velocity of that particle, i.e. $x_k(t + \Delta t_k^{(n)}) = \sigma_k^{(n)}$). Since the amplitude of the walls can vary in time, two different situations may occur, namely the height of the particle can be either below ($y_k^{(n)} < A_n$) or above ($y_k^{(n)} > A_n$) the current amplitude of the barriers. In the first case a collision will take place, so:

1. the position of the k-th particle is advanced to the position of the barrier;

2. the motion of the particle is reversed;

3. the amplitude of the barriers is changed accordingly.

The discrete dynamics of the collision can be written as:

$$\begin{aligned} x_k^{(n+1)} &= \sigma_k^{(n)} \\ \sigma_k^{(n+1)} &= -\sigma_k^{(n)} \\ A_{n+1} &= \sqrt{A_n^2 + \Delta E_k^{(n)}} \end{aligned} \tag{3.10}$$

where $\Delta E_k^{(n)} = \sigma_k^{(n)}(4|v_k|v_p/N)$ is the normalized energy exchanged during a single collision. A picture of a collision with $\sigma > 0$ is reported in Fig. 3.1, whereas Fig. 3.2 represents the case of collision of a particle with $\sigma < 0$.

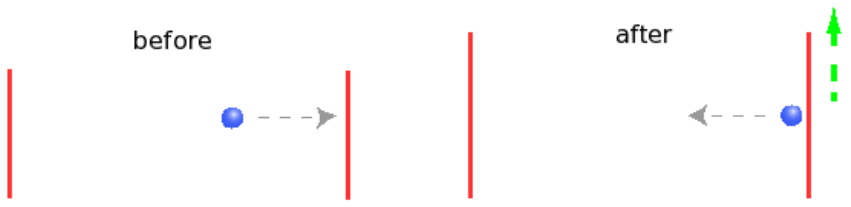

Figure 3.1: The modified Fermi model: representation of the dynamics in case of a collision of a particle with positive velocity (faster than the walls in the frame at rest). After the collision the length of the barriers increases.

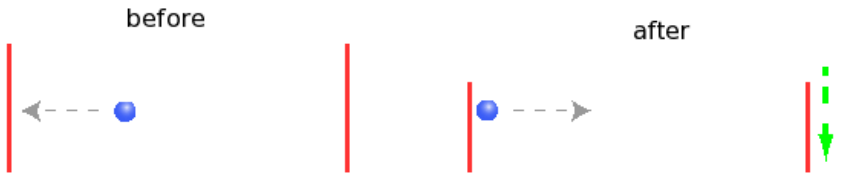

Figure 3.2: The modified Fermi model: representation of the dynamics in case of a collision of a particle with negative velocity (slower than the walls in the frame at rest). After the collision the length of the barriers decreases.

In the second case, namely if the height of the particle is above the oscillating extremities of the walls, the particle undisturbed continues its flight, thus:

1. the particle goes out from the box. But, since periodic boundary conditions are imposed on the numerical domain, this is equivalent to enter the same box from the opposite wall (in Fig. 3.3 a picture of this situation is given). In other words, the particle is placed at the position of the opposite barrier. It is worth noting that this solution preserves the number of particles;

2. the sign of the velocity of the particle remains unchanged;

3. the amplitude of the barriers remains unchanged.

The map in the case in which no collision takes place is:

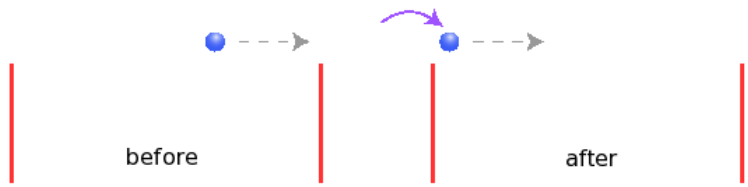

Figure 3.3: The modified Fermi model: representation of the dynamics in case of no collision. The particles enter the next box and the amplitude does not change.

$$\begin{aligned} x_k^{(n+1)} &= -\sigma_k^{(n)} \\ \sigma_k^{(n+1)} &= \sigma_k^{(n)} \\ A_{n+1} &= A_n. \end{aligned} \tag{3.11}$$

As a final step, in either cases, the positions of the remaining $N-1$ particles are advanced, viz:

$$x_j^{(n+1)} = x_j^{(n)} + v_j \Delta t_k^{(n)} \qquad (j \neq k). \tag{3.12}$$

3.4 Monte Carlo simulations

The map shown in the previous section is used to carry out numerical simulations. A particular attention has to be devoted to the distribution of particle velocities. Since Landau damping just depends on how the particles are distributed in velocity space, we have to chose an apt initial distribution function for the v's. We have seen that the driving process for Landau damping is the interaction of the electrostatic waves in the plasma with the particles at nearly resonant velocities. The non-resonant particles (the "bulk" as they are often called) participate with the dynamics via the small subset of collective Langmuir modes. We need to count in the model only the resonant region. This can be achieved by considering a Maxwellian distribution function with 0 mean and width $v_{th} = 1$, and take into account only the particles in an interval of size 2Δ around v_p, where the curve can be linearized. Then, in order to handle appropriate variables for a dynamical model we consider $\Delta = 1$. We refer to this new "normalized" velocities with u_j.

For each run, the free parameters have to be chosen. We have seen that the particles are scattered in the box with random x in $[-1:1]$ and $y = u^2$. Limits on velocity are found by imposing that, almost initially, no particle lies above the barriers (note that this condition is not necessary, since, as it can be inferred from the continuation, a particle that lies above the initial length of the walls will never interact with them). If the initial amplitude of the walls is A_0, velocities are distributed in the interval $[-\sqrt{A_0} : \sqrt{A_0}]$, with a distribution function of the form:

$$f(u) = a - bu, \quad b = \frac{u_p}{2\pi} \exp\left(-u_p^2/2\right) \tag{3.13}$$

where b is proportional to the derivative of a Maxwellian, and a given by the normalization conditions. Given the free parameters of the problem, namely the initial amplitude of the walls A_0 and the "phase velocity" u_p, the behaviour of the amplitude as a function of the step n can be obtained. Clearly, since each step n is determined by the instant of time in which a particle hits the barrier, this describes the time behaviour of our system.

The typical simulation is accomplished with $N = 10^5$ particles. This number seems to represent the right middle-way between good statistics and acceptable computational times. [1]

Fig. 3.4 reports the time evolution of the amplitude for $A_0 = 1$ and two values of u_p, namely $u_p = 1.4$ and $u_p = 1.8$, while Fig. 3.5 shows the evolution of the amplitude for $N = 800000$ and $N = 150000$ particles. As it can be seen in the latter picture, there are no important differences between the two graphs, despite the number of particles being very different. Clearly, computational times in the second case are shorter.

Looking at the plots, although some parameters are varied, some common characteristics can be noticed. For short times the amplitude of the barriers rapidly decreases from its initial value A_0 to a minimum value A_{min}. We refer to this stage as the *linear stage*.

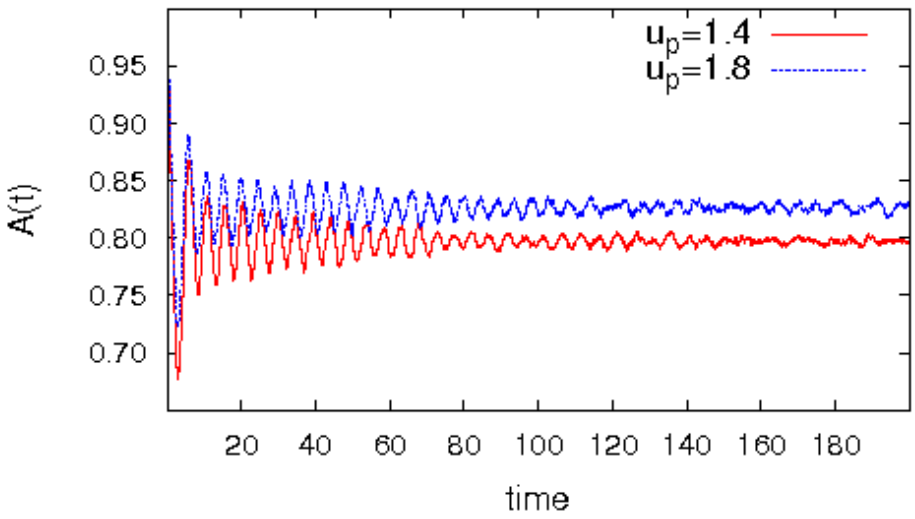

Figure 3.4: The behaviour of the amplitude of the wall in function of time for $N = 10^5$, initial amplitude $A_0 = 1$ and for $u_p = 1.4$ and $u_p = 1.8$.

[1] For a typical simulation with $N = 10^5$ particles and up to $t = 200$, on a computer with processor AMD Athlon(tm) 64 3200+, at 2.2 GHz and 1 Gb of memory, the computational time is less than one hour.

Later, in the *nonlinear stage*, the wave oscillates in a regular way around a constant saturation value of the amplitude, that we will indicate as A_{sat}. In the end, for long times, oscillations around A_{sat} change, becoming irregular and characterized by a lower amplitude. This is the *asymptotical stage*. We analyse now in detail these three stages.

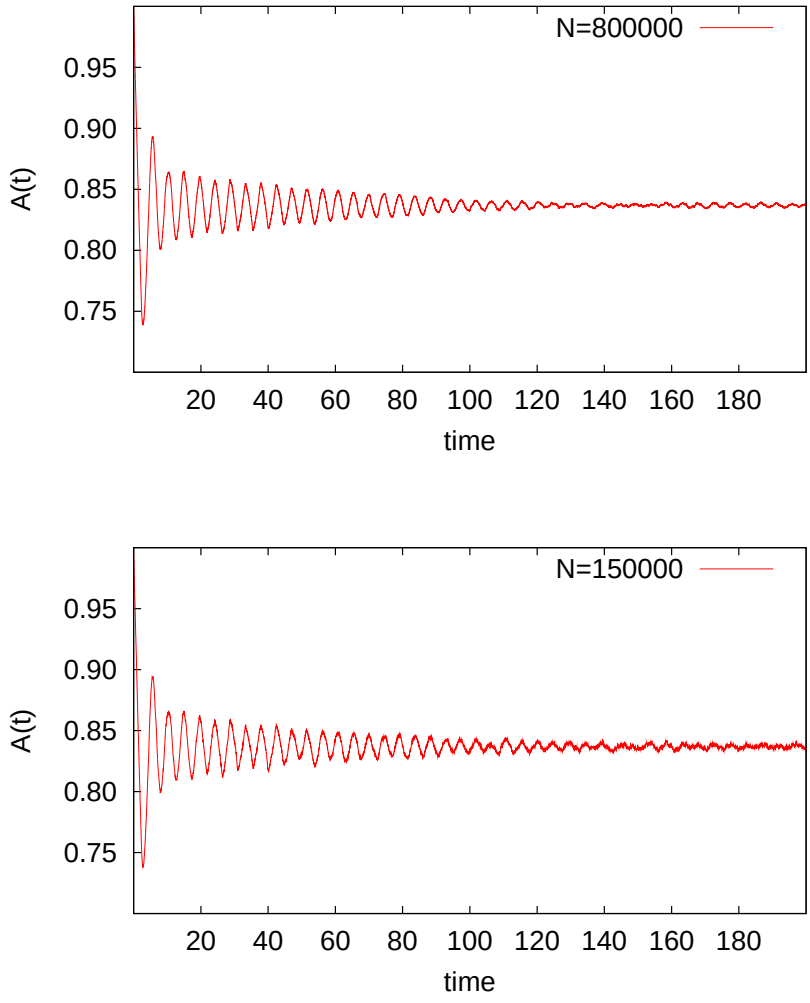

Figure 3.5: The behaviour of the amplitude of the walls in function of time for $N = 800000$ and $N = 150000$ particles, and for $A_0 = 1$ and $u_p = 1$.

3.5 Time behaviour of the wave

3.5.1 Linear stage

In Fig. 3.4, we see that for $t \lesssim 2$ the amplitude of the barriers rapidly decreases from its initial value A_0 to a minimum value A_{min}. A temporal window of the signal of Fig. 3.4 which highlight this stage is reported in Fig. 3.6. In this regime, the trapping phenomenon is not yet at work, and the bulk of particles has a single collision. We can say that this stage is the Landau (or linear) scenario.

An exponential function of the type $A_0 \exp(-\gamma^{exp} t)$ fits the data in the time range $0 < t < 2$, where γ^{exp} means that the rate derives from the experimental data set for each value of u_p. This rate can be compared to the theoretical one. An expression for the theoretical damping rate γ^{th} expected from our model, can be inferred by conjecturing that the time variation of energy is proportional to the energy exchanged in a single collision divided by a typical bounce time $\Delta t = L/|u|$ and then integrated over the whole of the particles:

$$\begin{aligned} \frac{dE_w}{dt} &= \int_{-\sqrt{A_0}}^{\sqrt{A_0}} \frac{\Delta E}{\Delta t} f(u) du \\ &= \int_{-\sqrt{A_0}}^{\sqrt{A_0}} \frac{4uu_p}{L/|u|} f(u) du \\ &= \int_{-\sqrt{A_0}}^{\sqrt{A_0}} 4u_p u|u| f(u) du \end{aligned} \tag{3.14}$$

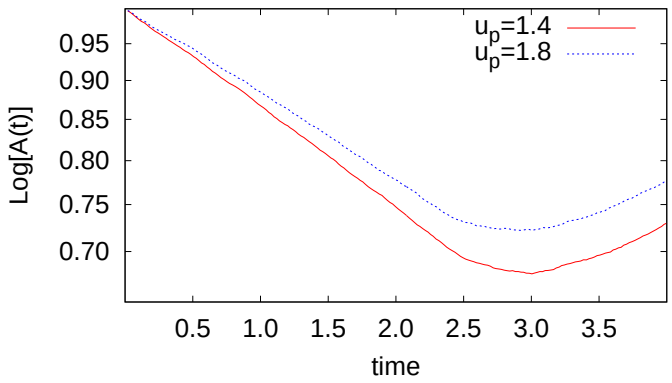

Figure 3.6: Time evolution of the amplitude for $0 < t < 2$ in log-linear scale, for the case $A_0 = 1$, and the value of $u_p = 1.4$ and $u_p = 1.8$.

By substituting Eq. (3.13) we immediately get:

$$\frac{dE_w}{dt} = -\gamma^{th} E_w \tag{3.15}$$

where the theoretical damping rate is:

$$\gamma^{th}(u_p) = \frac{\gamma_0}{\sqrt{2\pi}} u_p^2 \exp(-u_p^2/2) \tag{3.16}$$

(γ_0 is a proportionality constant). The above expression is proportional to the usual Landau damping rate of the linear theory [1] of Eq. 1.7. Fig. 3.7 shows the values of γ^{exp}, as a function of u_p, calculated through the fit of the curves $A(t)$ obtained for different u_p, in the range $t \leq 2$. Superimposed we report the curve (3.16) where $\gamma_0 \simeq 0.5 \pm 0.0001$ represents the best-fit on the data.

As regarding the behaviour of the damping rate with respect to different initial amplitudes, keeping u_p fixed, it has been verified that there are no important changes in γ^{exp} in this case.

It is worth noting that in deriving our model we haven't explicitly required to it to describe neither the linear non the nonlinear Landau damping. The

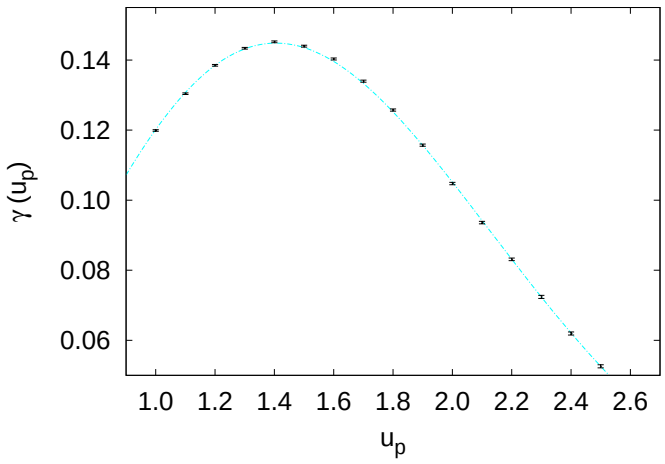

Figure 3.7: Different values of the damping rate γ^{exp}, calculated by numerical simulations with $N = 10^5$ and $A_0 = 1$ (black symbols), are plotted as a function of u_p. The curve represents the function of Eq. (3.16) with $\gamma_0 = 0.5$.

nice agreement of Fig. 3.7 is then a surprise. This means that our model is able to capture the basic physics of the non collisional damping. We are confident that also the long-time evolution of our system will describe at best the nonlinear Landau damping

3.5.2 Bifurcation value

Analytical and numerical works [26, 42] establish the existence of a critical initial amplitude that marks the transition between a state in which the field evolves to a nonzero time-asymptotic state from one in which the wave Landau damps to zero. A bifurcation between these two stages is experimentally found in our model. For every phase velocity u_p there exists a threshold value of A_0 above which the damping is stopped. This is due to a bifurcation between two states, namely $A_{sat} = 0$ for $A_0 \leq A_0^{(thr)}$ and $A_{sat} \neq 0$ for $A_0 > A_0^{(thr)}$. Fig. 3.8 shows the curve that separates the two regions, in the plane (A_0, u_p), obtained through some integrations of the model. If the initial parameters A_0 and u_p of a simulation are situated above the curve, after the initial damping to the minimum value A_{min}, the amplitude oscillates in the way we have seen above, while in the opposite case the dominant process is the damping of the wave.

However it must be said that the curve that represents the transitions

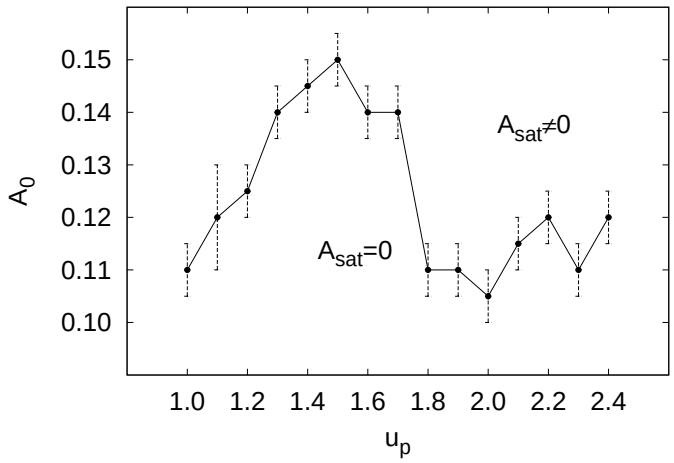

Figure 3.8: The curve, in the plane (A_0, u_p), that separates the region where the wave is completely damped, say $A_{sat} = 0$, from that where $A_{sat} \neq 0$. The curve has been built through some different simulations (black points) at fixed u_p and A_0.

between Landau and O'Neil scenario is to be taken with care, because of the finite number of digits in numerical simulations, so it has only an indicative value. In Fig. 3.9, as a matter of example, we report a case in which a complete dissipation of the wave takes place.

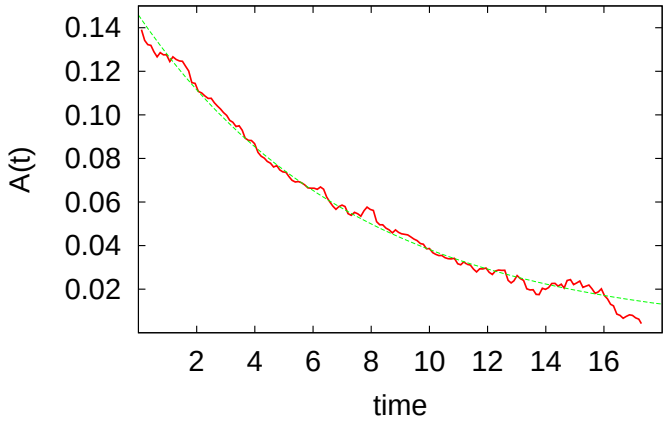

Figure 3.9: The time evolution of a wave with initial amplitude $A_0 = 0.14$ and $u_p = 1.3$ which Landau damps to zero (solid red line) and the best fit given by $A(t) = 0.14 \exp(-0.13t)$ (dashed green line).

3.5.3 Long-time behaviour: nonlinear stage

As the initial amplitude departs from its threshold value the behaviour of the wave become more and more regular, displaying high-amplitude oscillations (represented in detail in Fig. 3.10), observed also in numerical simulations of the Vlasov-Poisson system [28, 29, 31]. This represents the starting point of the nonlinear stage of Landau damping.

In this stage the trapping effects described in ch. 1 come into play. The bulk of particles begin to experience both tail-on collisions and head-on collisions, i.e. energy can be either gained or lost, thus stopping the linear damping. The saturation value A_{sat} around which the amplitude oscillates depends on the parameters of the model. In Fig. 3.11 the saturation value as a function of u_p and for a fixed initial amplitude is reported. It is easy to notice that the saturation value has its minimum for $u_p = 1.4$, i.e. where the maximum damping rate is found.

Let's now check what is the behaviour of the wave when the initial amplitude is varied. Fig. 3.12 shows the time evolution of the amplitude for four different values of the initial amplitude A_0.

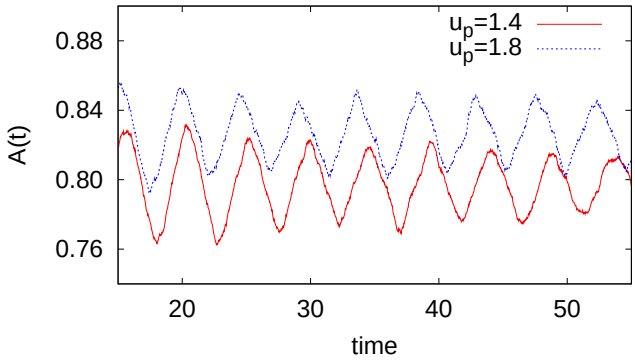

Figure 3.10: Particular of the oscillating part of the wave.

As it can be easily seen, the qualitative features of this evolution are similar for the cases taken into account. However, apart from the saturation level, that is increasing with increasing A_0, they differ in time scale, with lower amplitude having slower oscillations.

According to O'Neil [23], the period of oscillations τ should depend upon the amplitude of the wave as $\tau \approx A_0^{-1/2}$. However O'Neil treated the amplitude of the wave as if it were almost constant. Ivanov et al. [42], with numerical simulations of Vlasov-Poisson system, found a scaling relation between the period of oscillations and the saturation level of the form:

$$\tau \propto A_{sat}^{-\mu} \tag{3.17}$$

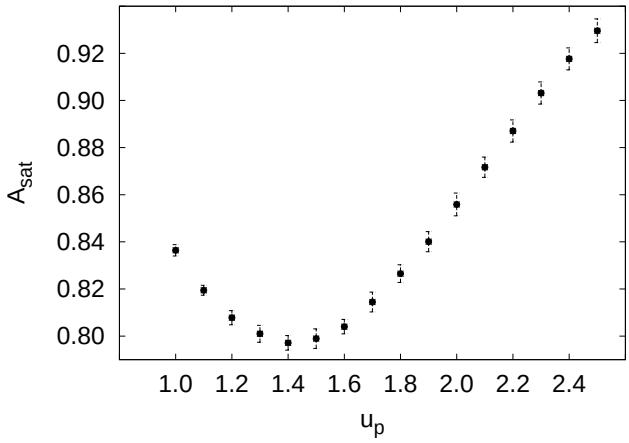

Figure 3.11: The saturation amplitude as a function of the wave phase speed and for $A_0 = 1$.

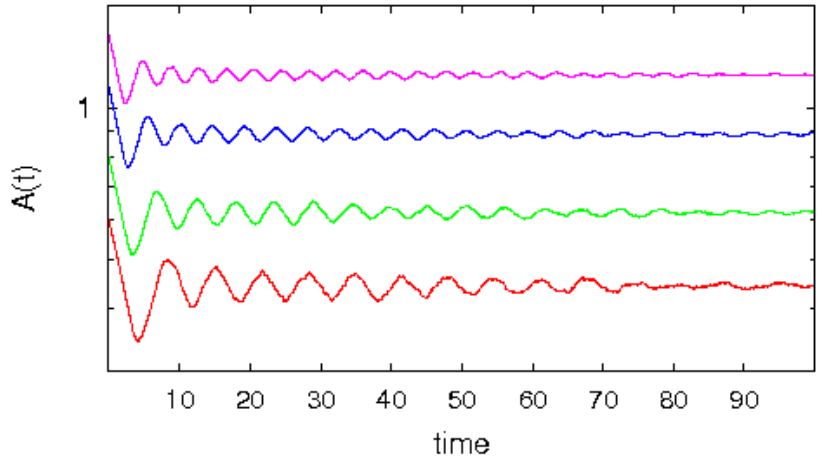

Figure 3.12: Time evolution of the amplitude $A(t)$ for $u_p = 1.4$ and for $A_0 = 1.4$, $A_0 = 1.1$, $A_0 = 0.8$ and $A_0 = 0.6$.

with $\mu = 0.52 \pm 0.02$. The previous relation is verified also our model. Even so, since the saturation amplitude varies with u_p, we found a little dependence of the exponent μ on this parameter. In the case $u_p = 1.0$ we find $\mu = -0.530 \pm 0.006$, for $u_p = 1.4$ and $u_p = 1.8$ we have $\mu \approx -0.55 \pm 0.01$. In Fig. 3.13 we report the values of τ as a function of A_{sat} for the cases indicated above, whereas Fig. 3.14 shows in a clearer way, the case $u_p = 1.0$ with the curve representing the best fit on the data. The value of the oscillation period τ has been obtained by considering mean and standard deviation of the data set of the measured peak-to-peak distances in the wave, until a cut-off time $t = 70$.

But we can say more about the saturation amplitude, the oscillation period and the way they vary with the phase velocity. In the first chapter we have seen that the saturation value should be of order of $(\tau_{tr}\gamma_L)$ lower that the initial value. A check that can performed is then to evaluate the function Γ given by:

$$\Gamma = \frac{A_0 - A_{sat}}{A_0 \tau_{tr}} \tag{3.18}$$

for a fixed value of u_p and for different initial amplitudes, and consequently, different saturation amplitudes and oscillation times. The function Γ should be proportional to $\gamma^{exp}(u_p)$. Since we have seen that the damping rate $\gamma(u_p)$

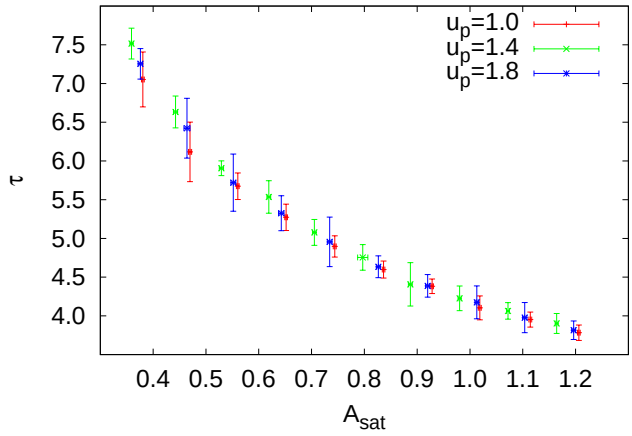

Figure 3.13: Oscillation time τ of the wave as a function of the saturation amplitude A_{sat} for the cases $u_p = 1.0, u_p = 1.4$ and $u_p = 1.8$.

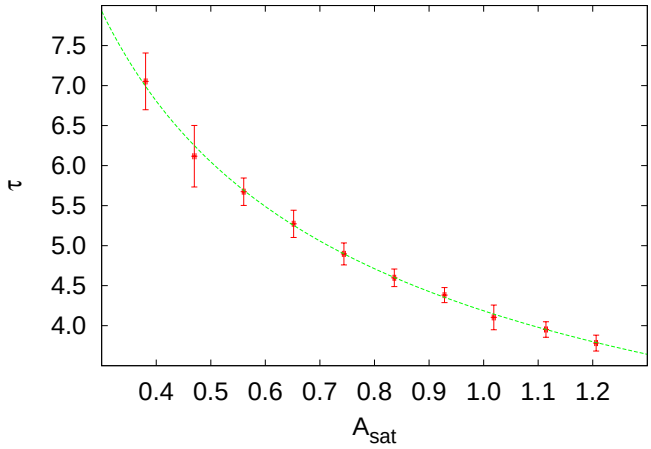

Figure 3.14: Oscillation time τ of the wave as a function of the saturation amplitude A_{sat} for $u_p = 1.0$. The dashed curve is the function $\tau = 4.18 * A_{sat}^{0.53}$.

depends on u_p but it does not vary with the initial amplitude A_0, for a fixed value of u_p, the function Γ should be approximately constant. Fig. 3.15 reports the value of Γ as a function of A_0 for three different value of u_p, i.e. $u_p = 1.0$, $u_p = 1.4$ and $u_p = 1.8$. We observe that the value of Γ is constant with A_0. Not a great difference exists between the three values of Γ, but the proportionality between them and the values of γ^{exp} (see Fig. 3.7) is preserved.

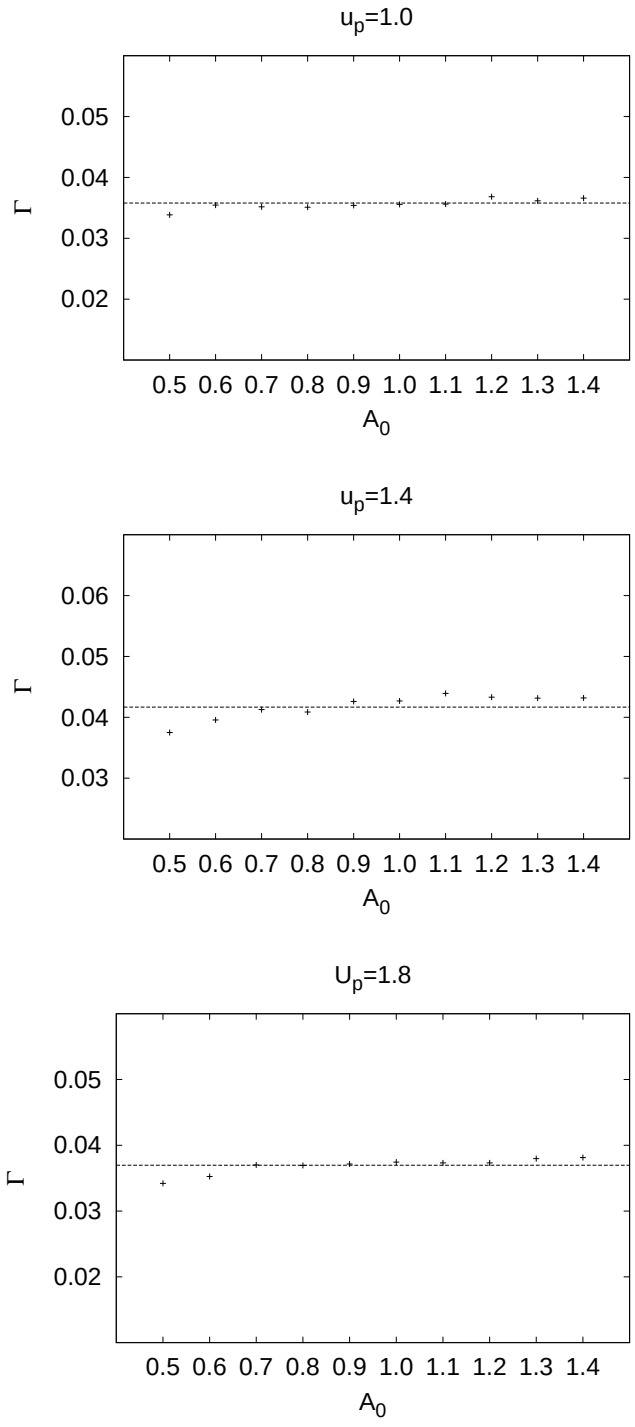

Figure 3.15: Evaluation of the function $\Gamma = (A_0 - A_{sat})/A_o\tau_{tr}$ for three values of u_p indicated on figures. The function is well fitted by a constant that is: $C = 0.036$ for $u_p = 1.0$, $C = 0.047$ for $u_p = 1.4$ and $C = 0.037$ for $u_p = 1.8$.

3.5.4 Asymptotical behaviour

Beyond the oscillatory regime a new behaviour is observed, namely oscillations of $A(t)$ around A_{sat} become rather irregular and with a lower amplitude (detail in Fig. 3.16). The time at which this new stage starts depends on

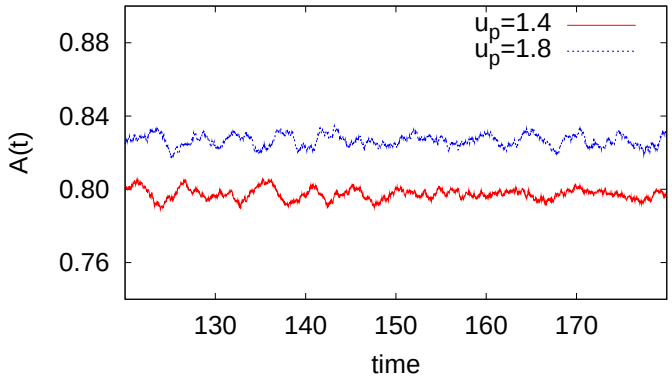

Figure 3.16: Particular of the asymptotic part of the wave.

the parameter u_p, namely the higher u_p the sooner this steady state appears. High u_p means an initial distribution function with a minor slope. This facet will be discussed in more detail in the next chapter.

Discrete-particle effects in the nonlinear evolution of wave-particle interaction have been investigated in the past, but the long-time behaviour, that resembles the O'Neil scenario [23] for the nonlinear Landau damping, where the oscillations in the electric envelope disappear in the long time limit, has never been obtained in numerical simulations, even if oscillations with decreasing amplitude have been observed [28, 31, 42].

We have seen that our simple *Fermi-like* model reproduces in a rather satisfying way the phenomenology of Landau damping. Therefore, it is possible to use it in order to delve into the question of Landau damping. In the next chapter we will discuss how the three stages derive from the collective dynamics of the particles and we will investigate some statistical features of the long-time behaviour of our model.

Chapter 4

Statistical features of wave-particle interaction derived from the modified Fermi model

4.1 Introduction

In the latest chapter some quantitative results of the Fermi-like model have been shown. We have seen that, although the model is very simple, and works in a rather basic way, it reproduces all the features of Landau damping. These results can be considered as a validation of the model.

In the present chapter we focus our attention on other facts. For example, what are the oscillations caused by? Are oscillations real or they represent a by-product of numerical calculations as conjectured in Ref. [30]. The next section is devoted to this question. Moreover we will discuss some statistical facts, like variations in statistical entropy and the calculation of correlations.

4.2 Oscillations

In Fig. 3.4 we see that the amplitude of the wave displays an abrupt descent in the beginning, soon after regular oscillations around a fixed amplitude appear. These oscillations are found also in numerical simulations of Vlasov-Poisson system. Here the oscillations continue as long as the simulations are continued, and even if they stop, this can be due the finite resolution of the numerical mesh. In our simulations, regular oscillations persist until a certain time, after which they disappear, giving rise to stochastic fluctuations

characterized by a low amplitude. The presence of oscillations both at intermediate times and in the long-time behaviour of the model is the result of the complex dynamics of particles. Keeping in mind that the decrease (increase) of the walls is due to collisions with particles with negative (positive) velocity, we can mediate collisions in time, to check how collisions with a given barrier are distributed and see whether they are related with the trend of the wave. Fig. 4.1 reports the time average of the difference between *tail-on* collisions (i.e. with particles with positive velocity) and *head-on* collisions (particles with negative velocity), in two time windows, with superimposed the wave in the same period. The time average of collisions has been scaled by a suitable amount to comparing it with the wave on the same scale, and the scaling is the same for the two figures. The pictures concern the nonlinear stage and the asymptotical stage.

In both cases, it is clear that collisions do not come one after the other at random, but, in a definite time interval, collisions happen *in average* all in the same direction. The number of collisions with a definite sign increases till it reaches a maximum, and after decreases, till the trend is reversed. It is easy to notice that, when *head-on* collisions dominate the wave amplitude decreases and vice versa. According to our model, oscillations stem from the dynamics of particles. The interaction between the whole of particles and the barriers is such that, at a certain time, particles coherently collide with one barrier, making the amplitude increase or decrease, and this behaviour is present both in nonlinear and in asymptotical stage. However, in the steady state the imbalance between *tail-on* collisions and *head-on* collisions become lower, as its easy to see looking at the units on the y-axis. Also the amplitude of oscillations decreases in the same time. The reasons of this behaviour can be better understood checking the velocity distribution function of the particles.

4.3 Changing in velocity distribution function

According to their heights, particles can be classified in, at least, three type of "population". By recalling that particles height is to be compared with the amplitude of the walls, we can say that first group is composed by particles with $y > A_{sat}$, the second group is composed by particles with $y \approx A_{sat}$. Particles with $y < A_{sat}$ belong to a third group. In Fig. 4.2 the sign of the velocity for particles with different heights are plotted, as a function of time. Particles which belong to the first group, namely those with $y > A_{sat}$, can

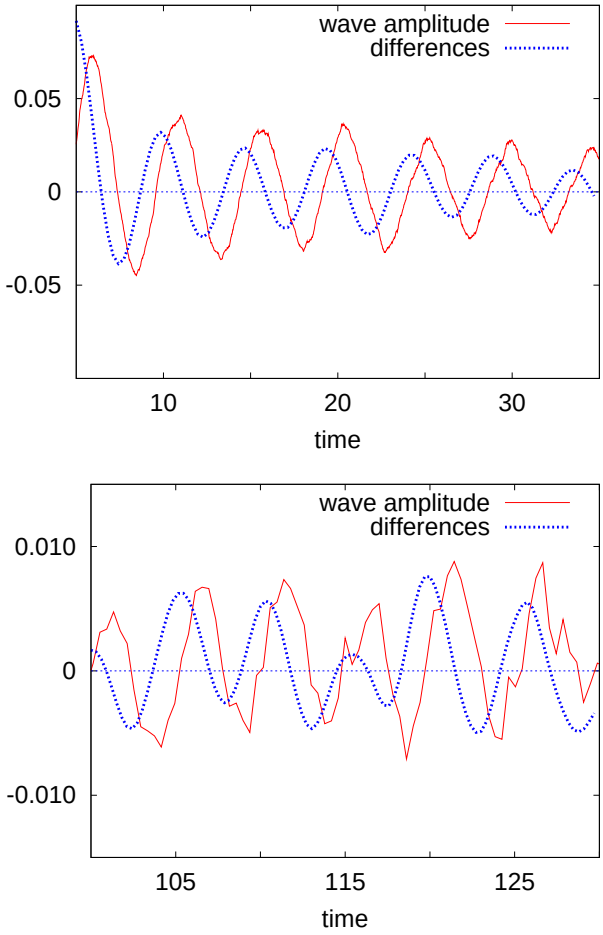

Figure 4.1: Dashed line: time average of the difference between *tail-on* collisions and *head-on* collisions for a run with $A_0 = 1$ and $u_p = 1.4$ in the nonlinear stage (top) and in the asymptotical stage (bottom). Solid line: wave amplitude in the same period. The wave amplitude has been shifted down by A_{sat} to compare the two graphs on the same scale.

be trapped at the beginning of the simulations, but, when the amplitude of the wave damps they are detrapped and free-stream unperturbed. The velocity sign, after a certain number of initial inversions, remains the same, indefinitely (see top panel of Fig. 4.2). These particles do not interact anymore with the wave. The second group is composed by the little fraction of particles that lie around the saturation amplitude A_{sat}. The changing in their velocity sign is chaotic. Indeed, if we consider two particles with heights that differ by a small amount, as the case shown in the two central panels of Fig 4.2, we see that, even if overall behaviour is the qualitatively same,

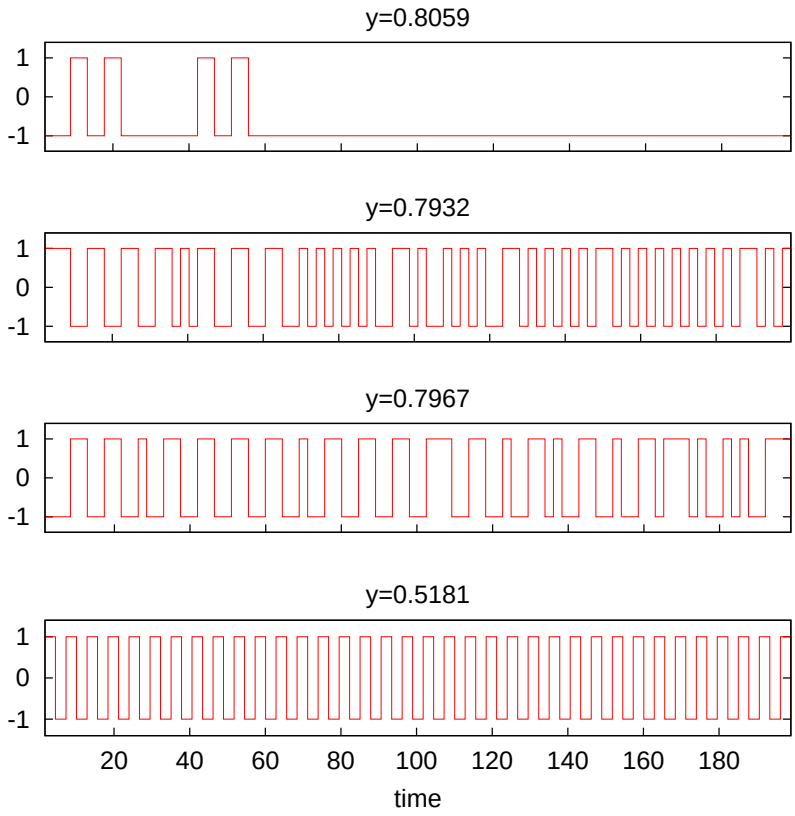

Figure 4.2: Velocity sign for particles of different height, reported on the figure, for a run with $A_0 = 1$ and $u_p = 1.4$.

inversions in velocity sign is not predictable and do not take place in the same sequence. This facet will be discussed in more detail in appendix B. They perform flights of different spatial length before being retrapped.

The third group is the more numerous. It is composed by the bulk of particles that lie below the saturation amplitude. They are always trapped and undergo to inversions of velocity sign each time that they reach a wall (bottom panel of Fig. 4.2). Even if their behaviour is trivial, they play the most important role in the wave–particle dynamics, since these are the particles that have the most effective exchange of energy with the wave. In the last section we discussed about particles that coherently collide with a definite velocity sign, making the amplitude increase and decrease. Going back and forth, particles with $y < A_{sat}$ are the particles that synchronize in colliding on a definite wall, and, in conclusion, they are responsible of the oscillation of the wave.

4.4 Distribution function

As result of the complex dynamics the velocity distribution function changes in time. The particle distribution function can be defined through the usual coarse graining of a point system in statistical mechanics, say $f(u,t)\Delta u$ represents the number of points that, at time t, lie within the box of (narrow but finite) size Δu. Fig. 4.3 reports the distribution function at different times. We see that at the beginning the distribution function is a straight line, most populated in the negative region of the velocity. When the wave damps, the shape of the distribution function changes accordingly. Particles start to cluster and the distribution function display empty and full region in velocity space. The distribution function remain always antisymmetric. As time goes on, the spikes become thinner and thinner, and their amplitude diminishes, till the distribution gets flat [41]. Particles with velocity at the extremes of the velocity domain are an exception. These are the fastest particles, with height above the saturation amplitude. Since, after few collisions at the beginning, they free–stream unperturbed, they are not affected by the wave, so their distribution in velocities doesn't change, even when the distribution becomes flat.

4.5 Phase mixing and the approach to the equilibrium

The transition to equilibrium can be better clarified by considering the entire phase space (x,u). A plot of the phase space at different times is given in Fig. 4.4. In this space each particle follows, at its own speed, a closed path (the "tori-KAM" whose corners are the four points $(\pm 1, \pm u_j)$). This generates regions characterized by different density in phase space. These zones are stripe-shaped. Stripes are thick in the beginning, but, due the the slightly different velocities of nearby particles, as time goes on, they become thinner and thinner. As the stripes get narrower, less and less particles collide almost synchronously on a given side of the potential well. Actually this is the dynamical process that is responsible for the presence of the amplitude oscillations shown in Fig. 3.4. In fact when the stripes are large enough, the synchronization of collisions on a given barrier is able to sustain or decrease the amplitude of the wave around the saturation value. When the filamentation goes on producing narrower velocity stripes, the synchronization of collisions is felt by a lower number of particles and the oscillations become less regular up to a complete phase-mixing. This means that, for long times, the system has reached the equilibrium configuration, and the only fluctua-

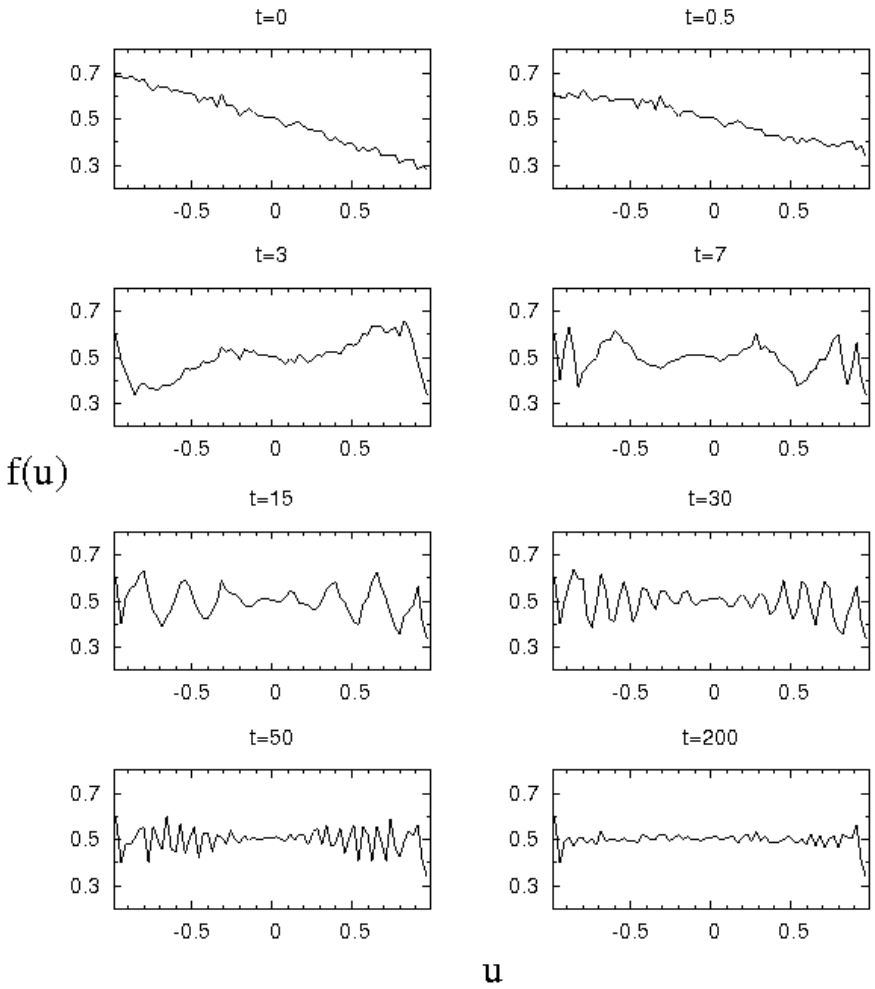

Figure 4.3: Distribution function (averaged on x) at eight different times, for $A_0 = 1$ and $u_p = 1.4$.

tions that one can observe are due to collisions that come one after another in a stochastic way.

Thus, the approach to equilibrium in the Fermi-like model, is described by a filamentation of the phase-space. The approach of systems to statistical equilibrium through a laminar filamentation is analogous to the well known phenomenon of laminar mixing between two fluids in statistical mechanics that has been investigated by Gibbs. The Fermi-like dynamical system plays the role of an area-preserving two-dimensional map, as the well known baker's

transformation [43]. Baker's map is described by the equations:

$$\begin{aligned} x_{n+1} &= 2x_n \\ y_{n+1} &= y_n/2 \end{aligned}$$

for $0 \leq x_n \leq 1/2$

$$\begin{aligned} x_{n+1} &= 2x_n - 1 \\ y_{n+1} &= (y_n + 1)/2 \end{aligned}$$

for $(1/2) < x_n \leq 1$.

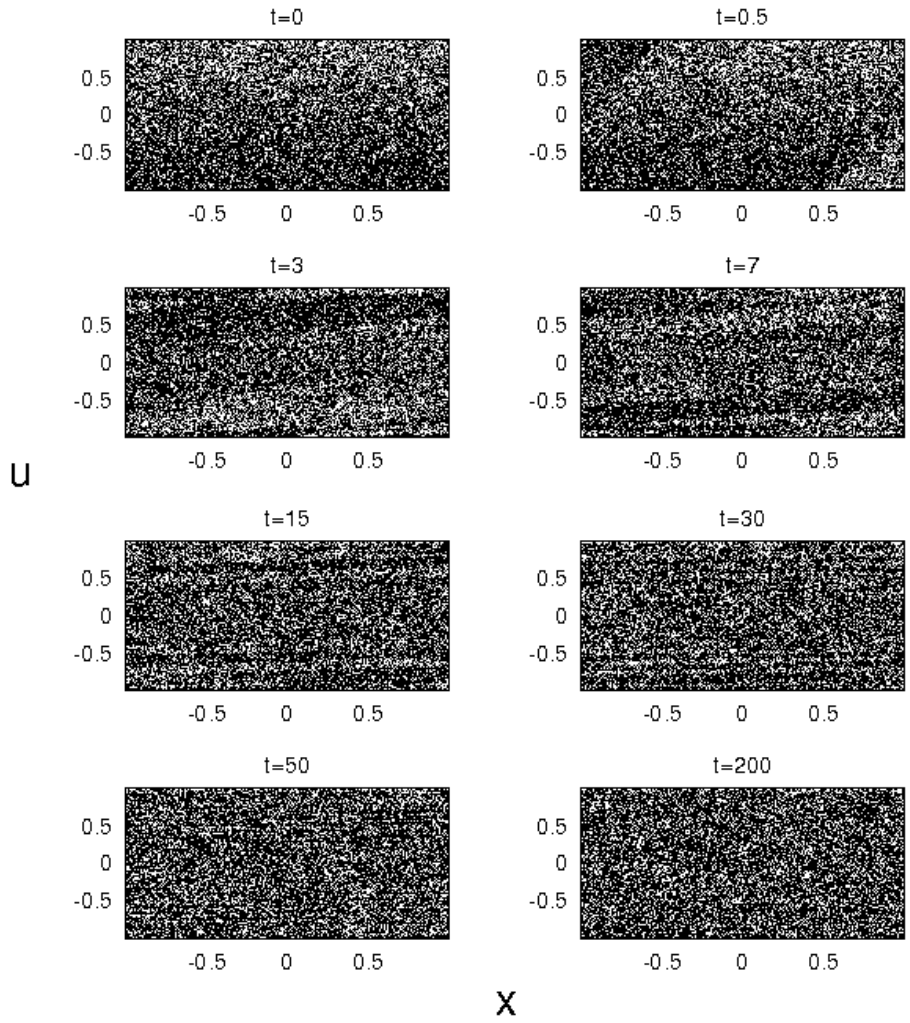

Figure 4.4: Phase space scatter plot at eight different times reported on figure, for $A_0 = 1$ and $u_p = 1.4$.

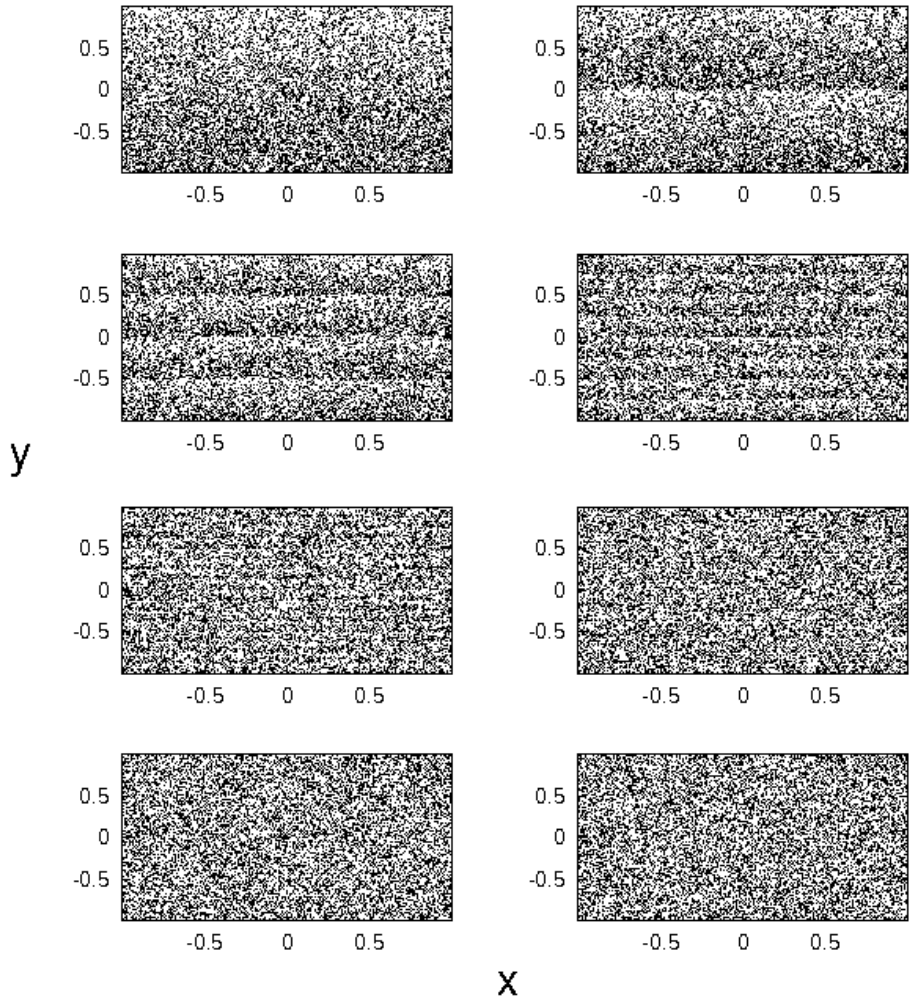

Figure 4.5: Phase space scatter plot for eight iterations of the baker's map. The initial distribution function is the same as the one used for the modified Fermi model.

A representation of the baker's map with an initial distribution in y analogous to that used in the Fermi-like model for the v's is displayed in Fig. 4.5. Even if the initial stages of the Fermi-like model and the baker's map differ, the last states are very similar. In both cases there are stripes that become smaller and smaller until they are no longer resolved.

4.6 Inter-particle separation

The phase space filamentation that drives the system towards equilibrium ends up to a complete mixing when the width of the velocity stripes gets smaller than the characteristic scale of discreteness of the system, i.e. the inter-particle separation. When this situation occurs, nothing can happen in term of oscillation in the wave: the system has reached its steady state, which we defined the asymptotical stage, that will last indefinitely.

This is one of the differences between the way the Fermi-like model and Vlasov theory describe the wave-particle interaction. Vlasov equation just expresses the fact that, in absence of collisions, the phase-space distribution function is constant along the trajectories of the system. In absence of collisions, as in the case of wave-particle interaction, trajectories in phase space are continuous lines. Volumes in phase space are conserved, even if they can be deformed. As a consequence, the filamentation process in Vlasov systems could keep going on and on producing thinner and thinner filaments in phase space (see for a representation of this situation, Fig. 4.6), never reaching the complete mixing stage. This means that Vlasov theory cannot describe a Gibbs process, because, in Vlasov theory, no characteristic length is present.

Conversely, the inter-particle distance appears as a natural typical distance in Fermi-like model, that takes into account the intrinsic discreteness of a plasma system.

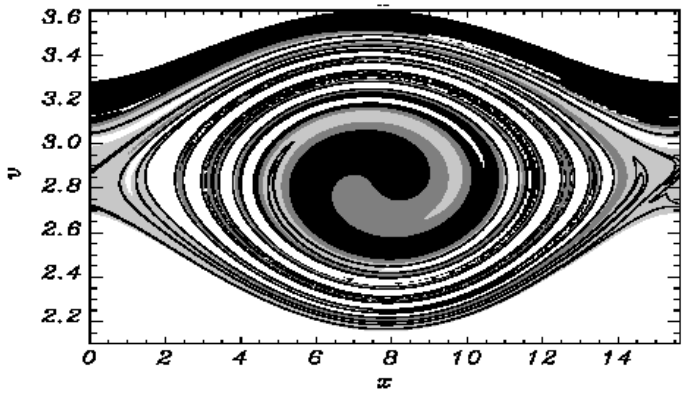

Figure 4.6: Contour of the distribution function in a Vlasov simulation [30].

4.7 Statistical entropy and correlations

We have seen that there exists a group of particles which are always trapped. These are the particles with height below the saturation amplitude, and they simply go back and forth between the walls, making the amplitude oscillate according to the mechanism described in sec. 4.2. In absence of Coulomb collisions between particles, the trapped region can be thought of as an isolated system with respect to the free region, where particles do not exchange energy with the wave (except for a few particles that can escape from the well and be retrapped after a finite time). It is straightforward to show that by imposing statistical entropy of the system of trapped particles $S = -\int f \log f dx du$ to be maximum, while conserving the total number of particles and assuming an infinite energy reservoir (the wave energy), the distribution function turns out to be flat over the velocity interval. As a consequence, the system naturally evolves towards the maximum entropy state, through the laminar mixing process discussed previously. In Fig. 4.7, we show the time evolution of the entropy variation $\Delta S = S(t) - S(0)$, with three different numbers N_c of numerical cells in phase space. After the initial growth, ΔS reaches a saturation level. The jump in the entropy of the system corresponds to the entropy difference ΔS^{th} between a flat velocity distribution (see the bottom right plot in Fig. 4.3) and a decreasing function (see the top left plot in Fig. 4.3).

The quantity ΔS^{th} is indicated in the figure by a horizontal solid line. It is worth noting that the jump in ΔS does not depend on the numerical resolution.

The curves in Fig. 4.7 can be fitted with a function $\Delta S \propto 1 - \exp(-t/\tau_G)$, τ_G being the time when a complete Gibbs mixing is reached. Repeating such simulations for many different numbers of particles N, gives the scaling law $\tau_G \propto N_\alpha$, where $\alpha = 0.55 \pm 0.02$.

Another consideration can be made by evaluating the correlations between trajectories in phase space. The normalized two-particle correlation function is defined as:

$$C_2(i,j) = \frac{|f_2(i,j) - f_1(i) f_1(j)|}{f_1(i) f_1(j)} \tag{4.1}$$

where f_2 and f_1 represent the two-particle and the single-particle coarse-grained distributions, respectively; the integers i and j indicate the i-th and j-th cells of area Δ in phase space. The distributions f_2 and f_1 can be evaluated dividing each phase space cell of area Δ in n_c subcells of area Δ_c.

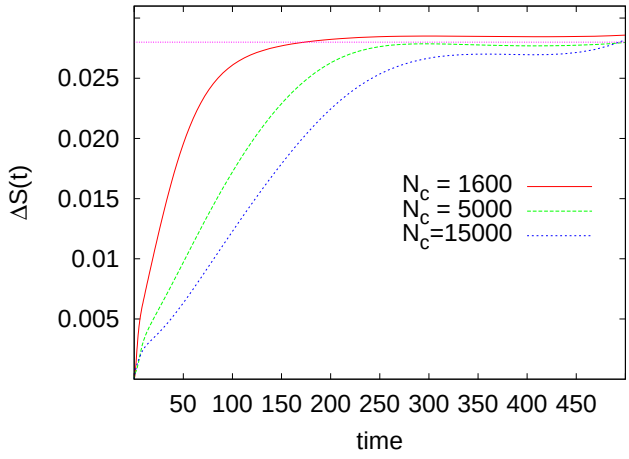

Figure 4.7: Time evolution of the entropy variation for three different number of cells N_c in the phase space. The straight line represents the theoretical entropy variation.

Using this subgrid in phase space, we define:

$$f_2(i,j) = \frac{\sum_{i'=1}^{n_c} g(i,i')g(j,i')}{n_c^2} \tag{4.2}$$

and:

$$f_1(i) = \frac{\sum_{i'=1}^{n_c} g(i,i')}{n_c} \tag{4.3}$$

where the integer i refers to the i-th subcell contained in a generic cell in phase space and $g(i,i')$ is simply the number of particles in a subcell of area Δ, divided by the total number of particles N (fine grained distribution). In Fig. 4.8, we show the time evolution of the maximum value of the two-particle correlation function C_2 in phase space. The evolution of $max(C_2)$ is followed up to the time when the first two oscillations occur in the signals described in Fig. 3.4. In the first trapping period, when the wave starts trapping the resonant particles, thus creating correlations in their phase space trajectories, we observe an increasing of the two-particle correlation function, that finally saturates when regular oscillations occur. This shows that wave-particle interaction creates correlation in the phase space particle trajectories [44, 45].

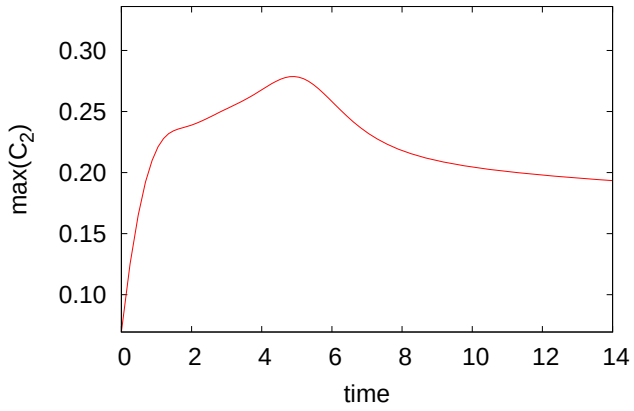

Figure 4.8: Time evolution of the maximum of the two-particle correlation function C_2.

4.8 Discussion

The fact that both the entropy of the system and the correlation function increase when trapping comes into play suggests that Vlasov theory, as it is, does not tell the whole story about wave-particle interaction. The entropy $S(t)$ is a constant for the exact Vlasov-Poisson system. The entropy of a statistical system is usually defined as:

$$S = -\int f \log f dx dv. \tag{4.4}$$

For a plasma:

$$\frac{dS}{dt} = -\int \frac{df}{dt}(1 + \log f) dx dv = 0 \tag{4.5}$$

since Vlasov equations states that $df/dt = 0$. This is consistent with the fact that Vlasov equation neglects the process (binary collisions) which causes statistical systems to increase their entropy and evolve toward a Maxwell-Boltzmann distribution.

This problem is closely related to that of irreversibility of Landau damping. The Vlasov-Poisson system possesses the property of reversibility and, if inversion of time is made at a certain point, the system will return to the

initial state. This seems to be in contrast with a dissipative phenomenon like Landau damping. It was Van Kampen and Felderhof [46] who pointed out that all forms of collisionless damping, including Landau damping, are largely due to a phase mixing effect caused by averaging over an essentially infinite velocity space. A *finite* number of electrons moving against a uniform charged background in a closed enclosure from which radiation is not allowed to leave will not exhibits damping of any kind: the system motion would be recurrent, as could be easily shown with the Fermi-like model. Also as discussed in Ref. [47], typically, irreversibility appears to be due to phase mixing (as in Landau damping) or waves radiating to infinity (radiation damping) or an incoherent interaction with an environment composed of a very large number of degrees of freedom in collisional contact with each other or with a "boundary" (thermodynamic reservoirs). The observed irreversibility of a dynamical system is not necessarily a property of the system, but may be a consequence of a certain types of measurements processes involving macro-averages and the loss of fine-scale information. This loss of information is often called coarse-graining.

The modified Fermi model plays a pedagogically fundamental role in the analysis of wave-particle interaction phenomena. Even though the trapping interaction is described in a very basic manner, the modified Fermi model catches the fundamental physics of the process, in which the phase mixing process appears as a straightforward consequence of the interaction. Conversely, Vlasov equations cannot describe phase mixing phenomenon, as observed in sec. 4.6. Moreover, the feedback of correlation growth on the dynamical evolution of the particle distribution function, which is described by the collision term, is neglected. The Fermi-like model, by considering the discreteness of plasma, can account for these effects.

4.9 The modified Fermi model in a case of instability

The modified Fermi model can be employed in a case of instability. An instability is the condition in which a small perturbation about a steady state grows in time. Conditions that may lead to a growing behaviour of the wave include: beams, in which fluxes of particles move in a plasma at rest, anisotropic distributions of pinch angles of the particles and non-equilibrium spatial distributions. Thus, the forcing term can be either in velocity or in physical space.

We have seen that Landau damping rate depends critically on the electron

distribution function f_0 in vicinity of the wave phase velocity $v_\phi = (\omega/k)$. If the derivative of the distribution function in $v = v_\phi$ is negative the wave is damped in time: the Maxwellian function is a stable distribution. If there were more particles at higher velocities than at lower ones, the distribution function would be not stable for waves resonant with these fast particles. This type of instability is called *bump-on-tail* instability.

Let's consider a distribution function of the form reported in Fig. 4.9, where a certain amount of electrons has been accelerated. It is possible to show that an analytical analysis [21] would give a result of the type of the one shown in ch. 1 (Eqs. 1.6 and 1.7), but now the amplitude increases for waves with phase speed in the velocity range where the particle distribution function has positive slope.

If we call γ_G the growing rate of an exponential increasing wave, we can say that we can use a linear approximation (see ch. 1) only for times shorter than $(1/\gamma_G)$. For longer times the linear mathematical treatment cannot be used.

The O'Neil theory remains valid in the case of growing waves. The amplitude grows in the beginning, then oscillates around a level that is τ_{tr}/τ_L (we use here the notation of the first chapter) higher than the initial value, till the distribution function forms a *plateau* in the region where electrons become trapped.

With the Fermi–like model it is easy to represent this case of instability. It suffices to change the sign of the slope of the initial distribution function, and consider a function of the form $f(u) = a + bu$ instead of the one in Eq. 3.13.

In Fig. 4.10 the time behaviour of the wave in the case of bump-on-tail

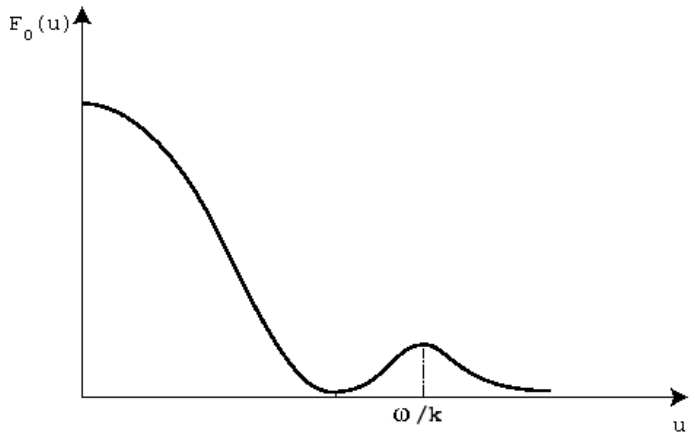

Figure 4.9: Distribution function with region of unstable ω/k.

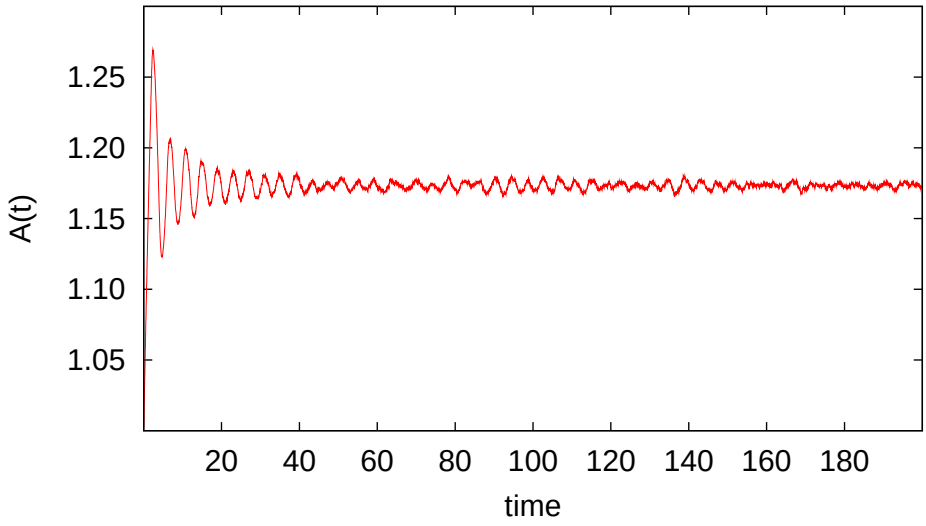

Figure 4.10: Wave behaviour in the bump-on-tail instability, for $A_0 = 1, u_p = 1.2$.

instability is reported. For short times, a steep increase of the amplitude appears. Later it oscillates around a constant value. The oscillations are regular in the beginning, but for long times they become stochastic.

In Fig. 4.11 the phase space and the coarse–grained distribution function are reported for the run in Fig. 4.10. In this case the phase mixing stops the increasing of the amplitude, making the wave oscillating around some constant value.

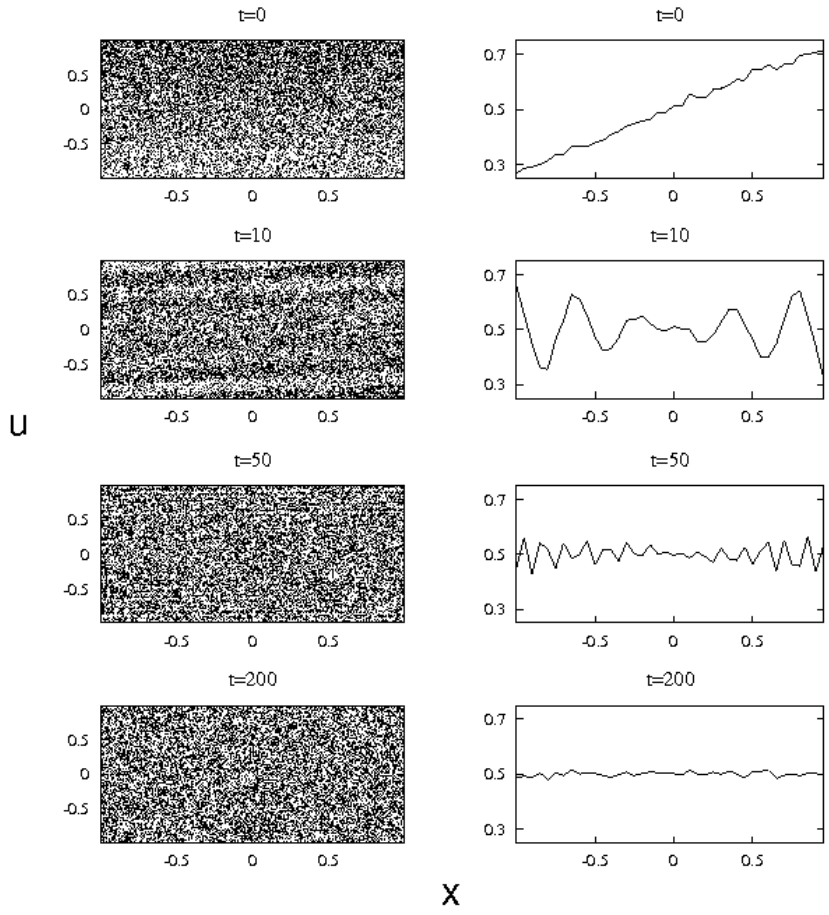

Figure 4.11: Bump-on-tail instability: phase space scatter plot (left column) and coarse-grained distribution function (right column) at four different times reported on figure, for $A_0 = 1$ and $u_p = 1.2$.

Chapter 5

Fermi-like model and PIC code: a comparison

5.1 Introduction

As mentioned in the first chapter, Vlasov codes are the designed programs that solve the Vlasov-Poisson system and consequently, they are used to investigate wave-particle interaction. But Landau damping is a tricky numerical problem, since different time scales are present, and the little physical effects must be separated from numerical noise. The numerical implementation of Vlasov codes demands a certain coarse graining of the space and momentum coordinates. This numerical uncertainty is quite sufficient to generate genuine dissipation [48], which leads the system to violate the conservative constraints of Hamiltonian dynamics and cause the reconnection (formally forbidden!) of nearby isolines of the distribution function. It is therefore important to perform a series of checks to rule out spurious numerical effects. These effects can be quantified checking the time evolution of the system invariants $\int f^i dxdv$, $i \geq 2$. Vlasov equation has the property that $\int G(f)dxdv$ is a constant for any isolated system in which f obeys Vlasov equation. In particular, the entropy $S(t)$ is a constant for the exact Vlasov-Poisson system. However, the entropy increases monotonically for the discrete numerical model (this is a property of the scheme, and can be proven rigorously), though the growth is slower for the higher resolution cases. The invariants $\int f^i dxdv$ give essentially the same result [28].

In sec. 4.6, we have seen that, as time goes on, smaller and smaller structures develop in phase space. Once the microstructures reach the mesh size, they are smoothed away by numerical diffusion (essentially due to the interpolation technique used in the code), and are therefore lost. Of course, this

has nothing to do with the phase mixing process discussed above. For these reasons, in order to test the modified Fermi-model, we consider, instead of Vlasov simulations, a standard PIC numerical simulations, performed in the regime of nonlinear Landau damping. Particle In Cell (PIC) code retains the discreteness of plasma, and therefore could display the same features of the Fermi-like model.

5.2 PIC codes

Particle in cell codes (PIC) [49, 50] refer to a method in which, individual particles (or fluid elements) in a Lagrangian frame are tracked in continuous phase space, whereas moments of the distribution such as densities and currents are computed simultaneously on Eulerian (stationary) mesh points. Since they make use of particles they seem more suitable to be used to perform comparisons with the results of the modified Fermi model. PIC codes represent historically widely adopted approach to numerical simulations of plasmas in the framework of the kinetic theory and in the past years they have been considered the most efficient tool in the description of the plasma dynamics, especially because such an approach allows to study much of the physical aspects in the full dimensional case, with a relatively small computational costs. On the other hand, the numerical study of the Vlasov-Maxwell system in the fully nonlinear regime and in the six-dimensional phase space, is still a very hard goal, even for modern parallel computers. However, a huge scenario of physical processes in plasma physics can be described in a phase space of lower dimensions and here Vlasov codes are extremely useful, for example in one spatial and one velocity coordinates phase space, one spatial and two velocity or in the four-dimensional description, with a relatively good numerical resolution. The main difference between PIC and Vlasov codes lies in the description of the particle distribution function. In a PIC code the distribution of particles is described in a statistical way where real particles are represented by so called *super-particles*. Each super-particle represents a given percentage of density and carries a given amount of momentum. The density and momentum is distributed among super-particles in such a way that their weighted summation at a given point of the spatial domain provides a correct value of the given moment of the particle distribution function with certain accuracy determined by the statistical properties of the set of super-particles. Moments are usually evaluated at nodes of 1-D, 2-D or 3-D spatial mesh. In Vlasov codes the distribution function of a given species is described by the set of values of a particle distribution function, itself evaluated on an uniform or adaptive grid defined on a 6-D phase space.

Moments needed for the time integration of the Maxwell equations are evaluated by straight numerical integration of the distribution function. The fact that values of the distribution function are given precisely with the given accuracy of n-th order implies that its moments are determined precisely with the same accuracy too. This cancels statistical noise caused by the fact that super-particles in PIC codes represent values of the distribution function at randomly selected points of the phase space. But, differently from PIC codes, where push of particles is not necessarily implemented with a scheme of some controlled order of precision, Vlasov scheme holds the precision of the given order at all steps of the algorithm. This has significant dissipative consequences at all effects of higher order.

5.3 Fermi-like model and PIC code: similar results

PIC simulations used here [44] follow the electron dynamics in the x-direction, which is the direction of wave propagation (the ions are considered motionless). The equations of motion of a large number of macro-particles ($N = 10^7$) are integrated numerically through a standard second-order leap-frog scheme. For convenience, we scale time by the inverse plasma frequency ω_p^{-1}, where $\omega_p = \sqrt{4\pi ne^2/m}$, and n is the electron density. Length is scaled by the Debye length $\lambda_D = v_{th}/\omega_p$. With these choices, velocity is scaled by the electron thermal velocity $\lambda_D\omega_p = v_{th}$ and electric field by $\sqrt{4\pi nmv_{th}^2}$. The electron phase space domain for the simulation is $D = [0, L_x] \times [-v_{max}, v_{max}]$, where $v_{max} = 5$. Periodic boundary conditions in physical space are imposed, then Poisson's equation is solved using a standard Fast Fourier Transform (FFT) routine. The initial distribution function is a Maxwellian in the velocity space, over which a modulation in the physical space with amplitude A and wave vector $k = 2\pi/L_x$ is superposed:

$$f(x, v, t = 0) = \frac{1}{\sqrt{2\pi}} e^{-\frac{x^2}{2}} [1 + A\cos(kx)]. \tag{5.1}$$

The length of the spatial domain is chosen to be $L_x = 20$, the amplitude of the perturbation is $A = 0.064$. The simulations follow the evolution of electrons for many plasma periods ($t_{max} = 4000$). For a PIC simulation with one spatial dimension and with grid spacing smaller than the Debye length, the effective collision time (see Ref. [49]) is longer than $t = (1/\omega_p)n\lambda_D$, where

$n = N/L_x$ is the 1-D density of particles in the simulation. In scaled units, the collision time is larger than $t = N/L_x \approx 10^6$ (for $L_x = 20\lambda_D$), which is much longer than duration of our runs, $t_{max} = 4000$. In these conditions, our simulations can be considered fully collisionless.

The runs for the Fermi-like model are conducted as described in the previous chapters.

The top plot in Fig. 5.1 shows the numerical results of the PIC code for the time evolution of the amplitude of the electric-field spectral component $E_k(t)$, while the bottom plot reports the typical time evolution of the barriers amplitude resulting from the Fermi-like model. As it can be seen, the plots are very similar: in both figures, after an initial decay, the amplitude starts oscillating around a saturation value.

The amplitude of the field initially decreases, then oscillates regularly and finally, for long times, the dynamics becomes completely stochastic. The time evolution described in Fig. 5.1 is determined, in both cases, by the interaction of the particles with the potential well of the wave, that is sinusoidal for the PIC simulation, and squared for the Fermi-like model. The particle dynamics is similar: as we have already discussed (sec. 4.3), particles whose energy is larger than the potential barrier free–stream unperturbed; a few particles at the border of the trapped region can be trapped and detrapped periodically, performing more or less long flights [31]; finally, the bulk of particles with energy well below the potential barrier is ever trapped. The discussion made in sec. 4.5 about the particle trajectories in the phase space, is also valid for the PIC model: each of trapped particle follows a closed path in the phase space (x, u); this path has an elliptical form for the PIC simulation and a rectangular one for the Fermi–like model. In the left panels in Fig. 5.2, the phase space (x, u) for the PIC code is reported (in the region around the wave phase velocity $v_p = 3.7$). This picture is to be compared with those in Fig. 4.3 and Fig. 4.4. Also in the case of the PIC model, as time increases, the dynamic of particles generates a filamentation of the structure in phase space, and stripes become narrower, up to a time where an apparently complete mixing settles up. In the right panels in Fig. 5.2, the distribution function $f(x_M, u, t)$ is plotted as a function of the velocity u for a given point in the physical space x_M at different times. The point x_M corresponds to the coordinate in the physical space where the velocity width of the trapped region is maximum. A quick reflection is enough to realize that, in the PIC code as in the Fermi-like model, the occurrence of velocity stripes produces a synchronization of collisions on each barrier. As the stripes get narrower, less and less particles collide almost synchronously on a given side of the potential well, and this generates the decreasing oscillation of the field. When the filamentation goes on producing narrower structures in

phase space, the synchronization of collisions is felt by a lower number of particles and oscillations become less regular till a complete phase mixing is reached.

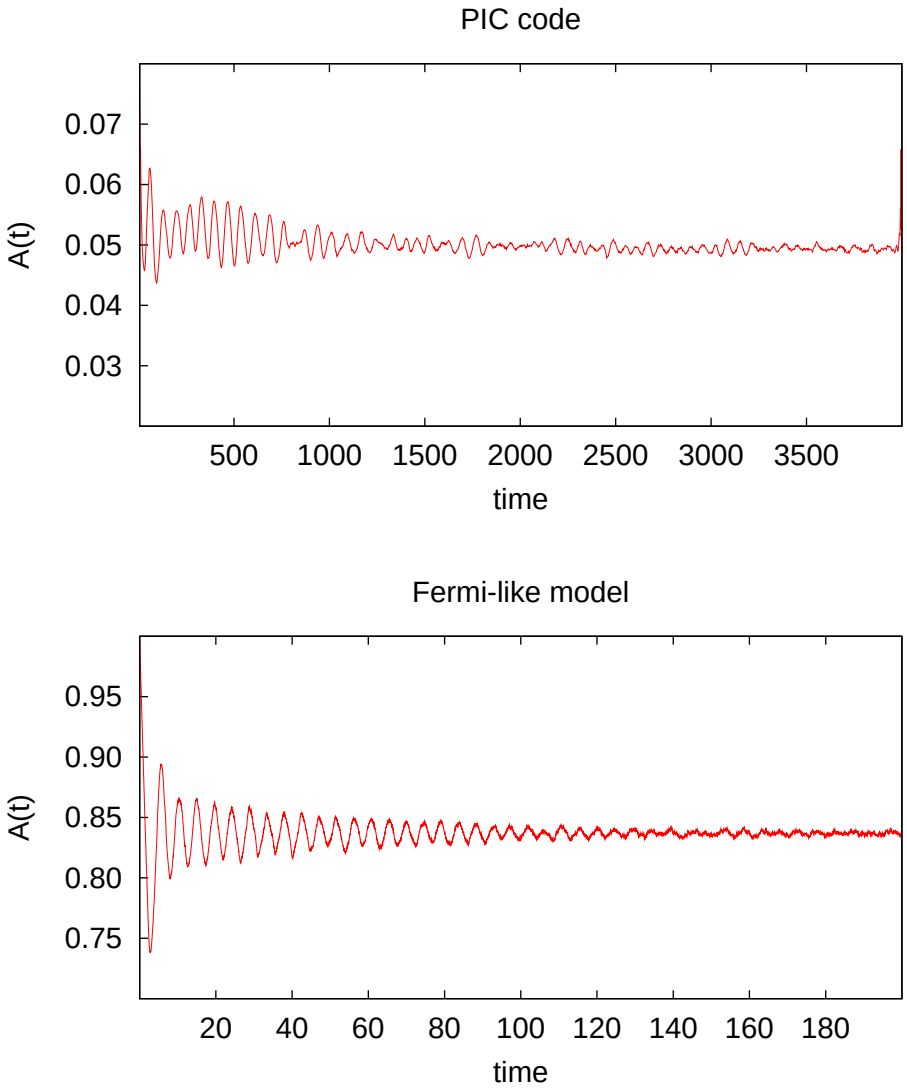

Figure 5.1: At the top: Time evolution of the electric-field amplitude (PIC simulation). At the bottom: Time evolution of the barrier amplitude (Fermi-like model).

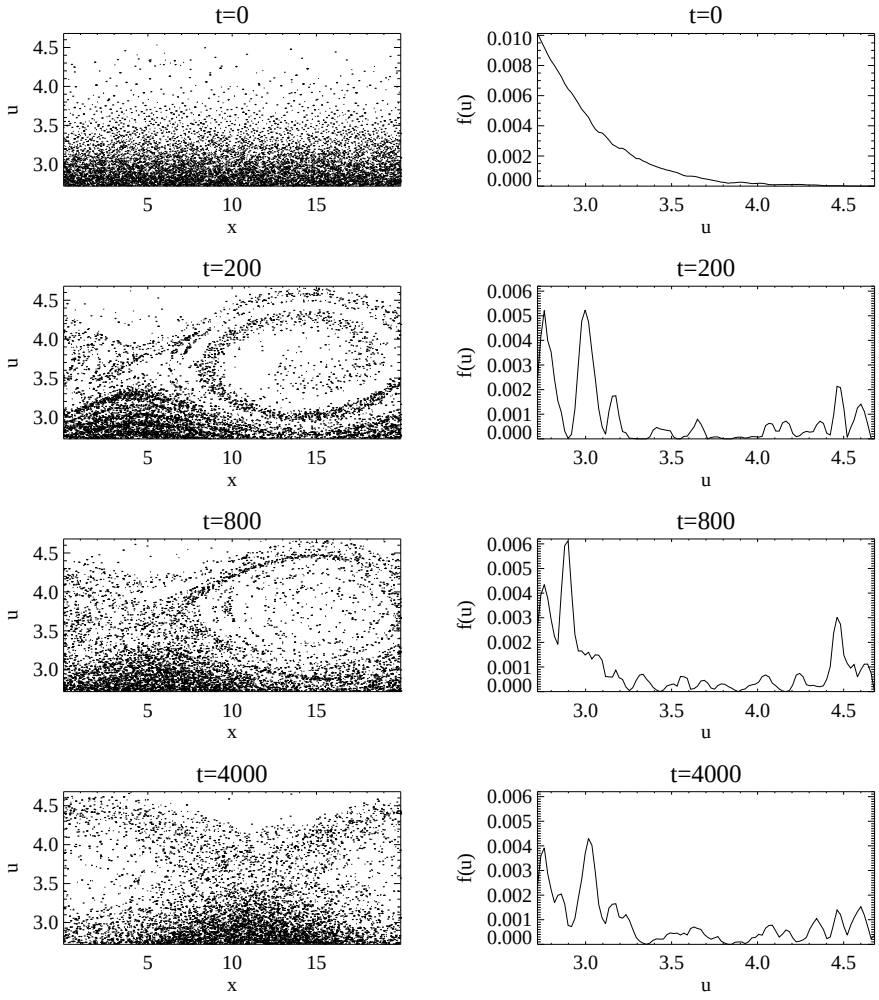

Figure 5.2: PIC simulation: phase space scatter plot at four different times (left panels); distribution function $f(x_M, u)$ as a function of u, at four different times (right panels).

5.4 Correlations

Also for the PIC code we compute the correlations between the trajectories of particles in phase space, in the same way as we did for the Fermi-like model. As described in sec. 4.7, the phase space has been divided in a series of cells and subcells in which the correlation function 4.1 has been evaluated. In Fig. 5.3, we show in logarithmic scale the time evolution of the maximum value of the two-particle correlation function C_2 in phase space.

The trend of $max(C_2)$ is followed until the time when the first two oscillations take place in the PIC simulation plotted in Fig. 5.1. When the

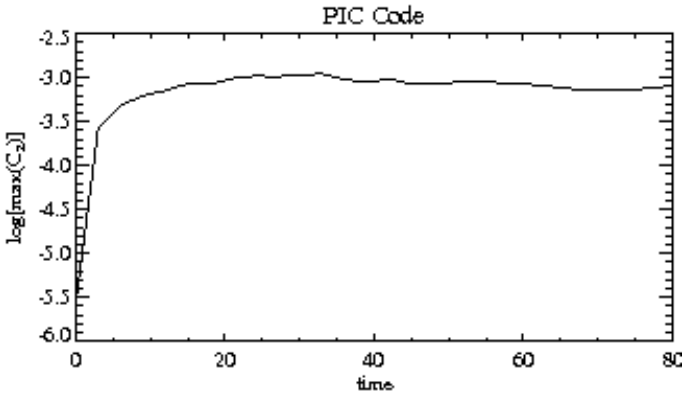

Figure 5.3: PIC simulation: time evolution of the maximum of the two-particle correlation function C_2 in the resonant region, in logarithmic scale.

wave starts oscillating and trapping the particles, correlations in phase space rapidly increase. An analogous behaviour has been observed for the Fermi-like model (see Fig. 4.8).

We have seen that the simple dynamical model gives results very similar to that of a PIC code. In both cases, the wave starts with a steep damping, then oscillates in a well-ordered way around a fixed value, finally it becomes almost constant. We have seen that this behaviour is the result of the collective wave-particle interaction. The particles trapped in the potential well of the wave, going back and forth, make the wave increase or decrease following the exchange of energy with particles. The oscillating stage run out when a complete mixing is established between particles. From this moment on, they are no longer able to exchange energy in a coherent manner. Both in Fermi-like model and in PIC code, two-particle correlations rise when the trapping phenomenon begin. The fact that both the entropy of the system and the correlation function increase when trapping becomes important suggests that Vlasov description fails in describing wave-particle interaction. In fact, in Vlasov theory the feedback of correlation growth on the dynamical evolution of the particle distribution function, which is described by the collision term, is neglected. Moreover Vlasov equation cannot describe increasing entropy processes, because as time increases it produces continuous structures at smaller and smaller scales, missing the intrinsic discreteness of the plasma system.

5.5 Conclusions

In this work we have introduced a dynamical model in the form of a modified Fermi model, that describes the wave-particle interaction in plasma physics. In a very simplistic and pedagogical way, the interaction is explained as the result of a large number of collisions between a certain number of particles and two walls of variable length. The model describes the linear part of Landau damping, and the trapping phenomenon, which leads to a saturation in the wave amplitude. A threshold amplitude below which the wave is always damped is found. Above this threshold, the wave, after an initial damping, oscillates regularly around a constant value, the period of these oscillations being correlated to the saturation amplitude of the wave. The particle distribution function changes in time, displaying regions of velocity space which are relatively full of particles and regions which are less populated. This clustering is the underlying phenomenon which generates the oscillations of the wave, since the energy exchanges between wave and particles, in a given interval of time, are all in the same direction. As time goes on, this synchronization become weaker and weaker, regular oscillations disappear, giving way to stochastic fluctuations. This lost of synchronization is due to a phase mixing between particles.

The phase mixing is produced by the filamentation of the phase space, a process analogous to the Gibbs laminar mixing, described by the baker's map. The Gibbs mixing time τ_G increases with the number N of particles as $\tau_G \propto N^0.55$.

In principle, this laminar mixing process cannot be described within the Vlasov theory, since in Vlasov theory smaller and smaller structures are created in phase space, never reaching the mixing stage. The system of trapped particles evolves from an unstable state towards the state of maximum entropy, where nothing can happen anymore.

Moreover we have shown that wave-particle interaction creates correlations between trajectories. Vlasov theory cannot describe increasing entropy phenomena and it cannot account for correlations in phase space, since it neglects collisions between particles.

Finally we compared the results of the Fermi-like model with those of a rigorous PIC code. We have seen that the results are very similar. Both this methods can describe the phase mixing and the rising of correlations. But, computer simulation of the Fermi model is faster than those of the PIC code, so only with Fermi-like model it is possible to examine the entropy increase for an increasing number of particles.

Appendix A

A simple treatment to get Landau damping

A.1 Introduction

A drawback common to many investigations of Landau damping is that they tend to be rather lengthy and technical, and although the single steps may appear not so complicated, the overall impression is that the analysis has lost the basic physics involved in the Landau damping.

The analysis that we report here is due to Anderson, Fedele, and Lisak [51] and it represents an effort to provide an intuitive generalization of the cold plasma wave theory to allow for the interaction between an electrostatic plasma wave and a continuous distribution of electron beams with different velocities co-propagating in a background of neutralizing immobile ions. The analysis starts by considering high frequency electrostatic plasma waves within a cold plasma description. Two cases are discussed, one in which the electron fluid is at rest and another when the electron fluid is moving with a velocity v_0 with respect to the neutralizing stationary ion background. In the next step it is assumed that the electron fluid consists of two species, one at rest relative to the stationary ion background, the other moving with a velocity v_0 . The analysis is then generalized by considering a large number of interstreaming electron fluids, each characterized by its density and velocity relative to the rest frame. In the final step, the infinite sum over electron beams is generalized to an integral over an electron velocity distribution and the characteristic dispersion relation containing the kinetic effect of the Landau damping is derived without going into the details required for mathematical rigor.

A.2 Basic equations

In the discussion we assume that a plane high frequency electrostatic electron plasma wave is propagating in the x direction in a homogeneous plasma. Due to the high oscillation frequency of the plasma wave, ions can be considered as a stationary neutralizing background. The relevant equations determining the interaction between the electron plasma wave and the plasma electrons are the equations of motion and continuity for the electron fluid together with Poisson's equation, which provides the self-consistent coupling between the electrostatic wave and the electron motion. Since the electron velocity, the electrostatic electric field as well as the propagation vector all lie in the x direction, the problem is truly one-dimensional and the governing equations read:

$$\begin{aligned} &\frac{\partial v}{\partial t} + v\frac{\partial v}{\partial x} = -\frac{e}{m}E \\ &\frac{\partial n}{\partial t} + \frac{\partial}{\partial x}(nv) = 0 \\ &\frac{\partial E}{\partial x} = -\frac{e}{\epsilon_0}(n - n_0) \end{aligned} \tag{A.1}$$

where v and n denote the velocity and density, respectively, of the electron fluid and E is the electrostatic electric field. Furthermore, n_0 is the constant density of the neutralizing ion background, e and m are the electron charge and mass, respectively, and ϵ_0 is the dielectric constant in vacuum.

A.3 Plasma oscillations

In order to analyse the characteristic propagation properties of the electron plasma wave, we consider the evolution of small perturbations of density, velocity and electric field on a stationary and homogeneous background according to:

$$v = v_0 + v_1, \qquad n = n_0 + n_1, \qquad E = E_0 + E_1 \tag{A.2}$$

where index 0 denotes a stationary and homogeneous equilibrium quantity

and index 1 denotes a small perturbation around the corresponding equilibrium quantity.

Let's consider a situation in which the equilibrium electric field is zero, $E_0 = 0$, and the electrons are stationary with respect to the background ions, i.e. $v_0 = 0$. Inserting Eq. (A.2) into Eq. (A.1) and linearizing, we obtain:

$$\begin{aligned} \frac{\partial v_1}{\partial t} &= -\frac{e}{m} E_1 \\ \frac{\partial n_1}{\partial t} + n_0 \frac{\partial v_1}{\partial x} &= 0 \\ \frac{\partial E_1}{\partial x} &= -\frac{e}{\epsilon_0} n_1 \end{aligned} \tag{A.3}$$

Looking for travelling plane wave solutions proportional to $\exp[i(kx - \omega t)]$ and with constant amplitude, where and k and ω are the frequency and wave number, respectively, of the electron plasma wave, Eq. (A.3) can be written as:

$$\begin{aligned} -i\omega v_1 &= -\frac{e}{m} E_1 \\ -i\omega n_1 + i n_0 k v_1 &= 0 \\ ikE_1 &= -\frac{e}{n_0} n_1 \end{aligned} \tag{A.4}$$

Eliminating v_1 and n_1 from the two first equations, Poisson's equation reduces to:

$$\left(1 - \frac{\omega_p^2}{\omega^2}\right) E_1 = 0 \tag{A.5}$$

where the characteristic plasma frequency ω_p is defined as $\omega_p^2 = n_0 e^2/(\epsilon_0 m)$. In order to have nontrivial solutions of Eq. (A.5) we must require that $\omega = \pm\omega_p$, which is the classical result of an electrostatic wave with frequency equal to plasma frequency.

Consider next a situation when the undisturbed situation corresponds to an electron fluid streaming through a neutralizing stationary ion background. In this case the zero order velocity of the electron fluid does not vanish. Linearizing as before around the background solution, Eqs. (A.3) become:

$$\begin{aligned}
&\frac{\partial v_1}{\partial t} + v_0 \frac{\partial v_1}{\partial x} = -\frac{e}{m} E_1 \\
&\frac{\partial n_1}{\partial t} + n_0 \frac{\partial v_1}{\partial x} + v_0 \frac{\partial n_1}{\partial x} = 0 \\
&\frac{\partial E_1}{\partial x} = -\frac{e}{\epsilon_0} n_1
\end{aligned} \tag{A.6}$$

The transformed equations now read:

$$\begin{aligned}
&-i(\omega - kv_0)v_1 = -\frac{e}{m} E_1 \\
&-i(\omega - kv_0)n_1 + in_0 k v_1 = 0 \\
&ikE_1 = -\frac{e}{\epsilon_0} n_1
\end{aligned} \tag{A.7}$$

Eliminating n_1 and v_1 as before and substituting into Poisson's equation, we find:

$$\left[1 - \frac{\omega_p^2}{(\omega - kv_0)^2)}\right] E_1 = 0. \tag{A.8}$$

The corresponding condition for nontrivial solutions becomes:

$$\omega = \omega_D \pm \omega_p \tag{A.9}$$

where we have introduced $\omega_D = kv_0$. This result represents the characteristic oscillation frequency of the previous case, now shifted by the Doppler frequency ω_D, due to the streaming electron velocity.

A.4 The two-stream instability

We now take a further generalizing step by combining the two previously studied cases. We assume that the electron fluid consists of two fluid species, one at rest relative to the stationary ion background, the other moving with a velocity v_0. The densities of the two fluids are denoted n_{01} and n_{02}, respectively. The condition of plasma neutrality requires that $n_0 = n_{01} + n_{02}$.

The dynamics of an electrostatic wave propagating in such a medium is determined by separate equations of motion and continuity for the two electron fluids, in fact Eqs. (A.3a) and (A.3b) and Eqs. (A.4a) and (A.4b) . However, Poisson's equation couples the dynamics of the two fluids and the electrostatic wave field. Now the Poisson's equation becomes:

$$ikE_1 = -\frac{e}{m}(n_{11} + n_{21}) \tag{A.10}$$

where n_{11} and n_{21} denote the perturbations on the two electron densities. Solving as before for n_{11} and n_{21}, Poisson's equation can be written as:

$$E_1 = \left[\frac{n_{01}e^2}{m\epsilon_0} \cdot \frac{1}{\omega^2} + \frac{n_{02}e^2}{m\epsilon_0} \cdot \frac{1}{(\omega - \omega_D)^2}\right] E_1 \tag{A.11}$$

which leads to the dispersion relation

$$1 = \frac{\omega_{p1}^2}{\omega^2} + \frac{\omega_{p2}^2}{(\omega - \omega_D)^2} \tag{A.12}$$

where ω_{p1} and ω_{p2} are the characteristic plasma frequencies of the two electron fluids. We are not concerned here with the solution of Eq. (A.12). We simply mention that, under some conditions (essentially the case in which Eq. (A.12) has complex roots, viz $\omega = \omega_{re} + i\omega_{im}$), the phenomenon of two-stream instability may appear, namely the electrostatic wave amplitude has a solution that grows in time during propagation as $\exp[i(kx - \omega_{re}t) + \omega_{im}t]$. In particular, the instability occurs when the electrostatic wave and the streaming electron fluid are close to being in resonance, i.e. the phase velocity v_f is close to v_0. In this situation, the coupling between the streaming electrons and the wave becomes very strong and energy is transferred from the electrons, which are moving with a velocity slightly larger than the phase velocity, to the wave, which grows.

A.5 Landau damping

We can generalize the dispersion relation given in Eq. (A.12) to a situation where the electron fluid is composed of a large number of interstreaming

electron fluids, each characterized by its streaming velocity, v_j, its density, n_{0j} and its plasma frequency ω_{pj} . The density of each electron fluid can be more conveniently expressed as $n_{0j} = f_j n_0$, where n_0 is the background ion density and f_j is the fractional density of the fluid j. Note that:

$$\sum_j f_j = 1. \tag{A.13}$$

With these assumptions, the proper generalization of Eq. (A.12) is:

$$1 = \sum_j \frac{\omega_{pj}^2}{(\omega - kv_j)^2} = \omega_{p0}^2 \sum_j \frac{f_j}{(\omega - kv_j)^2} \tag{A.14}$$

where ω_{p0} is the plasma frequency corresponding to the background density n_0. The last step of generalization can now be taken by assuming that the electron fluid consists of electrons of all velocities, the corresponding electron density being determined by a normalized distribution function, $f(v)$, where $n_0 f(v)dv$ is the total number of electrons in the infinitesimal velocity range between v and $v+dv$. The fractional density f_j in Eq. (A.14) is then replaced by $f(v)dv$, the sum turns into an integral and the dispersion relation becomes:

$$1 = \omega_{p0}^2 \int_{-\infty}^{+\infty} \frac{f(v)}{(\omega - kv)^2} dv. \tag{A.15}$$

A partial integration of this integral gives the dispersion relation:

$$1 = -\frac{\omega_{p0}^2}{k} \int_{-\infty}^{+\infty} \frac{df/dv}{\omega - kv} dv \tag{A.16}$$

where it is assumed that $f(\pm\infty) = 0$. Eq. (A.16) is exactly the same dispersion relation that is obtained from a fully kinetic treatment of the electron wave interaction based on the collisionless Vlasov equation for plasma electrons.

In the integration, care must be taken with those electrons which have velocities close to the phase velocity of the wave, i.e., for $v = \omega/k$, where, in

fact, the integral becomes singular. However, the theory of analytical functions supplies the recipe for evaluating this integral. The result contains two contributions, the principal value (PV) due to the main body of the distribution and half the residue contribution (Res) due to the resonant electrons at $v = \omega/k$ where the denominator of the integral vanishes. This gives:

$$1 = \frac{\omega_{p0}^2}{k^2}\left(\int_{-\infty}^{+\infty} \frac{df/dv}{v-\omega/k} dv + i\pi \mathrm{Res} \int_{-\infty}^{+\infty} \frac{df/dv}{v-\omega/k} dv \right). \tag{A.17}$$

Assuming that the phase velocity of the wave is much larger than the velocities in the bulk of the distribution, we can expand the denominator around $kv/\omega = 0$ when evaluating the principal value. This yields:

$$\mathrm{PV} = \frac{k}{\omega} \int_{-\infty}^{+\infty} \left(1 + \frac{kv}{\omega} + \frac{k^2v^2}{\omega^2} + \frac{k^3v^3}{\omega^3} + \cdots \right) \frac{df}{dv} dv. \tag{A.18}$$

The integrals in the previous equation can be evaluated by partial integration an by using the properties of $f(v)$:

$$\begin{aligned} \int_{-\infty}^{+\infty} f(v)dv &= 1 \\ \int_{-\infty}^{+\infty} vf(v) &= 0 \\ \int_{-\infty}^{+\infty} v^2 f(v)dv &= \frac{1}{2}v_{th}^2 \end{aligned} \tag{A.19}$$

The principal value then becomes:

$$\mathrm{PV} \int_{-\infty}^{+\infty} \frac{df/dv}{\omega - kv} dv \approx -\frac{k^2}{\omega^2}\left(1 + \frac{3k^2v_{th}^2}{\omega^2} \right) \tag{A.20}$$

and the residual integral is:

$$\mathrm{Res} \int_{-\infty}^{+\infty} \frac{df/dv}{v-\omega/k} dv = f'(\omega/k) \tag{A.21}$$

Then the dispersion relation in Eq. (A.17) reads as:

$$1 = \frac{\omega_{p0}^2}{\omega^2}\left(1 + \frac{3k^2 v_{th}^2}{\omega^2}\right) + i\pi\frac{\omega_{p0}^2}{k^2} f'(\omega/k). \tag{A.22}$$

The thermal as well as resonant contributions in Eq. (A.22) are small and to lowest order the dispersion relation reduces to our previous result from Sec. II, viz. $\omega^2 \approx \omega_{p0}^2$. Using this approximation perturbatively to simplify the correction terms we obtain the dispersion relation in the form:

$$\omega^2 = \omega_{p0}^2 + \frac{3}{2}k^2 v_{th}^2 + i\pi\omega^2\frac{\omega_{p0}^2}{k^2} f'(\omega/k). \tag{A.23}$$

Separating the real and imaginary parts, $\omega = \omega_{re} + i\omega_{im}$ where, $|\omega_{im}| \ll |\omega_{re}| \approx \omega_{p0}$ we obtain the classical result for the propagation of an electrostatic high frequency electron plasma wave in a warm plasma:

$$\begin{aligned} \omega_{re}^2 &\approx \omega_{p0}^2 + \frac{3}{2}k^2 v_{th}^2 \\ \omega_{im} &\approx \frac{\pi}{2}\frac{\omega_{p0}^3}{k^2} f'(\omega/k). \end{aligned} \tag{A.24}$$

In order to interpret this result we note that the two-stream instability implies that electrons with velocities almost equal to but slightly higher than the phase velocity of the wave cause an increase of the wave amplitude. The concomitant increasing energy of the wave must cause a slowing down of the fast electrons. Conversely, we expect that electrons, which are moving with velocities almost equal to but slightly slower than the phase velocity of the wave, will gain energy from the wave, thus increasing their speed at the expense of the wave energy, which consequently decreases. For an ordinary (Maxwellian) velocity distribution, the distribution function is a decreasing function of velocity, the derivative at the resonant velocity, ω/k, is negative, and the wave experiences Landau damping.

The physical mechanism behind the damping mechanism is intuitively clear; there are more electrons moving slightly slower than electrons moving slightly faster than the phase velocity of the wave and the net energy transfer

must be from the wave and to the electrons. If around the resonant velocity, there are as many electrons moving faster as there are electrons moving slower, i.e., the electron distribution function has a plateau with $f'(v) = 0$, no energy transfer will take place between the wave and the electron fluid, and ω_{im} should be zero, as indeed is predicted by Eq. (A.24).

One more time we point out that this analysis skips some formal mathematical issues in order to concentrate on the physics involved in the process.

Appendix B

The Shannon entropy

B.1 Introduction

We have seen in sec. 1.6 that a particular attention has been devoted by some authors to the investigation of chaos in the region of the phase space where the separation between trapped and free particles occurs. Among others, Valentini *et al.* [31] used a Lagrangian approach to the nonlinear Landau damping to understand why Isichenko's idea [24] does not work in the numerical simulations. From an accurate analysis of the Poincaré sections and of the Lyapunov exponents of the phase space trajectories, they conclude that in the zone of the separatrix, in correspondence of the maximum and minimum value of the electric field envelope, the particles exhibit an ergodic and chaotic dynamics. Due to the time oscillation of the wave amplitude, these particles are able to escape from the well and perform flights, in agreement with the Isichenko conjecture. However, a statistical study of the spatial and time length of these flights has shown that they have a limited length, because after a characteristic re-trapping time, almost all the particles are retrapped by the wave. In this situation, in the numerical solution no algebraic damping is allowed due to the fact that the wave-particle energy balance is kept on a time scale equal to the retrapping time.

In the case of the modified Fermi model, we have seen that the its dynamics is generated by the particular sequence of collisions that takes place. In particular, we have seen that, according to the regularity of their motion, particles can be distinguished in three groups (sec. 4.3): particles that are always trapped and thus exhibit regular motion, particles that have only an initial interaction with the wave, and particles that are trapped and detrapped in a non regular way, and hence show an unpredictable motion.

But is it possible to characterize this irregular motion? Is it completely

stochastic or there is a kind of *memory* in it? To address this question we make use of a statistical tool known in literature as Shannon (or information) entropy [52, 53]. Shannon introduced this concept in the area of the information theory to qualify the sources emitting sequences of discrete symbols (e.g. binary digit sequences). Originally information theory was introduced in the practical context of electric communications, nevertheless in a few years it became an important branch of both pure and applied probability theory with strong relations with other fields as computer science, cryptography, biology and physics [54].

The idea to use Shannon entropy has been suggested by the fact that in the Fermi-like model, the regularity of the motion of a particle can be inferred by observing the sequence of signs of its velocity in time (see Fig. 4.2), and these signs, in turn, can be considered as a sequence of binary digits, i.e. 1 and -1.

We will give a brief description of the Shannon entropy.

The regularity of a sequence of $N-1$ symbols, produced by any source, can be characterized through the ability in predicting the N-th symbol. Consider a source that can output a sequence of m different symbols (in our case $m = 2$), denote with $s(t)$ the symbol emitted by the source at time t and with $P(C_n)$ the probability that a given "word" $C_n = (s(1), s(2), ..., s(n))$ of length n is emitted. We assume that the source is stationary, so that for the sequence $\{s(t)\}$ the time translation invariance holds: $P(s(1), \ldots, s(n)) = P(s(t+1), \ldots, s(t+n))$. Then, the entropy associated to a generic n-digits word can be defined as:

$$H_n = -\sum_{\{C_n\}} P(C_n) \log P(C_n) \tag{B.1}$$

where the sum is computed over all the possible combinations of length n. The quantity $h_n = H_{n+1} - H_n$, indicated as differential entropy, thus represents the average information provided by the $(n+1)$-th digit, once the previous n digits are known. One can also say that h_n is the average uncertainty about the $(n+1)$-th symbol, provided the n previous ones are given. For a stationary source, the limits in the following equation exist, are equal and define the Shannon entropy h_{Sh}:

$$h_{sh} = \lim_{n\to\infty} h_n = \lim_{n\to\infty} \frac{H_n}{n}. \tag{B.2}$$

This quantity is a measure of the regularity of the sequence. For example, for a given regular (say periodic) sequence, the information carried by the next digit after one period is zero, since the full knowledge of the sequence in contained into the first period. The predictability of such a sequence is then trivially high, and the signal is completely correlated with long range memory. On the contrary, if the sequence is chaotic, the information provided by the knowledge of each digit can be high. For example, for a random realization, namely if all digits have the same chance to be -1 or 1, any next digit carries with it the same amount of information of the previous ones. Such a sequence is completely unpredictable, and neither memory nor correlations are present. In this case the limit in Eq. (B.2) can be easily shown [53] to be $h_{sh} = \log 2$. Thus, the quantities defined so far represent a tool to describe the complexity of the source, through the regularities of the emitted sequences. Note that although the theoretical Shannon entropy is defined as the limit to infinity of the word length, in the real experiments the convergence of the limit (B.2) is normally already obtained for small values $n < 8$.

B.2 Analysis of the data of the simulation

We have computed the quantities defined above, namely the entropy H_N, and the Shannon entropy h_{Sh}, using words of length up to $n = 8$ for four particles in a run of the modified Fermi model. We have considered the case $A_0 = 1$ and $u_p = 1.4$. With these conditions the saturation amplitude is around $A_{sat} = 0.797$. Three particles taken into account have an height near the saturation amplitude, namely one has height $y = 0.7999$, another one has height $y = 0.7997$ and the last one has an altitude $y = 0.7965$. The fourth particle is always trapped ($y = 0.197$), and thus displays a regular motion. Results are collected in Fig. B.1. For comparison, on the same figure, is reported, together with the data of the simulation, the results obtained using an artificial datasets composed by a completely random realization. All sequences include 446 digits.

Looking at Fig. B.1 (top panel), it is possible to notice that, for the regular string, there is no increase of information when the number n of digit of the words increases. This corresponds, as expected, to a vanishing differential entropy leading to $h_{sh} = 0$ (see bottom panel of the same figure). The random case, conversely, displays a constant growth of entropy H_n with the number of digits, indicating that all of them bring the same amount of information. This correspond to a constant differential entropy h_n. For the experimental dataset, we have $h_{Sh} \approx 0.55$ in two cases and $h_{Sh} \approx 0.68$ in the case of the particle with the minimum height. This indicates that

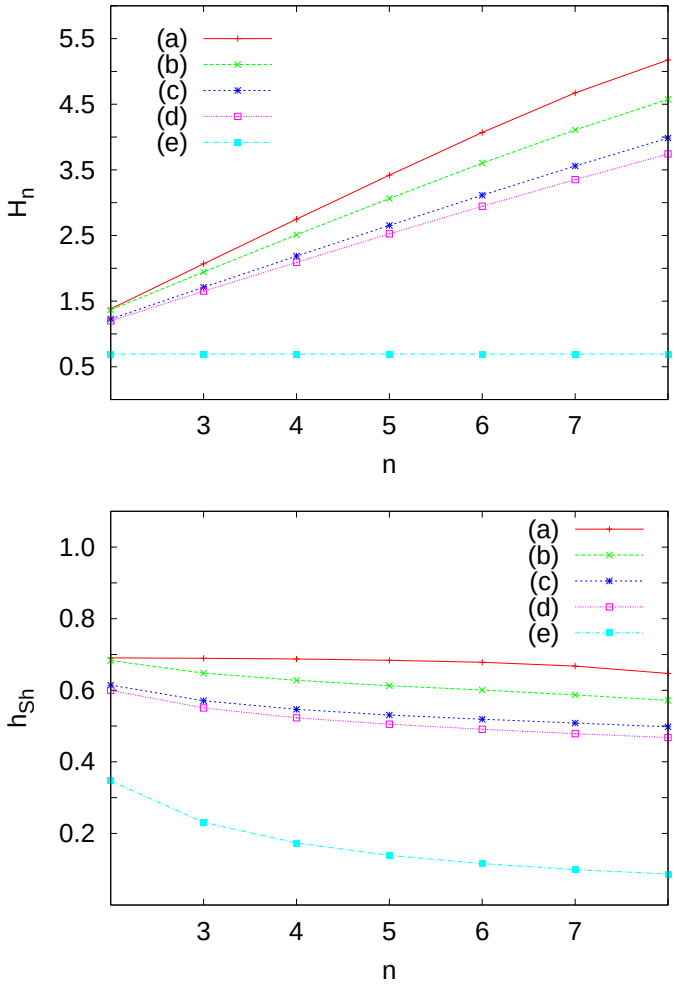

Figure B.1: Values of the entropy H_n (top panel) and of the Shannon entropy h_{Sh} (bottom panel) as a function of the words length n. Different colours refer to the different dataset: in particular: (a) random string, (b) $y = 0.7965$, (c) $y = 0.7997$, (d) $y = 0.7999$, (e) $y = 0.197$.

the system is chaotic, but with some degree of regularity. This is evidenced by the fact that the information entropy H_n grows more slowly than with respect to the random case (Fig. B.1 top panel). Moreover, for the particle with the minimum height (curve b) we see that the two-word entropy h_2 is near to the completely random case, but if we consider longer words ($n > 2$) the entropy become smaller. This means that the system appears as to be random if we look at it for short time periods but, for longer intervals of time, it keeps some kind of memory. It could be conjectured that the

particles in the saturation region are not subject to a random motion, but rather their dynamical behaviour has long range correlations. The presence of correlations, and thus of a memory effect, corresponds to evidence of some degree of regularities in the signal obtained through this procedure.

A more careful examination of this issue, although interesting, is left to a future work.

Bibliography

[1] L. Landau, J. Phys., (USSR), **10**, 25-34 (1946).

[2] A. Vlasov, J. Phys (USSR), **9**, 25-40, (1945).

[3] N. G. Van Kampen, Physica **21**, 949-963 (1955).

[4] J. H. Malmberg, C. B. Wharton, Phys. Rev. Lett. **13**, 184-186 (1964).

[5] A. W. Chao, *Physics of Collective Beam Instabilities in High Energy Accelerators* Wiley, New York, (1993), pp. 218-268.

[6] B. Fak, K. Guckelsberger, M. Korfer, R. Scherm, A. J. Dianoux, Phys. Rev. B, **41**, 8732-8748 (1990)

[7] R. Baier, H. Nakkagawa, A. Niegawa, K. Redlich, Z. Phys. C **53**, 433-438 (1992).

[8] S. Strogatz, R. Mirollo, P. Matthews, Phys. Rev. Lett. **68**, 2730-2733 (1992).

[9] J. Buck, Q. Rev. Biol.,**63**, 256-289 (1988).

[10] A. T. Winfree, *The Geometry of Biological Time* (Springer, New York, 1980) pp. 315-336.

[11] I. Langmuir, L. Tonks, Phys. Rev., **33**, 195 (1929).

[12] D. Bohm, E. P. Gross, Phys. Rev., **75** 1851, 1864 (1949).

[13] M. Bernstein, J. M. Greene, M. D. Kruskal, Phys. Rev., **108**, 546 (1957).

[14] D. D. Ryutov, "Landau damping: half a century with the great discovery", Plasma Phys. Control. Fusion, **41**, A1-A12(1999).

[15] J. M. Dawson, Phys. Fluids, **4**, 869 (1961).

[16] K. Miyamoto, *Plasma Physics for Nuclear Fusion*, MIT Press, Cambridge, MA, 1997.

[17] P. Bertrand *et al.*, Phys. Rev. E, **49**, 5656 (1994).

[18] J. M. Dawson, Phys. Scr., **T52**, 7 (1994).

[19] S. R. Cranmer, A. A. van Ballegooijen, Ap. J. **594**, 573 (2003).

[20] I. Lerche, R. Schlickeiser, A&A **366**, 1008, (2001).

[21] N. A. Krall, A. W. Trivelpiece, *Principles of Plasma Physics*, McGraw-Hill, Tokio, 1973.

[22] A. A. Sagdeev, A. A. Galeev, *Nonlinear Plasma Theory*, Benjamin, New York, 1969.

[23] T. M. O'Neil, Physics of fluids, **8**, 2255 (1965).

[24] M. B. Isichenko, Phys. Rev. Lett., **78**, 2369 (1997).

[25] C. Lancellotti, J. J. Dorning, Phys. Rev. Lett. **80**, 5236 (1998).

[26] C. Lancellotti, J. J. Dorning, Phys. Rev. Lett. **81**, 5137 (1998).

[27] C. Z. Cheng, g. Knorr, J. Comput. Physics., **22**, 330 (1976); R. J. Gagne, M. Shoucri, ibid. **24**, 445 (1977); J. Canosa, J. Gazdag, Phys. Fluids **17**, 2030, (1974); M. Shoucri, ibid. **22**, 2038 (1979); A. J. Klimas, J. Comput. Physics., **50**, 270 (1983); A. Ghizzo et al., Phys. Fluids **31**, 72 (1988).

[28] G. Manfredi, Phys. Rev. Lett., **79**, 2815 (1997).

[29] M. Brunetti, F. Califano, F. Pegoraro, Phys. Rev. E, **62**, 4109 (2000).

[30] L. Galeotti, F. Califano, Phys. Rev. Lett., **95**, 015002, (2005).

[31] F. Valentini, V. Carbone, P. Veltri, Phys. Rev. E, **71**, 017402 (2005).

[32] Tie Zhou, Yan Guo, Chi-Wang Shu, Physica D **157**, 322 (2001).

[33] M. Firpo, F. Doveil, Phys. Rev. E, **65**, 016411, (2001).

[34] J. R. Danielson, F. Anderegg, and C. F. Driscoll, Phys. Rev. Lett. **92**, 245003 (2004).

[35] R. May, Nature, **261**, 459 (1976).

[36] B. V. Chirikov, Phys. Rep., **52**, 263 (1979).

[37] E. Fermi, Phys. Rev., **75**, 1169 (1949).

[38] A. K. Kerlis *et al.*, Phys. Rev. Lett. **97**, 194102 (2006)

[39] S. Ulam, in Proceedings of the Fourth Berkley Symposium on Mathematics, Statistics and Probability, California U.P., Berkeley, 1961, Vol. 3, p. 315.

[40] A. J. Lichtemberg, M. A. Lieberman, Appl. Math. Sci., **38**, Springer-Verlag, New York (1992).

[41] R. De Marco, V. Carbone, P. Veltri, Phys. Rev. Lett., **96**, 125003 (2006).

[42] A. V. Ivanov, I. H. Cairns and P. A. Robinson, Phys. of Plasmas, **11**, 4649 (2004).

[43] J. L. McCauley, *Chaos, dynamics and fractals*, Cambridge University Press (1993).

[44] V. Carbone, R. De Marco, F. Valentini, P. Veltri, Europhysics Letters, **78**, 65001 (2007).

[45] V. Carbone, R. De Marco, F. Valentini, P. Veltri, Communications in Nonlinear Science and Numerical Simulation, **13**, 34 (2008).

[46] N. G. Van Kampen, B. U. Felderhof, *Theoretical Methods in Plasma Physics*, Amsterdam (1967).

[47] A. Thyagaraja, Eur. J. Phys., **9** (1988).

[48] C. Jarzynski, G.F. Bertsch, Phys. Rev. C, **53** (1996).

[49] C. K. Birdsall, A. B. Langdon, *Plasma Physics via Computer Simulation*, McGraw-Hill Book Co., Singapore, 1985.

[50] D. H. Dubin, *Numerical and Analytical Methods for Scientists and Engineers Using Mathematica*, Wiley-Interscience, Hoboken, New Jersey, 2003.

[51] D. Anderson, R. Fedele, M. Lisak, Am. J. Phys. **69** (2001).

[52] C. E. Shannon, The Bell System Technical J. **27** 623, **27** 379 (1948).

[53] G. Boffetta, M. Cencini, M. Falcioni, A. Vulpiani, Physics Reports **356** (2002).

[54] W. H. Zurek, *Complexity, Entropy and Physics of Information*, Addison-Wesley, Redwood City, 1990.